Aggregate dissolution in different pore solutions

Mahsa BAGHERI

École
polytechnique
fédérale
de Lausanne

2021

To my parents and my sister

for their endless love

Acknowledgements

It has been a new journey with amazing experiences, but I am almost at the end! This thesis would not have been possible without the inspiration and support of a number of wonderful individuals.

My deep and sincere gratitude to my thesis director, Karen, giving me a wonderful opportunity to be a member of her amazing team, LMC. I really appreciate her unflagging support and encouragement.

A hug thank to Barbara for all rewarding discussions and providing valuable feedback throughout this research. I really acknowledge all of her insightful comments.

I really appreciate the time and effort of my jury members to revise my thesis: Prof. Klaartje De Weerdt, Prof. Benoît Fournier and Dr. Erich Wieland.

I would like to give special thanks to Lionel, Jean and Antonio for sharing their expertise and experiences. It is a pleasure to thank my friends, who were my second family in Switzerland: Anna (Natechanok), Sarra, Diana, Fabien, Maya, Franco, Andrea, Solene, Qiao, Mai and Khalil.

In this journey, I spent three months of my PhD at Empa, and I wold like to thank my collegues and my friends there: Andreas, Luigi, Boris, Sonya and Yiru. Also especial thanks to Mahdieh for all helpful discussions and collaborations.

Finally, my deep and sincere gratitude to my parents for their continuous and unparalleled love, help and support. I am grateful to my sister for always being there for me as a friend. I am forever indebted to my parents for giving me the opportunities and experiences that have made me who I am.

Lausanne, April 2021

Abstract

The occurrence of cracking due to alkali silica reaction (ASR) affects the service life of concrete structures. The dissolution of silica-containing minerals within aggregates causes the formation of ASR products, which fill macroscopic cracks and cause the opening of additional cracks.

Three ASR-reactive aggregates from Switzerland were studied to find the chemical composition and crystalline structures of the dissolvable minerals. The ASR reactivity of these Swiss aggregates was assessed using the conventional expansion tests and the dissolution experiments. Quartz (possibly with inclusions of amorphous SiO_2), K-feldspar ($KAlSi_3O_8$) and Na-feldspar ($NaAlSi_3O_8$) were observed to be the most reactive minerals within the studied aggregates. Although similar reactivity trends were observed from the results of expansion and dissolution tests, the results of these approaches cannot be simply correlated.

The effect of different factors on dissolution kinetics was studied for the simple model systems. Different approaches were used to measure the extent of silica and feldspars dissolution; directly with the scratch-tracking method, as a new method, with the observation of solid surface and indirectly by measuring the amount of released Si from each solid. The formation of new solids, such as C-S-H and lithium silicates, means that the dissolution rates measured by the released Si may be misleading. An increase in dissolution rates of silica and feldspars was observed in the presence of lithium, calcium and sulfate. However, no noticeable effects on dissolution rates were measured in the presence of iron, magnesium and additional NaCl, KCl or CsCl at high pH. Among all studied elements, aluminium is the only element slowing down dissolution rates of quartz, amorphous silica and Na and K-feldspar at 20, 40 and 60 °C.

The effect of paste composition was studied on the pore solution composition over 17 months and on the ASR expansion. Pastes, containing metakaolin, had the lowest amount of alkalis and the highest amount of aluminium in the pore solution. Significant effect of aggregate mineralogy to take up alkalis from the pore solution composition was observed for the feldspar-rich aggregate, Bend aggregate. The lowest ASR expansion was measured for the concrete samples made of blended cement pastes mainly due to having low alkali and pH in the pore solutions.

Keywords: Alkali silica reaction, dissolution kinetics, silica, feldspar, high pH, temperature, pore solution.

Résumé

L'apparition de fissures dues à la réaction alcali-granulat (RAG) affecte la durée de vie des structures en béton. La dissolution des minéraux contenant de la silice dans les agrégats provoque la formation de produits RAG, qui comblent les fissures macroscopiques et provoquent l'ouverture de fissures supplémentaires.

Trois agrégats réactifs de Suisse ont été étudiés pour trouver la composition chimique et les structures cristallines des minéraux solubles. La réactivité RAG de ces agrégats a été évaluée à l'aide des tests d'expansion conventionnels ainsi que des expériences de dissolution. Le quartz (éventuellement avec des inclusions de SiO_2 amorphe), le K-feldspath ($KAlSi_3O_8$) et le Na-feldspath ($NaAlSi_3O_8$) ont été observés comme les minéraux les plus réactifs dans les agrégats étudiés. Bien que des tendances de réactivité similaires aient été observées à partir des résultats des tests d'expansion et de dissolution, les résultats de ces approches ne peuvent pas être simplement corrélés.

L'effet de différents facteurs sur la cinétique de dissolution a été étudié pour des systèmes modèles simples. Différentes approches ont été utilisées pour mesurer le degré de dissolution de la silice et des feldspaths ; directement avec la nouvelle méthode de suivi des rayures, en observant la surface solide, et indirectement en mesurant la quantité de Si dissout. La formation de précipités, tels que le C-S-H et les silicates de lithium, indique que les vitesses de dissolution mesurées par le Si dissout peuvent être trompeuses. Une augmentation des taux de dissolution de la silice et des feldspaths a été observée en présence de lithium, de calcium et de sulfate. Cependant, aucun effet notable sur les taux de dissolution n'a été mesuré en présence de fer, de magnésium et de NaCl, KCl ou CsCl supplémentaire à pH élevé. Parmi tous les éléments étudiés, l'aluminium est le seul élément ralentissant les taux de dissolution du quartz, de la silice amorphe et du Na et du K-feldspath à 20, 40 et 60 ° C.

Dans la troisième partie, l'effet de la composition de la pâte de ciment a été étudié sur la composition de la solution de pore pendant 17 mois et sur l'expansion ASR. Les pâtes, contenant du métakaolin, avaient la plus faible quantité d'alcalis et la plus grande quantité d'aluminium dans la solution interstitielle. Un effet significatif de la minéralogie des agrégats pour absorber les alcalis de la composition de la solution interstitielle a été observé pour un agrégat riche en feldspath, l'agrégat Bend. L'expansion ASR la plus faible a été mesurée pour les échantillons de béton constitués de pâtes de ciment composées, principalement en raison de la faible teneur en alcali et le bas pH dans la solution interstitielle.

Mots-clés: Réaction alcali-granulats, cinétique de dissolution, silice, feldspath, pH élevé, température, solution interstitielle.

Contents

List of Figures

Figure 3-16 (a) An example SEM image for amorphous silica illustrating the 2D cross-section of powder particles (the micrograph was obtained by stitching several SEM

List of Tables

List of Equations

Chapter 1   Introduction

1.1   Background

Building materials are used in infrastructure and housing for modern societies. In particular, cement based materials are in high demand because of their high performance, availability of raw materials, low cost and relatively low environmental footprint per unit mass produced [1]. However, Alkali Silica Reaction (ASR) is an important durability issue, which causes expansion and deterioration of concrete in the long term (Figure 1-1). ASR is a worldwide durability problem and many concrete structures are suffering from ASR. For instance, in Switzerland, ASR was detected in around 10 to 20% of concrete dams [2], and more than 90% of the Swiss aggregates are classified as ASR–reactive aggregates [3].

a)

b)
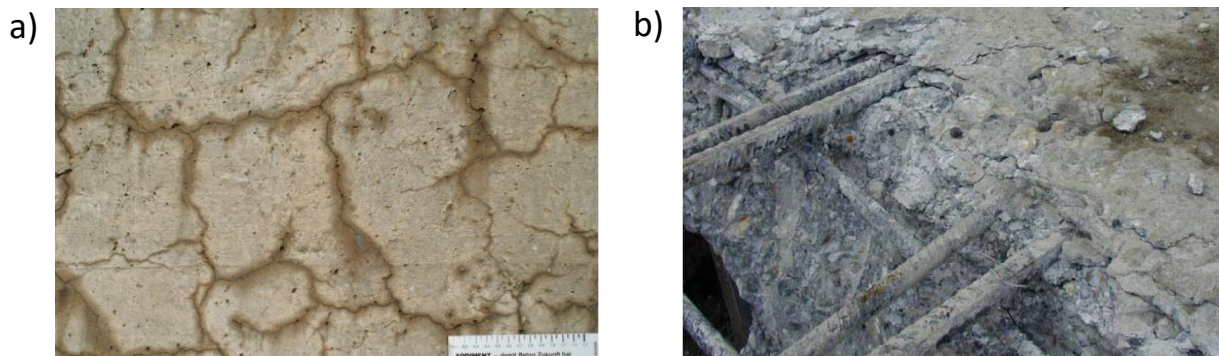
Figure 1-1 a) Typical crack pattern caused by ASR (image from Dr. Andreas Leemann – Empa, Swiss Federal Laboratories for Materials Science and Technology) and b) severely cracked deck of a 142 m long bridge (image from Ruedi Gall).

ASR produces an expansive gel because of a chemical reaction between amorphous or poorly crystalline silica (from certain reactive aggregates) and alkali hydroxides (mainly from the pore solution of the cement paste), which is able to create macroscopic expansion in concrete [4]. The formation

of ASR products and thus the rate at which cracking occurs depends on the rate of dissolution of the reactive phase inside the aggregates, amorphous silica or poorly crystallized quartz [5].

So far, it seems that there is not any possibility to stop ASR in existing structures. In the past, two approaches were tried to treat the affected structures; i) water proofing and ii) slot cutting (to release stresses due to concrete expansion) of the dams. However, none of them is known as an efficient solution to preserve concrete from ASR. In the first approach, there is always enough water for the expansion to progress, and in the second approach, the concrete continues expanding.

In newly build structures, the use of non-reactive aggregate can be one solution to avoid ASR. However, from both environmental and economic aspects, local aggregates are preferable and in remote locations (such as for dams) may be the only choice. Another solution to lower damage risk of ASR is decreasing dissolution kinetics of silica-containing minerals within aggregates, as the dissolution of metastable silica from aggregate is the initial reaction of ASR [6]. This goal can be achieved by the use of appropriate cement paste and consequently changing pore solution composition (by using blended cement paste with Supplementary Cementitious Materials (SCMs)). Therefore, a systematic study is needed to clarify the effect of pore solution composition (the presence of different ions such as Al, Li, Fe, Na, … with different concentrations) on the dissolution kinetics of reactive silica within ASR-reactive aggregates.

Most studies of dissolution kinetics of minerals have been carried out under acid to neutral pH conditions and studies under high pH conditions are still rare. This means we lack a fundamental understanding of the different factors and their interplay. As a result, numerous questions are still open and both, mitigation of ASR and prediction of expansion due to ASR are linked to a high degree of uncertainty. To answer these questions, the dissolution kinetics of the reactive aggregate, as the initial ASR step, should be studied in simulated pore solutions at high pH with different compositions.

1.2   Context and objective of the study

The present project was a part (subproject I) of a bigger project, funded by SNSF under the Sinergia programme, consisting of six different subprojects, bringing an interdisciplinary approach to ASR (Figure 1-2). The main goal of the present study was to investigate and quantify the factors governing the initial dissolution of aggregate and its kinetics. The effect of solution composition on dissolution kinetics was studied for three ASR-reactive aggregates from different locations in Switzerland (Uri, Brienz and Praz) and the simplified model solids.
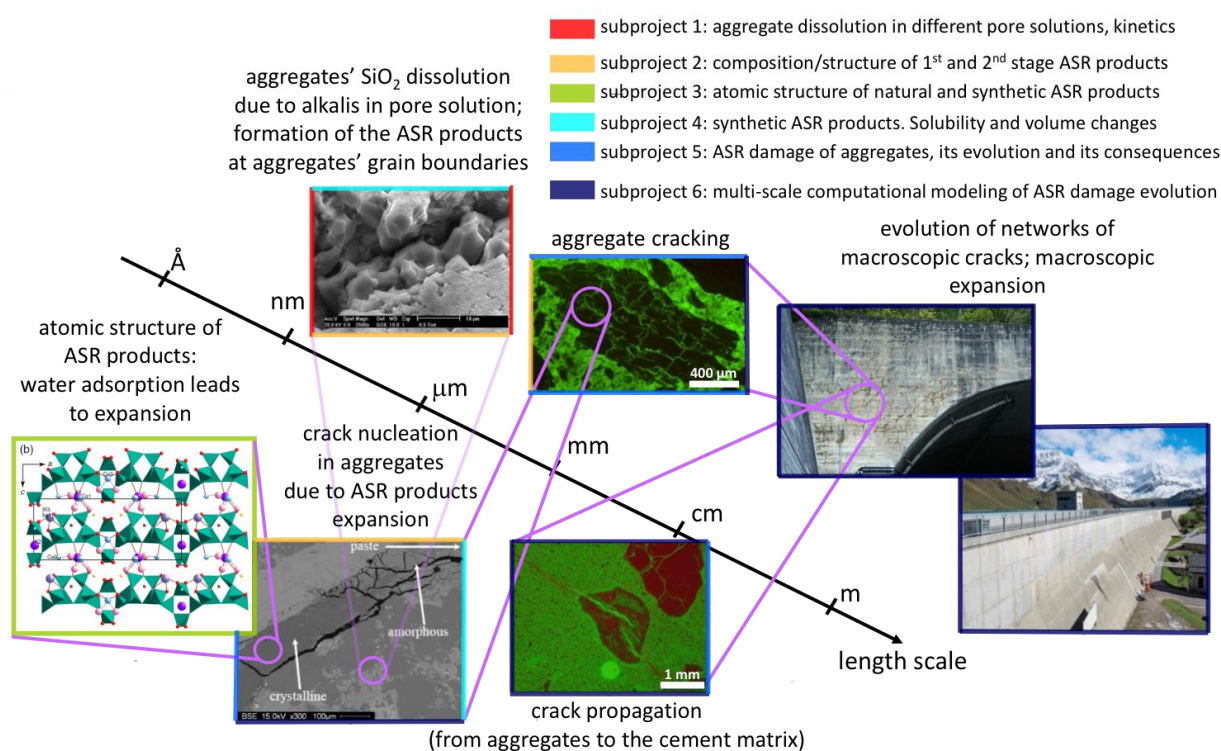
Figure 1-2 Overview of the aspects of ASR studied within the Sinergia project considering the different length scales (graph designed by Dr. Michele Griffa- Empa, Swiss Federal Laboratories for Materials Science and Technology).

Since natural aggregates have complicated mineralogy, the following strategy was applied to study some simple model solids in addition of investigation of natural aggregates:

•   Identification of the chemical composition of reactive minerals in the natural aggregates

• Selection of representative and pure model solids with the same chemical composition and crystalline structures as the reactive minerals in the studied aggregates

• Investigation of the effect of different parameters on the dissolution kinetics of minerals such as presence of Al, Li, Na, K, s … in a simplified pore solution, pH and temperature.

The next step was to track evolution of pore solution composition of cement and concrete samples made by different blended cement pastes in long term. Pore solution composition from paste and concrete samples made by different blended cements (stored at different temperatures and with different water to binder ratio) was measured as long as possible to obtain pore solution by extraction method.

In parallel, expansion tests (based on LMC method) on the same samples were done to link the effect of pore solution composition on the extent of expansion due to ASR.

1.3   Experimental approach

Different techniques and experiments were used to study the target materials and their reactions in this project, as summarized in Figure 1-3.
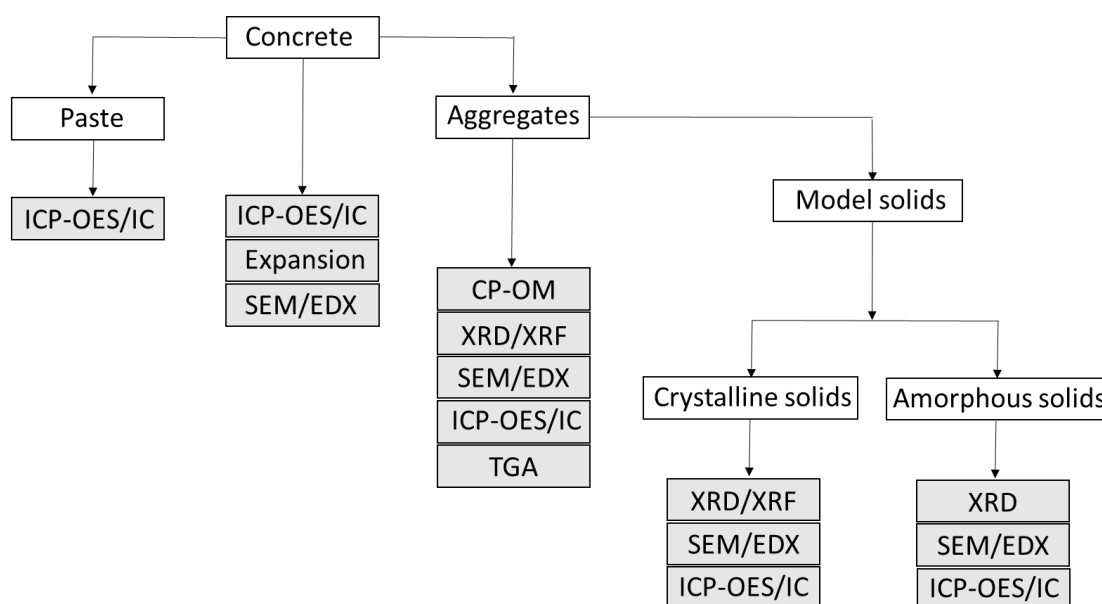
Figure 1-3 Schematic of the used techniques and experiments.

Dissolution experiments were done using natural aggregates and simplified model solids with crystalline and amorphous structures. The materials were characterized using different techniques; X-ray Powder Diffraction (XRD), X–ray fluorescence (XRF), Optical Microscopy with Crossed Polarizers and inserted gypsum plates (CP-OM), Scanning Electron Microscopy (SEM) and Energy Dispersive X–ray (EDX). The amounts of released component from the target solids were quantified using Inductively Coupled Plasma Optical Emission Spectrometry (ICP-OES) and Ion Chromatography (IC). The aggregates were analysed before and after dissolution experiments using Thermo Gravimetric Analysis (TGA) as well.

Different paste and concrete samples were made of Supplementary Cementitious Materials (SCMs) such as metakaolin, fly ash, micro silica and limestone. The extracted pore solutions of the paste and concrete samples were analysed using ICP-OES/IC. Expansion of the concrete samples was followed by measuring the relative length change based on LMC method. The formed ASR products and ASR cracking were analysed using SEM/EDX.

Finally, the results of expansion tests revealed which pastes suppressed ASR. The results of dissolution experiments and pore solution analysis were considered to explain why ASR was suppressed for some samples while for the others higher expansion values were measured. We hope the results of this work provide useful and basic knowledge to select the best paste composition to lower damage risk of concrete structures due to ASR.

1.4   Structure of the work

Chapters 2, 3 and 4 have been prepared as papers; and chapter 2 was already submitted.

This work is structured as following:

Chapter 2 shows the results of aggregate dissolution in different alkaline solutions. In addition to solution study by using ICP-OES/IC, a new method, called scratch-tracking method, is introduced. Scratch-tracking method is to observe directly the solid surfaces using SEM and measure dissolvable minerals within natural aggregates.

Chapter 3 shows the effects of different parameters such as degree of solid crystallinity, solution composition, pH and temperature on dissolution rates of silica and feldspars, which were used as the simplified model solids. The dissolution study was done with both approaches, solution analysis using ICP-OES/IC and the newly introduced scratch-tracking method.

Chapter 4 is about the pore solution analysis of different paste and concrete samples. The extent of concrete expansion is shown as a function of time for different samples. The pore solution composition on the extent of ASR expanding is discussed to link dissolution results with the observed ASR-expansions.

Chapter 5 determines the overall conclusions and perspective of this thesis.

Chapter 2　　　Dissolution of aggregates subject to alkali silica reaction

Mahsa Bagheri, Barbara Lothenbach, Mahdieh Shakoorioskooie, Andreas Leemann, Karen Scrivner

Abstract

Alkali silica reaction (ASR) can significantly affect the service life of concrete structure. The dissolution of aggregates has a direct impact on gel formation and thus on the macroscopic expansion. The ASR reactivity of three aggregates from different locations in Switzerland were studied by conventional expansion tests and other investigations. Scratch tracking on polished surfaces in the SEM showed faster dissolution of feldspars and quartz while muscovite was hardly affected. The dissolution of the aggregates in solution confirmed these differences between minerals. The trends in expansion and aggregate dissolution were the same, but due to the differences between dissolution experiments and expansion tests and presence of complex interactions in both studies, dissolution studies should not be simply correlated to the extent of expansion.

Keywords: Aggregate dissolution, ASR expansion, Alkali effect.

2.1   Introduction

Alkali-silica reaction (ASR) can cause serious problems for the durability of concrete. ASR is a chemical reaction between silica-containing minerals within aggregates and the alkaline pore solution of concrete. The formation of reaction products leads to cracking of the aggregates; the cracking starts inside the aggregates and then propagates into the cement paste [2,4,6–8]. ASR starts with aggregate dissolution, and this is an important parameter affecting expansion. Aggregate dissolution in concrete occurs mainly at the grain boundaries, where amorphous or poorly crystalline materials is found [4]. Many granitic and sedimentary aggregates contain different minerals such as quartz, feldspar, biotite, labradorite, calcite, which have very different dissolution rates in alkaline solution [9]. Usually only reactive silicates such as poorly crystalline forms of quartz are considered to be susceptible to ASR [10]. However, feldspar has a similar dissolution rate to quartz at high pH [9]. If feldspar dissolves, the release of alkali may speed up dissolution and/or the release of Al may slow it down [11]. In dissolution experiments, the dissolution of other minerals (such as calcite [12]) may lead to the formation of new solids with dissolved Si from silica-containing minerals.

Previously, aggregate dissolution has been proposed as a way to assess the ASR susceptibility of aggregates. For example, in *ASTM C 289* [13] 25 g of crushed and sieved aggregates with size fraction of 150 to 300 μm is dissolved in 25ml of 1 M of NaOH at 80 °C for 24 hours, and the amount of dissolved silica is measured. However, such a highly concentrated alkaline solution at 80 °C can dissolve non-expansive silicates, such as crystalline quartz, and the interference of some other minerals within aggregates are rather troublesome. For example, the dissolution of calcite and calcium silicate precipitation consumes the dissolved Si. *RILEM TC 219-ACS* [14] has proposed a method to assess alkali release from feldspars. Two representative samples (500 g) of the aggregate (size fraction ≤ 4 mm) are immersed in containers, one having 2 l of 0.7 M of KOH and the second having 2 l of 0.7M of NaOH solution with excess $Ca(OH)_2$ at 38 and 60 °C. After 14, 42, 91, 182 and 364 days, 10 ml of the solution is removed to measure the amount of released alkalis (the amount of K in NaOH and/or Na in KOH solution) from aggregates. Nevertheless, formation of new solids in the presence of $Ca(OH)_2$ leads to misinterpretation of the results.

The most widely accepted way to assess the alkali silica reaction is through its impact on expansion in mortar bars or concrete prisms [15].

In the present study, three aggregates from different locations in Switzerland, Uri, Brienz and Praz (U, B and P), were assessed by expansion tests of concrete samples at 38°C. In parallel, the dissolution of various minerals within these aggregates was studied at high pH and at the same temperature as the expansion tests. Dissolution studies were done to measure the released ions from each aggregate at high pH. In addition, a scratch-tracking technique was used to determine chemical composition of minerals, which dissolved at high pH.

2.2 Materials and Methods

2.2.1 Aggregate characterization

0.5 kg of each aggregate was taken from a well–mixed batch (size fraction of 0 to 4 mm), and was ground for X–ray fluorescence (XRF) analysis, using fused beads according to EN 196–2. Total carbon content was determined by combustion analysis according to ISO 10694 and used to calculate the CO_2 content. For X-ray Powder Diffraction (XRD), a representative portion of each aggregate, from a well–mixed batch, was crushed and sieved between 0.315 and 0.630 mm, then washed with water to remove any fine particles, and dried at 100 °C for 1 day. Samples of 20 g were taken randomly and ground to obtain fine powder for XRD analysis. A PANalytical X'Pert Pro MPD diffractometer with $CuK\alpha_{1,2}$ radiation was used to record the patterns. All the diffractograms were recorded between 5° to 70° 2θ over 30 min with a step size of 0.017°. After recording the patterns, Rietveld analyses were done to quantify the crystalline composition of the samples.

Thin–section petrographical investigations were made on all the aggregates using optical microscopy with crossed polarizers and inserted gypsum plate (CP-OM) to study texture and mineralogy of the aggregates. The CP-OM images of the thin cross-sections of concrete samples (with U, B and P aggregates) were recorded from the most representative microstructure (observed in more than 80 % of the pieces).

2.2.2 Expansion test

Concrete prisms with standard size of 40 × 40 × 160 mm^3 were produced with U, B and P aggregates. An aggregate mass of 1790 kg/m^3 was used in the mix, with the following grain size distribution: 0 – 4 mm (40 wt. %), 4 – 8 mm (25 wt. %) and 8 – 11 mm (35 wt. %). All specimens were cast using 440 kg/m^3 of Portland cement (CEM I/42.5 N, Na$_2$O-equivalent of 0.79%) and with water to cement mass ratio of 0.5. The specimens were kept at 100% relative humidity for 24 h before unmolding. Our laboratory-based ASR acceleration protocol was an adaptation from the SIA MB 2042 standard [16,17], which included immersion of the concrete prisms in an alkaline solution (a mix of 0.3 M KOH and 0.1 M NaOH to simulate the alkalinity of the pore solution within concrete based on Chapter 4) to prevent alkali leaching. The volume of concrete to immersion solution ratio was appropriately 0.25 (with no unit, m^3/m^3). The specimens were stored at 38 °C and the length changes of at least 10 specimens for each type of aggregate were regularly measured up to 250 days (9 months). Scanning electron microscopy (SEM) imaging (Thermo Scientific™ Quanta™ 650, pressure between 3.0 and 5.0 × 10^{-6} Torr) and energy dispersive X–ray (EDX) point analysis (Thermo Noran Ultra Dry 60 mm^2 detector and Pathfinder X-Ray Microanalysis Software) were used to track formation of the ASR products and study their chemical composition for all aggregate types at 56 and 250 days.

2.2.3 Identification and dissolution rate of reactive minerals

In order to identify which minerals dissolved in the aggregates, all three aggregates (U, B and P) were studied in two series of experiments a) topography analysis and b) dissolution in solution.

2.2.3.1 Topography analysis

It is possible to directly observe dissolution of polished surfaces by SEM and EDX (to identify the chemical composition of the dissolved minerals). Therefore, randomly selected pieces of aggregates (with size fraction 10-20 mm) were impregnated in epoxy, and kept in the room temperature. After hardening, the samples were polished down to ¼ μm (with diamond sprays). The polished samples were cleaned several times by isopropanol and then deionized (DI)-water ultrasonically to

remove any fine particles and impurities. Then, the samples were coated with carbon. The silica-containing areas (such as quartz, Na–feldspar, K–feldspar and muscovite) and calcite areas were found by EDX analysis. SEM secondary electron images from these areas of interest (at least five areas for each mineral) were recorded as reference images before doing dissolution experiments. After collecting the reference images, the carbon coating was removed by gently polishing for some minutes with a soft polishing disc and petroleum lubricant. The samples were cleaned ultrasonically with DI-water and isopropanol three times each, and dried in the oven at 50°C for 1 day. The samples were recoated and observed in the SEM to check whether the carbon-removing procedure produced any visible changes. The coating was then removed again and the samples were immersed in 0.4 M KOH solution at 38 °C for 21 and 60 days. After each period of dissolution, the samples were washed gently with isopropanol, dried, coated with carbon and re–examined in the SEM. After each SEM and EDX investigations, the carbon coating was removed as explained previously and was put back in the fresh 0.4M KOH solution. Ultra-pure water was used for the preparations of all solution. The SEM images from the surface of the specimens after 21 and 60 days were aligned with respect to the first image of the same region using a rigid body registration (alignment) algorithm. Registration was conducted using a Python interface of SimpleElastix image registration library provided by Insight Segmentation and Registration Toolkit (ITK), based on a mutual information similarity metric [18]. To quantitatively compare the dissolution degree at different times (21 and 60 days), a threshold was applied to the aligned grey level SEM images to segment the scratches. The changes in the width size distribution (nm) and area fraction (%) were computed for segmented scratches.

2.2.3.2 Dissolution in solution

The homogeneity of the five subsamples of P aggregate (fine powder, obtained by grinding of 20 g of crushed aggregate with size fraction 0.315 – 0.630 mm) was checked by XRF and XRD analyses. The 5 subsamples showed very low deviation, confirming the homogeneity for dissolution experiments (Supplementary Information, Table 2-2). To study the type and amount of the dissolved ions from each aggregate at high pH, 20 g was put in either 120 ml of 0.4 M KOH or 0.4 M NaOH solution (to be able to measure both released Na and K) and stored at 38 °C. After different reaction times, an aliquot of the solution (5 ml) was sampled, and filtered with 0.2 μm nylon micro filter. 1 ml of the solution was diluted by a factor of 10 using ultra–pure water to avoid any precipitation (without acidification), and measured by Inductively Coupled Plasma Optical Emission Spectrometry (ICP–OES (Shimadzu ICPE–9000)) and Ion Chromatography (IC (Thermo Scientific Intergrion HPIC)). The amount of released component (wt. %) from each aggregate in 0.4M KOH and 0.4M NaOH was calculated by Equation 2-1:

$$\text{Released component (wt.\%)} = (\frac{C_t \times V_{sol}}{W}) * 100$$

Equation 2-1 Released component (wt.%)

where C_t is the concentration of released component (g/l) from U, B and P aggregates at any time, V_{sol} is the solution volume (l) and W is the mass of available crystalline amount of the component (g) existing in 20 g of each aggregate before dissolution (calculated based on XRD Rietveld results).

A pH meter (electrode BlueLine 14 pH (SI Analytics), pH meter (Lab 850)), calibrated against standard solutions, was used to record pH values at ambient temperature. At the end of the dissolution experiments, the solids were collected by filtration, washed with ultra–pure water and isopropanol to remove the remaining KOH or NaOH solution and dried at 38°C, and were analysed by XRD and thermogravimetric analysis (TGA) to check for any precipitation during the dissolution experiments.

2.3   Results

2.3.1 Aggregate characterization

The XRD and XRF results of U, B and P aggregates are summarised in Table 2-1. The XRF analysis indicates that silica is the dominant oxide in all studied aggregates; the B aggregate contains more aluminium than U and P aggregates. Based on the Rietveld analysis, U and P aggregates contain around 50 wt. % of quartz (SiO_2) and 26 wt. % and 16 wt. % of potassium and sodium feldspars ($KAlSi_3O_8$ or $NaAlSi_3O_8$), while B aggregates consist of about 25 wt. % quartz and 50 wt. % of feldspars.

Table 2-1 Chemical and mineralogical composition of the U, B and P aggregates.

Technique	Component	U	B	P
XRF (wt. %)	SiO_2	64.3	69.1	68.0
	Al_2O_3	8.8	14.3	7.2
	CaO	8.7	2.9	8.9
	K_2O	2.1	3.4	2.2
	MgO	2.1	1	1.9
	Fe_2O_3	2.0	2.3	1.4
	Na_2O	1.7	3.7	1.4
	SO_3	0.4	0.1	0.1
	LOI	9.5	3	9
XRD (wt. %)	**Quartz**: SiO_2 [ICSD 174]	51.4	25.1	56.3
	Feldspar: Albite: $NaAlSi_3O_8$ [ICSD 87657]	18.3	33.5	8.3
	Feldspar: Microcline: $KAlSi_3O_8$ [ICSD 83531]	7.3	11.7	8
	Feldspar: Orthoclase: $KAlSi_3O_8$ [ICSD 9543]	—	5.9	—
	Mica: Muscovite: $KAl_2(AlSi_3O_{10})(OH)_2$ [ICSD 75952]	8.8	10.8	7.5
	Calcite: $CaCO_3$ [ICSD 73446]	7	10.4	15.4
	Dolomite: $CaMg(CO_3)_2$ [ICSD 66333]	6.7	0.3	4.6
	Chlorite: Clinochlore $Mg_5Al(AlSi_3O_{10})(OH)_8$ [ICSD 66258]	0.9	2.4	—

Figure 2-1 shows illustrative CP–OM images of the thin cross-sections of the concretes produced out of U, B and P aggregates. The uniformly dark blue areas are the paste areas. Microstructures of P (Figure 2-1 (a and d)) and B aggregates (Figure 2-1 (b and e)) are quite similar and both of them

are granitic. A bimodal grain size distribution of coarse quartz grains with highly undulose extinction can be observed in both P and B aggregates. However, the quartz grains are more elongated in P aggregate and more isometric in B aggregate. The matrix between the quartz grains consists of a mixture of muscovite and microcrystalline quartz. The U aggregate is a sedimentary rock and shows a significantly different texture. Coarse and microcrystalline quartz grains both with little undulose extinction and isometric form are present. Mica flakes are uniformly distributed in the interstitial regions between quartz grain boundaries. Amorphous silica exists at the quartz grain boundaries (Figure 2-1 (c)), as reported in [19]. Calcite is detected by XRD and was also identified in the CP–OM images of all aggregates (Figure 2-1 (d, e and f)). For P and B aggregates (Figure 2-1 (d) and (e)), it was observed mainly as individual particles containing a mixture of quartz and calcite. However, in the case of U, calcite occurs mainly as detrital component in a size similar to the coarse quartz. Less frequent it is present as sparitic veins (Figure 2-1 (f)).
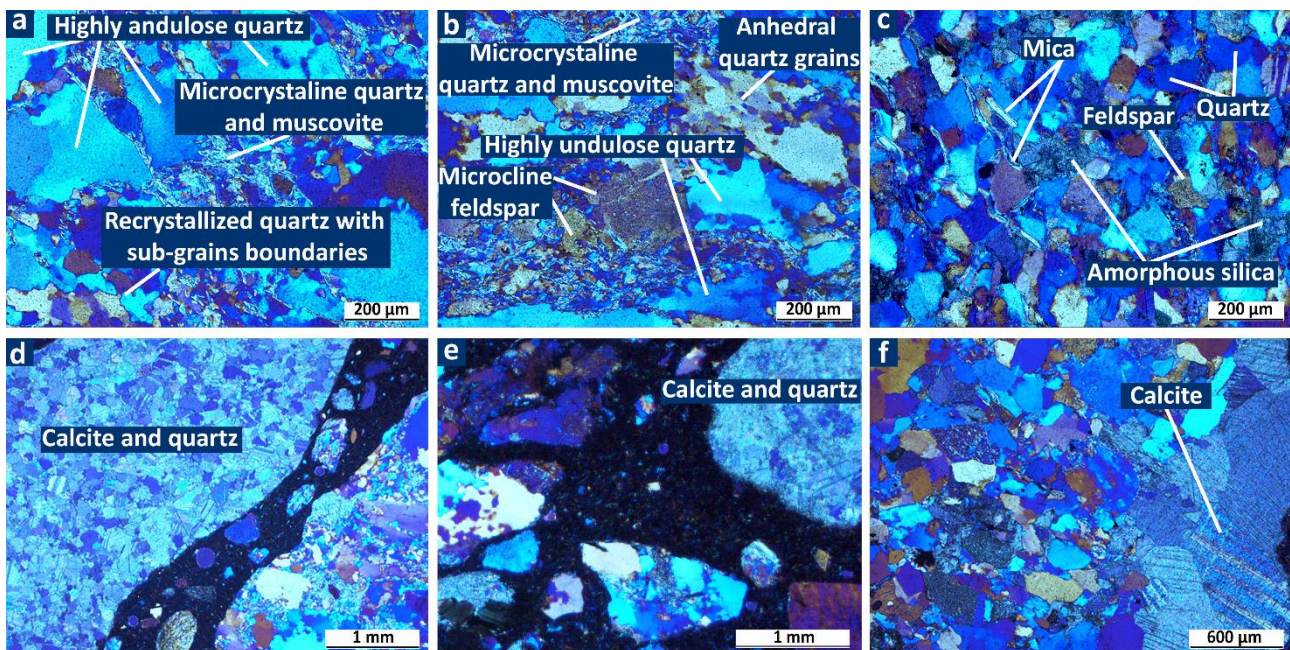
Figure 2-1 CP-OM images of P (a and d), B (b and e) and U (c and f) aggregates

2.3.2 Concrete Expansion

The relative length (Figure 2-2) and mass (Supplementary Information, Figure 2-10) changes of concrete prisms produced with three types of aggregates were measured as a function of time. The concrete sample with U aggregate showed the highest increase in length and mass. Since the samples were submerged in an alkaline solution (0.3 M KOH and 0.1 M NaOH), the expansion continuously increased over the course of 250 days. This behavior is in contrast with the conventional concrete performance laboratory–based tests [20,21] where reactions slow down after a certain time due to leaching of alkalis. In the case of concrete produced from U aggregates, the rate of expansion slowed down after 112 days. This is probably due to the extent of damage and crack filling, which is not investigated further here. SEM and EDX examinations of the cross-section of concrete samples (made of U, B and P aggregates) after 250 days confirmed the formation of ASR products, and the ASR-product compositions in all samples (Supplementary Information, Figure 2-11) were similar to values that were already reported [22].
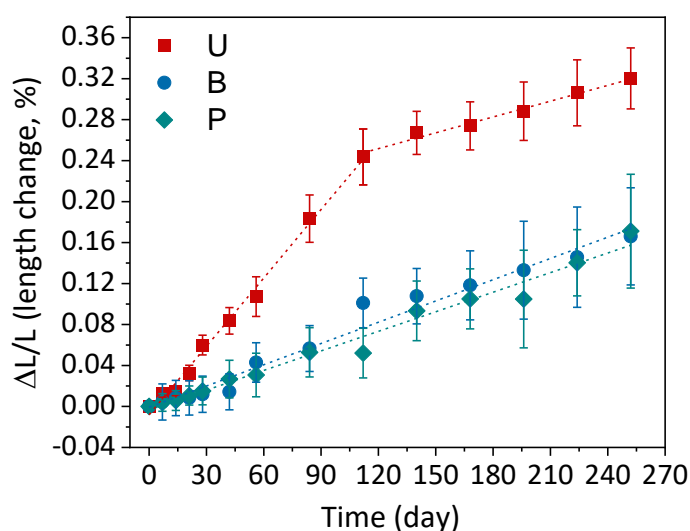
Figure 2-2 Relative length change (%) of different concrete samples produced with U, B and P aggregates as a function of time.

SEM images of the concretes were examined at 56 days and 250 days (Figure 2-3). At 56 days, the ASR products have formed at the grain boundaries of the different minerals (Figure 2-3 (a, b and c)).

This causes opening of cracks between the grains. After 250 days, several larger cracks opened in the aggregates, Figure 2-3 (d, e and f). The ASR gel exudes into the cement paste, where it takes up calcium [23].
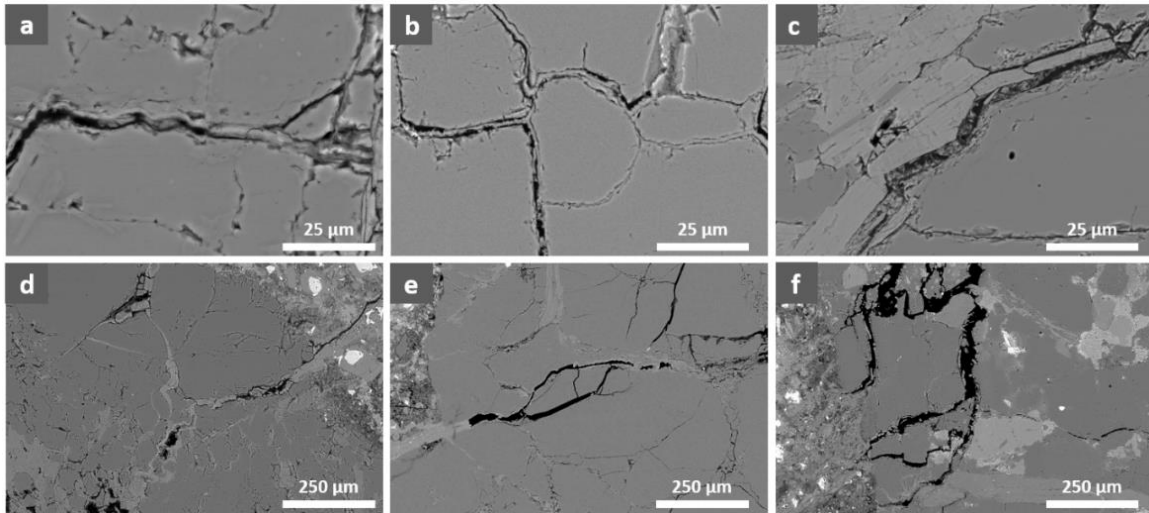
Figure 2-3 SEM backscattered images of the cross-section of concrete samples with (a) P (b) B (c) U aggregates after 56 days, and (d) P (e) B (f) U aggregates after 250 days.

2.3.3 Identification and dissolution rate of reactive minerals

2.3.3.1 Topography analysis

Figure 2-4 shows SEM secondary electron images of quartz, muscovite, K-feldspar and Na-feldspar areas of the P aggregate (a, d and g) before dissolution, (b, e and h) after 21 days and (c, f and i) after 60 days of immersion in 0.4M KOH at 38 °C.
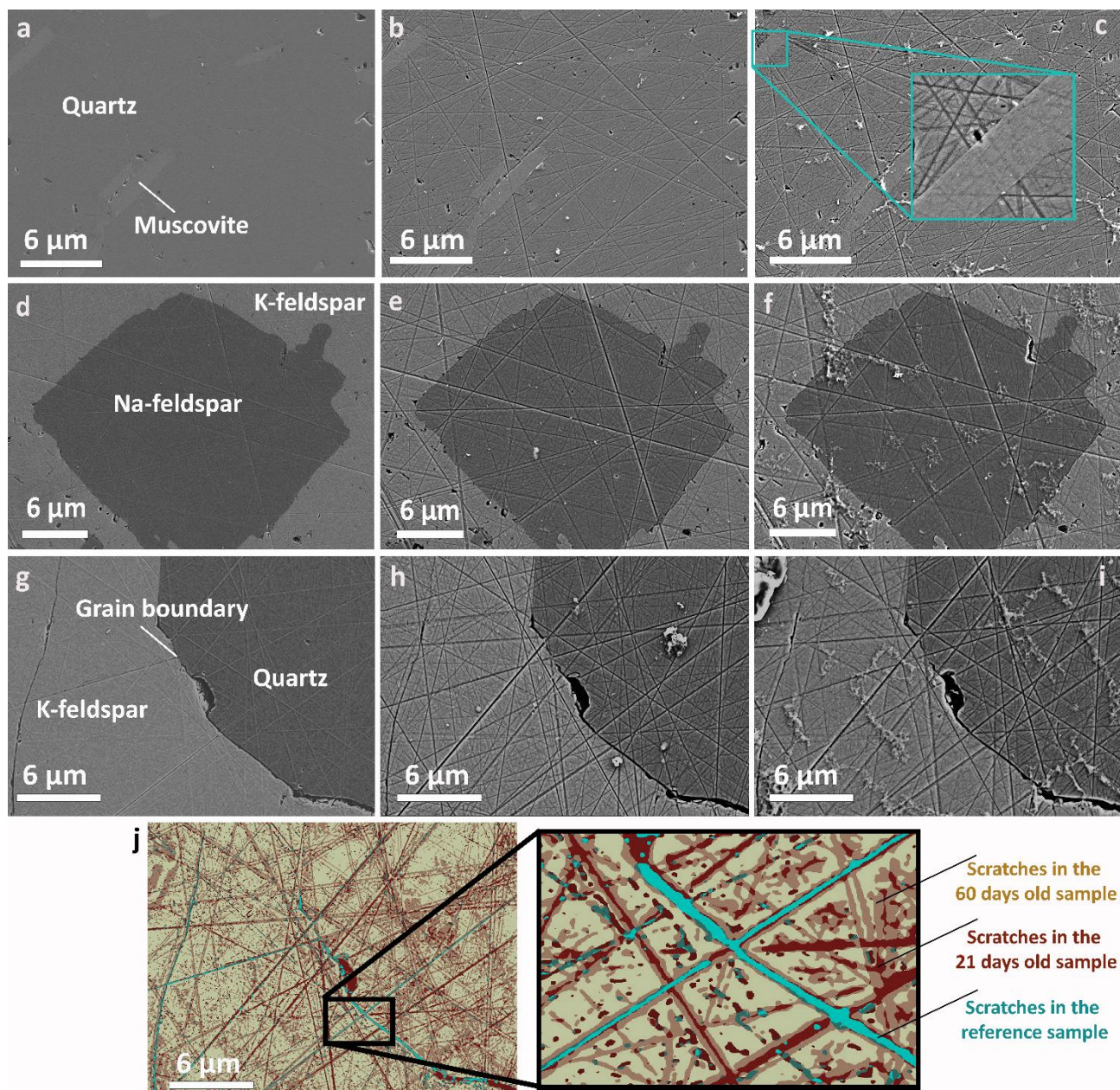
Figure 2-4 Aligned SEM secondary electron images of (a, b and c) quartz and muscovite, (d, e and f) K–feld-spar and Na–feldspar and (g, h and i) quartz and K–feldspar areas of P aggregate (a, d and g) before dissolution, (b, e and h) after 21 days and (c, f and i) 60 days of dissolution in 0.4 M KOH solution at 38 °C and j) overlapped image of segmented scratches in all the three SEM images (g–i) to quantify the width changes over time by dissolution increment.

In the SEM images before immersion, it is just possible to see some feint scratches from the polishing process (Figure 2-4 (a, d and g)). During immersion in the alkaline solution, the scratches in quartz, K–feldspar and Na–feldspar areas deepen and widen, and in addition, obvious dissolution occurs at the grain boundaries, while muscovite showed negligible changes after immersion in the

alkali solution for 21 and 60 days (Figure 2-4 (b and c), (e and f) and (h and i)). Additionally, there was severe dissolution of some calcite grains at the high pH as shown in Figure 2-5. The calcite dissolution may be attributed to the absence of Ca in the solution. In concrete, where calcium is present from portlandite, very little dissolution of calcite is expected.
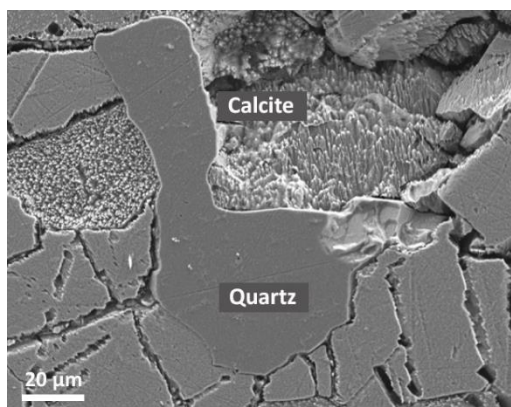
Figure 2-5 SEM secondary electron images of quartz (darker grey area) and calcite (lighter grey area) areas of P aggregate after 60 days immersion in 0.4M KOH solution at 38 ℃.

Figure 2-4 (c, f and i) shows some precipitation on the sample surface after 60 days of immersion, which can be either ASR products or C–S–H (due to reaction of released Si from quartz and feldspars dissolution and released Ca from calcite dissolution). It was not possible to determine the chemical composition by EDX analysis because of the small amounts.

Figure 2-4 (j) shows an example of alignment of SEM images (Figure 2-4 (g) to (i)) to quantify the dissolution extent based on the changes in the scratch width for quartz and K–feldspar areas of P aggregate. Figure 2-6 shows (a) scratch width size distribution (nm) for quartz areas and (b) scratch area fraction (%) for quartz, K–feldspar, Na–feldspar and muscovite areas before dissolution of P aggregate and after 21 and 60 days of immersion. In the width distribution histograms for the quartz areas (Figure 2-6 (a)), the peak of the fitted Gaussian distribution plot shifts to higher values after 21 and 60 days. Before immersion, the average scratch width was around 50 nm, after dissolution for 21 days and 60 days this increased to approximately 85 nm and 135 nm respectively. Figure 2-6 (b) indicates similar dissolution rates in quartz, K-feldspar and Na-feldspar areas, while the very slow

dissolution of muscovite is clear. The low reactivity of muscovite agrees with that reported by Lee-mann and Holzer [10]. However, they observed a higher reactivity of quartz compared to K-feldspar, this may be related to different feldspar polymorphs being present in the samples of this study.
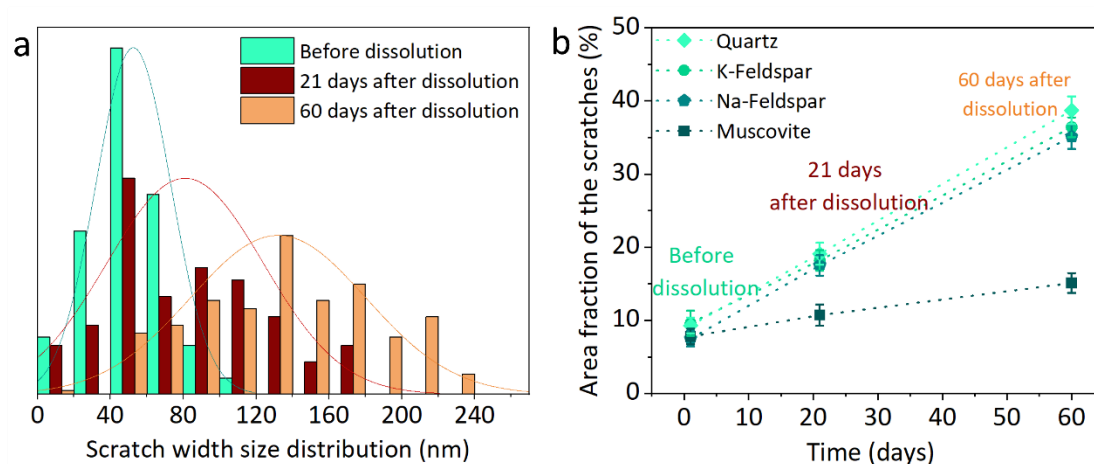
Figure 2-6 Quantification of scratch parameters obtained from the alignment of the SEM images of P aggregate; (a) scratch width size distribution (nm) for quartz area and (b) scratch area fraction (%) for quartz, K-eldspar, Na-feldspar and muscovite areas of P aggregate before dissolution, after 21 and 60 days of immersion in 0.4 M KOH solution at 38 °C.

Dissolution data for minerals at high pH values are scarce. Figure 2-7 shows dissolution rates of quartz, Na-feldspar (albite) and K-feldspar as a function of pH (9 < pH < 13) at 25 °C from previous studies. At pH 12.3 and 25 °C, comparable dissolution kinetics for quartz (5.4×10^{-11} mol/m^2/s) as for Na-feldspar (albite, 4.2×10^{-11} mol/m^2/s) were reported, while the one for K-feldspar at pH 12.7 and 25 °C (0.5×10^{-11} mol/m^2/s) was somewhat slower (Figure 2-7) [9,24–29]. Reported dissolution rates of muscovite at high pH are much lower ($\approx 10^{-12}$ mol/m^2/s) [30–32], in agreement with the observations made in this study.
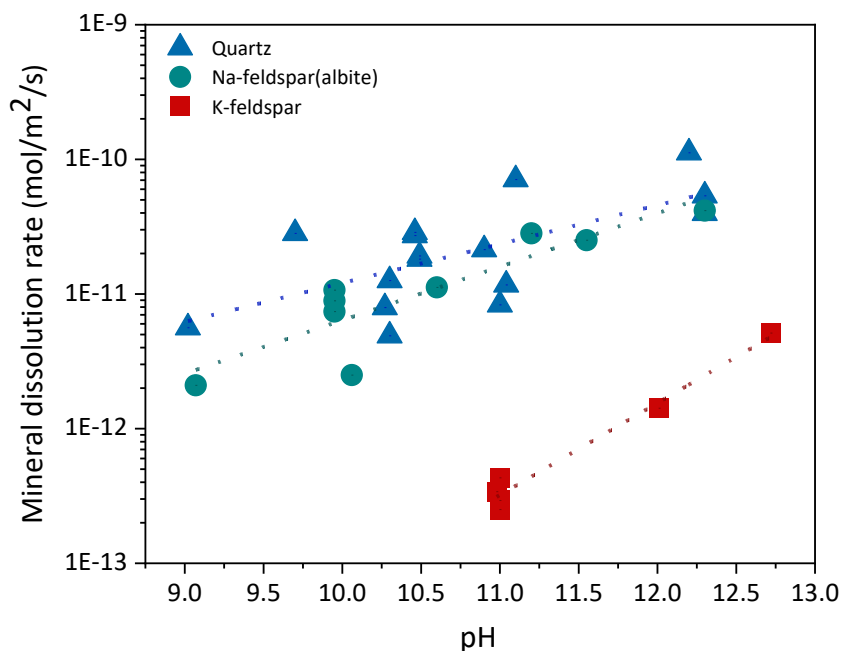
Figure 2-7 Dissolution rates of quartz, K–feldspar and Na–feldspar (albite) (mol/m^2/s) at high pH (9 < pH < 13) and at 25 °C [9,24–29].

In this topography study, the scratches from polishing process were preferential areas for mineral dissolution, but comparative results are in good agreement with previous studies.

2.3.3.2 Dissolution kinetics of aggregates

The ICP-OES results showed linear increases of Si concentrations with time for all aggregates immersed in 0.4M KOH and 0.4M NaOH (Supplementary Information, Table 2-3). The amount of SiO$_2$ dissolved for each measurement was calculated per g/l by Equation 2-1. Since the topography study indicated the preferential dissolution of quartz and feldspars (2.2.3.1), W in Equation 2-1 was considered as the total mass of SiO$_2$ from quartz and feldspars before dissolution of the 20 g sample, based on the XRD Rietveld analysis (Table 2-1). All three aggregates have approximately similar content of silica based on the XRF analysis and total amount of quartz and feldspars from XRD (Table 2-1).

Figure 2-8 indicates a linear increase of released SiO_2 (wt. %) for U, B and P aggregates. The U aggregate released the most silicon in both solutions with more in 0.4M KOH (0.48% after 63 days) than 0.4M NaOH (0.34% after 63 days) (Figure 2-8 and Supplementary Information, Table 2-3). Less silicon was released from B and P aggregates with KOH and NaOH leading to similar amounts of dissolution (0.2% after 63 days). The higher reactivity of U aggregate can be explained by the petrographic observation of amorphous silica at grain boundaries and the small-sized quartz grains in U aggregate (2.3.1) [33].
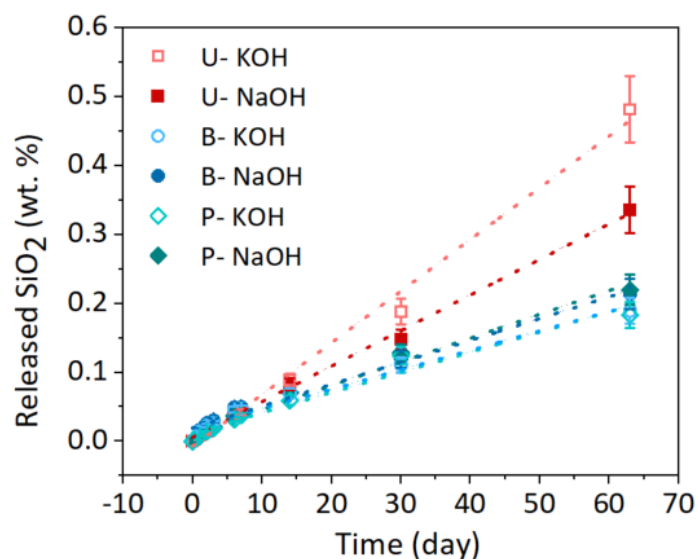
Figure 2-8 Released SiO_2 (wt. %) from U, B and P aggregates in 0.4M KOH and 0.4M NaOH solutions as a function of time at 38°C.

The calcium concentrations (Supplementary Information, Table 2-3) were always below the detection limit of ICP-OES. However, calcite dissolution is visible in the TGA data (for example see Supplementary Information, Figure 2-12, which showed a small decrease in the amount of $CaCO_3$ after doing dissolution experiment) and topography study (2.3.3.1). As high alkali concentration can damage the ICP-OES machine, solutions with high-dilution factor were used for ICP-OES measuring. This limits the measurement precision for minor elements such as Al and Ca, and could explain why the Ca concentrations were below the ICP–OES detection limit. The other reason can be formation of

new solids, which consumed the dissolved Ca as indicated by the formation of some products on the surface of samples in the topography study Figure 2-4 (c, f and i). It should be noted that, for aggregates with calcite, the measured Si released may be lowered by reaction with Ca from calcite dissolution.

In addition to silicon, Al and alkalis were released in both 0.4M KOH and 0.4M NaOH as summarised in Supplementary Information, Table 2-3. The concentration of Al increased initially, but then stabilised after 30 days, indicating either a decrease in feldspar dissolution with time and/or precipitation of Al containing solids (Supplementary Information, Table 2-3). The highest amount of dissolved Al was observed for the B aggregate, which also contains the highest amount of Al and feldspar as indicated by XRF and XRD/Rietveld analysis (Table 2-1). A slight increase with time was observed for the measured K or Na concentrations as both the NaOH and KOH solutions used already contained traces of K or Na. However, the small increase of K in the case of NaOH solutions, confirmed the dissolution of K-feldspar in agreement with the results from the topography study (2.3.3.1), in particular for the B aggregate with the highest feldspar content. The pH values did not change significantly during the experiments (Supplementary Information, Table 2-3).

2.3.4 Comparison of aggregate dissolution and concrete expansion

The rates of expansion for concrete samples with different aggregates (U, B and P) (%/day) were obtained from the slope of the curves shown in Figure 2-2. As the expansion rate of concrete made with U aggregate slightly changed over time (Figure 2-2), the initial expansion rate was considered. The rates measured in 0.4 M KOH were used, as potassium is the major source of alkali (almost 75%) in the pore solution. Figure 2-9 shows the rates of expansion versus the rates of SiO_2 release.
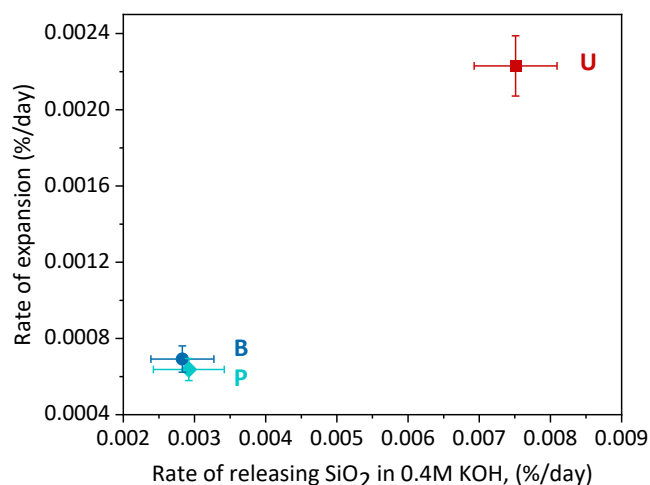
Figure 2-9 Rates of expansion of the concrete samples with U, B and P aggregates (%/day) versus rates of releasing SiO$_2$ from U, B and P aggregates (%/day) in 0.4 M KOH at 38 °C.

The concrete sample with U aggregate had the highest rate of expansion (%/day) and the highest rate of release of SiO$_2$ (%/day) in 0.4 M KOH. The concrete samples with B and P aggregates showed almost the same rates of expansion (%/day) and rates of SiO$_2$ release (%/day) (Figure 2-9). As there are essentially only 2 data points in Figure 2-9, it would be necessary to study many more aggregates to confirm such a possible general correlation. However, aggregate dissolution in concrete occurs (mainly at the grain boundaries and areas of amorphous or poorly crystalline material) in contact with a limited amount of pore solution, while dissolution experiments are done by immersion of the aggregates in an abundant amount of solution. The particle size distribution of aggregates in concrete is wide, which introduces different surface areas of silica-containing and dissolvable minerals contributing to ASR, while for dissolution experiments a narrow size fraction of aggregates was used. The composition of pore solution in concrete is complex depending on the used paste and aggregates, while simplified solution (0.4M KOH) was used for dissolution experiments. Some of the critical reactions, such as complex interaction of ASR-gel formation, play a key role in the extent of expansion, and are not considered in dissolution experiments. All of these factors mean that the study of dissolution kinetics only gives an indication of ASR–reactivity of aggregates, and is unlikely to directly relate to the extent of expansion across a range of aggregates.

2.4   Conclusions

In the present study, expansion tests confirmed the ASR susceptibility of three aggregates from Switzerland (U, B and P aggregates). The concrete with U aggregate showed the highest rate of expansion. Two series of experiments a) topography analysis and b) investigation of solution composition were done to identify the chemical composition and dissolution kinetics of the reactive minerals within the three aggregates. The results identified quartz, K-feldspar and Na-feldspar as dissolvable minerals, while the reaction of muscovite was negligible. The scratch-tracking technique is a useful way to monitor reactivity of minerals within aggregate. It was observed that the type of alkali (NaOH or KOH) only slightly affected the dissolution of the aggregates at 38 °C.

The U aggregate showed the highest rate of release of SiO_2 in the dissolution experiments, corresponding to the highest rate of expansion in concrete. These results underline the importance of aggregate dissolution as the first step in expansion due to ASR. However, a direct correlation is not possible given the limited data available from this study. A simple direct correlation across a broad range of aggregates is unlikely due to the complex combination of dissolution, ASR product formation and crack formation involved in damage due to ASR.

Acknowledgements:

Suplementary Information

Table 2-2 (a) XRF and (b) XRD analyses of five crushed subsamples (from a portion of 20 g, 0.315–0.630 mm) of the P aggregate.

Technique	Component	P 1	P 2	P 3	P 4	P5	Standard deviation	Average	Range
XRF (wt. %)	SiO_2	67.6	67.2	66.8	67.6	67.6	0.36	67.4	66.8-67.6
	CaO	12.2	12.4	12.6	12.7	12.1	0.25	12.4	12.1-12.7
	Al_2O_3	4.4	4.4	4.6	4.6	4.5	0.10	4.5	4.4-4.6
	K_2O	1.8	1.8	1.9	1.8	1.8	0.04	1.8	1.8-1.9
	MgO	1.5	1.5	1.5	1.5	1.5	0.00	1.5	1.5
	Fe_2O_3	0.8	0.8	0.8	0.8	0.8	0.00	0.8	0.8
	Na_2O	0.6	0.6	0.6	0.7	0.6	0.04	0.6	0.6-0.7
XRD (wt. %)	**Quartz**: SiO_2 [ICSD 174]	53.1	51.8	55	54.2	52.4	1.30	53.3	51.8-55
	Feldspar: Albite: $NaAlSi_3O_8$ [ICSD 87657]	8.6	7.7	7.7	7.2	8.2	0.54	7.9	7.2-8.6
	Feldspar: Microcline: $KAlSi_3O_8$ [ICSD 83531]	7.4	6.3	6.3	5.6	8	0.96	6.7	5.6-8
	Calcite: $CaCO_3$ [ICSD 73446]	18.6	19.5	18.7	19.2	19	0.37	19.0	18.6-19.5
	Dolomite: $CaMg(CO_3)_2$ [ICSD 66333]	4.8	6.8	5.1	5.5	5.1	0.79	5.5	4.8-6.8
	Mica: Muscovite: $KAl_2(AlSi_3O_{10})(OH)_2$ [ICSD 75952]	7.6	8	7.1	8.3	7.3	0.49	7.7	7.1-8.3

Table 2-3 Amount of dissolved ions from different aggregates in (a) 0.4 M KOH and (b) 0.4 M NaOH at 38°C, saturation index values by GEMS and pH values by different methods.

(a) Aggregate	Time (day)	Al (mmol/L)	Ca (mmol/L)	K[2] (mmol/L)	Na (mmol/L)	Si (mmol/L)	Sulfate (mmol/L)	Saturation index of C-S-H	Saturation index of SiO$_2$	pH [3]	pH [4] (GEMS)
U	0	< LOQ [1]	< LOQ	276	3.97	< LOQ	< LOQ	-1.4	-7.4	13.5	12.9
	1	< LOQ	< LOQ	266	3.65	0.173	0.090	-1.0	-5.4	13.5	12.9
	2	< LOQ	< LOQ	269	3.61	0.284	0.095	-1.0	-5.2	13.5	12.9
	3	< LOQ	< LOQ	276	3.98	0.442	0.113	-0.9	-5.0	13.5	12.9
	6	< LOQ	< LOQ	289	4.11	0.787	8.833	-0.9	-4.7	13.5	12.9
	7	< LOQ	< LOQ	309	4.39	0.958	0.158	-0.8	-4.7	13.4	12.9
	14	0.196	0.048	327	3.04	2.136	0.287	-0.3	-4.3	13.5	13.0
	30	0.393	< LOQ	338	4.39	4.771	0.636	-0.7	-4.0	13.5	13.0
	63	0.272	< LOQ	394	5.44	12.926	3.779	-0.6	-3.5	13.4	13.0
B	0	< LOQ	< LOQ	276	3.97	< LOQ	< LOQ	-1.4	-7.4	13.5	12.9
	1	0.247	< LOQ	279	3.78	0.237	0.112	-1.0	-5.3	13.5	12.9
	2	0.332	< LOQ	297	4.04	0.392	0.114	-0.9	-5.1	13.5	12.9
	3	0.471	< LOQ	276	3.75	0.477	0.092	-0.9	-5.0	13.4	12.9
	6	0.519	0.129	338	4.65	0.876	1.199	-0.2	-4.7	13.4	13.0
	7	0.526	0.131	320	4.65	0.933	0.145	-0.2	-4.7	13.4	13.0
	14	0.650	0.058	322	3.11	1.453	0.098	-0.4	-4.5	13.5	13.0
	30	0.967	< LOQ	338	4.39	2.439	0.195	-0.7	-4.3	13.5	13.0
	63	1.056	< LOQ	389	5.44	4.415	1.291	-0.7	-4.0	13.5	13.0
P	0	< LOQ	< LOQ	276	3.97	< LOQ	< LOQ	-1.4	-7.4	13.5	12.9
	1	< LOQ	< LOQ	271	3.70	0.148	0.101	-1.1	-5.5	13.5	12.9
	2	< LOQ	< LOQ	286	3.95	0.271	0.111	-1.0	-5.2	13.4	12.9
	3	< LOQ	< LOQ	269	3.80	0.388	0.106	-1.0	-5.1	13.4	12.9
	6	< LOQ	< LOQ	294	4.19	0.677	0.151	-0.9	-4.8	13.4	12.9
	7	< LOQ	< LOQ	332	4.52	0.840	0.148	-0.8	-4.7	13.4	13.0
	14	0.053	0.052	284	2.70	1.390	0.089	-0.4	-4.5	13.4	12.9
	30	0.203	< LOQ	345	4.19	3.080	0.231	-0.7	-4.2	13.5	13.0
	63	< LOQ	< LOQ	353	4.57	4.807	1.405	-0.7	-4.0	13.5	13.0

(b)	Aggregate	Time (day)	Al (mmol/L)	Ca (mmol/L)	K (mmol/L)	Na [2] (mmol/L)	Si (mmol/L)	Sulfate (mmol/L)	Saturation index of C-S-H	Saturation index of SiO$_2$	pH [3]	pH [4] (GEMS)
		0	< LOQ[1]	< LOQ	0.30	326	< LOQ	< LOQ	-1.3	-7.1	13.1	12.9
		1	< LOQ	< LOQ	0.44	340	0.227	0.092	-0.9	-5.1	13.1	13.0
		2	< LOQ	< LOQ	0.53	345	0.377	0.102	-0.8	-4.9	13.1	13.0
		3	< LOQ	< LOQ	0.52	327	0.499	0.101	-0.8	-4.8	13.1	12.9
	U	6	0.211	< LOQ	0.58	334	0.858	0.124	-0.8	-4.5	13.1	12.9
		7	0.225	< LOQ	0.59	355	0.983	0.162	-0.7	-4.5	13.1	13.0
		14	0.284	0.047	0.72	352	1.994	0.187	-0.3	-4.2	13.1	13.0
		30	0.486	< LOQ	0.65	362	3.739	0.445	-0.6	-4.0	13.1	13.0
		63	0.448	< LOQ	0.95	428	9.009	2.634	-0.1	-3.7	13.1	13.0
		0	< LOQ	< LOQ	0.30	326	< LOQ	< LOQ	-1.3	-7.1	13.1	12.9
		1	0.263	< LOQ	0.34	336	0.275	0.100	-0.9	-5.0	13.1	13.0
		2	0.361	< LOQ	0.47	340	0.445	0.103	-0.8	-4.8	13.1	13.0
		3	0.404	< LOQ	0.54	327	0.548	0.107	-0.8	-4.7	13.1	12.9
	B	6	0.615	< LOQ	0.70	386	0.922	0.130	-0.7	-4.6	13.1	13.0
		7	0.641	< LOQ	0.78	389	0.976	0.126	-0.7	-4.6	13.1	13.0
		14	0.788	0.053	0.92	376	1.462	0.078	-0.3	-4.4	13.1	13.0
		30	1.245	< LOQ	0.92	414	2.628	0.198	-0.5	-4.2	13.1	13.0
		63	1.490	< LOQ	1.21	444	4.985	1.457	-0.4	-4.0	13.1	13.0
		0	< LOQ	< LOQ	0.30	326	< LOQ	< LOQ	-1.3	-7.1	13.1	12.9
		1	0.201	< LOQ	2.05	323	0.132	0.086	-0.9	-5.3	13.1	12.9
		2	< LOQ	< LOQ	0.42	329	0.280	0.105	-0.9	-5.0	13.1	12.9
		3	< LOQ	< LOQ	0.54	335	0.438	0.117	-0.8	-4.8	13.1	13.0
	P	6	< LOQ	< LOQ	0.64	358	0.787	0.133	-0.8	-4.6	13.1	13.0
		7	< LOQ	< LOQ	0.89	398	0.947	0.126	-0.7	-4.6	13.1	13.0
		14	0.090	0.059	0.91	385	1.661	0.095	-0.3	-4.4	13.1	13.0
		30	0.264	< LOQ	0.91	406	3.183	0.232	-0.6	-4.1	13.2	13.0
		63	0.154	< LOQ	1.20	386	5.768	1.686	-0.6	-3.8	13.1	12.8

1) LOQ = Limit of Quantification.
2) The ICP-OES results are underestimated due to presence of strong alkali content.
3) The pH values were measured at room temperature ~ 23°C.
4) The pH values by GEMS are at 38°C, and pH of 0.4M KOH equals to 13.5 at 23°C and to 13.0 at 38°C.
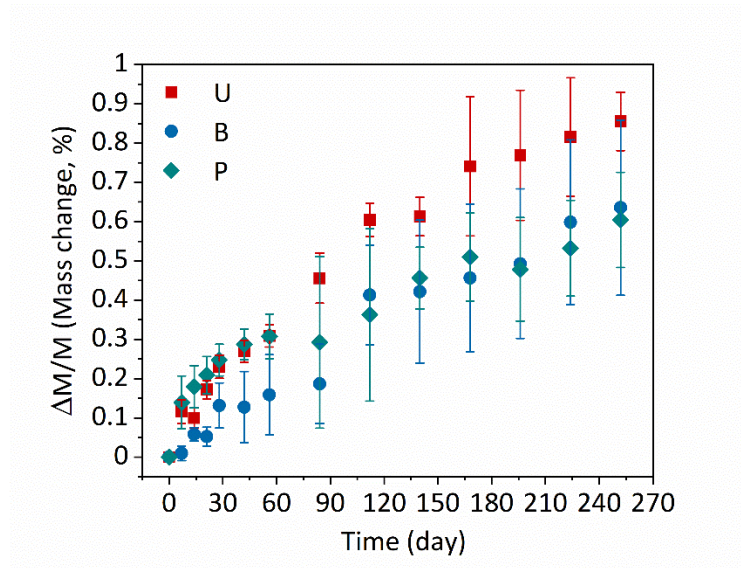
Figure 2-10 Mass change (%) of concrete samples with U, b and P aggregates as a function of time.
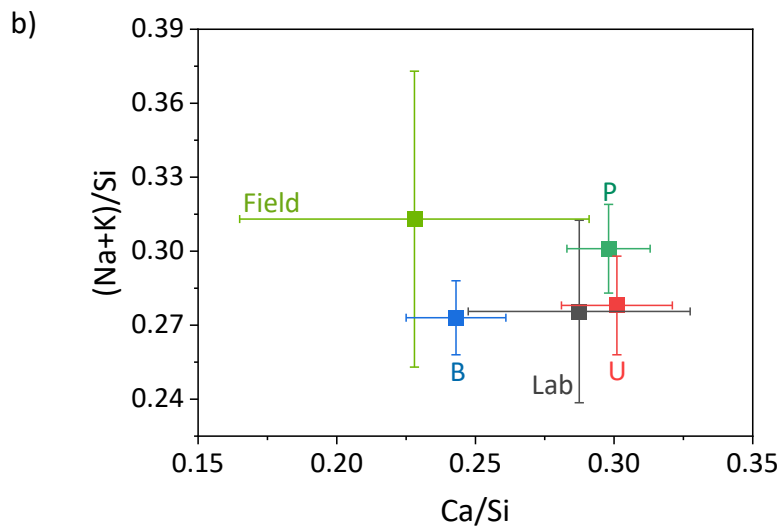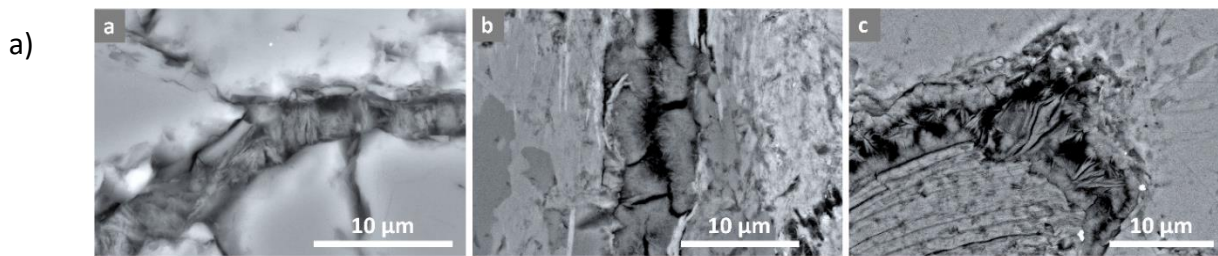
Figure 2-11 (a) SEM backscattered images of ASR products in concrete samples made of (a) P, (b) B and (c) U aggregates after 250 days and (b) EDX analysis of the samples from the present study (labaled U, B and P) after 250 days, and the reported values (labaled Field and Lab) [22].
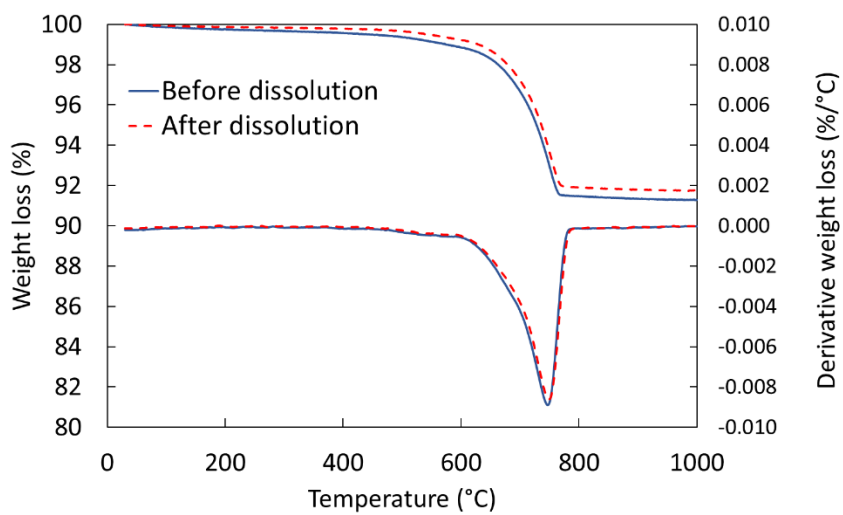
Figure 2-12 Thermogravimetric analysis of U aggregate (solid line) and of the collected solids at the end of dissolution experiments (dash line) in 0.4M NaOH at 38 °C.

Chapter 3　　Effect of different ions on dissolution rates of silica and feldspars at high pH

Mahsa Bagheri, Barbara Lothenbach, Mahdieh Shakoorioskooie, Karen Scrivner

Abstract

The dissolution kinetics of reactive silica minerals influences strongly the time when damage due to alkali silica reaction may occur in concrete aggregates. The effect of the presence of different ions on the dissolution rates of SiO_2 and feldspars at high pH values was studied directly by measuring the dissolution at scratched surfaces and indirectly by following the increase of silicon concentrations in dissolution experiments. The interpretation of the dissolution rate based on silicon concentrations was hampered by the formation of C-S-H and lithium silicates, while quantification of scratched surfaces allowed a direct observation of the dissolution kinetics. High pH values, lithium, calcium and sulfate increased the dissolution rates of silica and feldspars, while iron, magnesium and the presence of additional NaCl, KCl or CsCl showed no significant effect. In contrast, aluminium slowed down the dissolution rates of quartz, amorphous silica and Na and K-feldspar at 20, 40 and 60 °C.

Keywords: Dissolution kinetics, silica, feldspar, high pH, temperature.

3.1   Introduction

Building materials play a key role in modern infrastructures and housing for society. Cement based materials are in high demand because of their high performance, availability of raw materials, low cost and relatively low environmental footprint per unit mass produced [1]. The durability of concrete structures can be affected by the so-called alkali silica reaction (ASR), which can cause expansion and deterioration of the concrete in the long term. With susceptible aggregates, the high pH of the pore solution of concrete can lead to the dissolution of silica within the aggregate and to the formation of an expansive gel [4]. The formation of ASR products and thus the rate at which cracking occurs depends strongly on the dissolution rate of the reactive phases inside the aggregates [7]. The dissolution kinetics of reactive aggregates in concrete depends on different factors including i) the composition of the pore solution, which depends on cement and aggregate composition [10,34], ii) surface area, crystallinity and presence of crystal defects in the reactive aggregates [7], iii) moisture [35] and iv) temperature [34,36,37].

The composition of the pore solution can be influenced by the type of cement and by the kind and amount of supplementary cementitious materials (SCMs) [38]. Not only the alkali concentrations and pH affect the dissolution kinetics of reactive aggregates but also the concentration of other ions such as aluminium in the pore solution. An improved understanding of the role of different ions is thus fundamental to develop efficient mitigation strategies to control ASR in concrete.

The dissolution rates of silica, quartz, feldspars and silica–rich aggregates increase with temperature and with the pH value [9,36,39]. The type of alkalis has been reported to affect the dissolution of siliceous minerals [39–41].

Cements with aluminium-rich SCMs such as fly ash or metakaolin have been observed to prevent expansion due to ASR [4,42,43]. Aluminium decreases the rate of silica and quartz dissolution [2,44–46], and also the dissolution of aggregates [2,4]. This has been related to the tendency of aluminium to adsorb on silica surfaces, where it passivates the active silica sites and slows down further dissolution [44,47,48]. This effect is less distinct at high pH values

(≥13), as high pH values lower the tendency of aluminium to sorb on silica surface sites [2,4,44,47].

Some studies based on measurements of mass loss [49,50] or silicon concentrations [51] have suggested that calcium in solution decreases the dissolution of silica due to formation of C-S-H on the silica surface. However, the study of weight losses and dissolved concentrations in the presence of precipitates makes the interpretation of such results challenging. Other studies at near neutral pH, where no C-S-H can form, have suggested an increase of quartz dissolution in the presence of calcium [40].

The lithium can prevent expansion due to ASR as shown by McCoy and Caldwell [52] in 1951 and confirmed in several studies [53–55]. The presence of lithium lowers the CaO/SiO_2 as well as the $(Na+K)/Si$ ratio in the ASR products [54,55]. The amount and the availability of other alkalis $(Na+K)$ and the type of aggregate determine the amount of lithium required to control the expansion due to ASR [8,52–54,56]. It has been suggested that, Li^+, due to its smaller ionic radius and higher charge density, is more readily incorporated in ASR products than K^+ and Na^+ and that lithium-based ASR products are non-expansive [54,55]. Some studies suggested that lithium reduces silica dissolution [6,57,58], while others [39,40,59,60] observed no significant influence of Li measuring silicon in dissolution tests. It should be noted that lithium can precipitate as Li_2SiO_3 [50], which again can make the interpretation of results based on silicon concentration or weight loss difficult, similar to the case of C-S-H formation with calcium discussed above. In addition, in the present research the effect of sulfate on ASR expansion is studied, as high temperatures often used during ASR tests increase sulfate concentrations in solution significantly [61,62], which could affect the dissolution kinetics.

Most studies of dissolution kinetics of minerals have been carried out under acid to neutral pH conditions, while studies under high pH conditions are rare, such that we lack a fundamental understanding of different factors affecting dissolution kinetics and their interplay. As a result, numerous questions are still open and there is high degree of uncertainty in mitigation of ASR and prediction of expansion due to ASR.

The present study investigates the effect of solution composition on dissolution kinetics of silica (amorphous silica and quartz) and feldspars (K-feldspar and Na-feldspar) at high pH values by studying i) directly the dissolution of scratched surfaces, ii) indirectly by following the increase of silicon concentrations during dissolution experiments and iii) by observing weight changes.

3.2   Materials and methods

3.2.1 Mineral samples

The materials used were:

- amorphous silica: two powders (100 - 250 µm), coarse (100 - 360 µm), labelled (AmS-1 and AmS-2).

- quartz: two powders (100 - 250 µm), coarse (100 - 360 µm), labelled (Q-1 and Q-2).

- amorphous silica plates (diameter 25mm and thickness 2mm) with > 99.9 % purity from Lanno Quartz (Xinpu, China), labelled (AmS-Pl).

- albite (Na-feldspar): from Rantzauer Töpferbedarf (Barmstedt, Germany), labelled Alb-1,

- natural rocks containing mostly:

    o   microcline (K-feldspar): labelled MicrocR, orthoclase (K-feldspar) labelled OrthoR and

    o   albite (Na-feldspar), labelled AlbR.

Powder samples (labelled Microc and Alb-2) were prepared from the rocks (MicrocR and AlbR), with size fraction < 100 µm by crushing and sieving. In order to remove very fine particles, the powder samples were cleaned ultrasonically with deionized water and isopropanol three times for few minutes, and dried at 40 °C before doing dissolution experiments.

X–ray fluorescence (XRF) and X-ray Powder Diffraction (XRD) were used to determine chemical composition and crystalline structure of the materials used. The XRD patterns (between 5° to 70° in 2Θ during 30 min with a step size of 0.017°) were recorded using a PANalytical X'Pert Pro MPD diffractometer with CuK$\alpha_{1,2}$ radiation. Quantification of the crystalline and amorphous fractions was done using Rietveld analyses. Alb-1 contained 88% and AlbR/Alb-2 82% of albite. OrthoR and MicrocR/Microc samples contain almost 50% of orthoclase and microcline respectively; the non-crystalline content is mostly likely also feldspars with low crystallinity as feldspars were observed to be dominant phases using SEM/EDX. The amorphous silica samples, AmS-1/2 and AmS-Pl, showed no XRD peaks confirming amorphous structure, and Q-1 and Q-2 showed quartz (~94 %) as detailed in Table 3-1 and in Supplementary Information, Figure 3-18.

Table 3-1 Phase analysis of the materials used for dissolution experiments

Technique	Component	Alb-1[1]	AlbR/Alb-2[2]	OrthoR[3]	MicrocR/Microc[4]	AmS-1[5]	AmS-2[6]	Q-1[7]	Q-2[8]
XRF (wt. %)	SiO_2	69.6				-----			
	Al_2O_3	18.6				-----			
	Na_2O	10.4							
XRD (wt. %)	**Quartz**: SiO_2 [ICSD 174]	7.6		-----				93.9	
	Cristobalite: SiO_2 [ICSD 75300]			-----				0.2	
	Coesite: SiO_2 [ICSD 18112]			-----				2.8	
	Feldspar: Albite: $NaAlSi_3O_8$ [ICSD 37653]	88.2	82.0	-----	13.2				
	Feldspar: Microcline: $KAlSi_3O_8$ [ICSD 83531]		-----		48.8	-----			
	Feldspar: Orthoclase: $KAlSi_3O_8$ [ICSD 10270]		-----	52.4	8.2			-----	
	Feldspar: Sanidine: $K(AlSi_3O_8)$ [ICSD 10274]		-----	10.9	-----				
	Lawsonite: $CaAl_2Si_2O_7(OH)_2 \cdot H_2O$ [COD 9010839]	-----	17.0	-----					
	Amorphous/non-crystalline	4.2	1.1	36.8	30.1	100		3.1	
Specific S.A. (m^2/kg)[9]	------------	48.4 ± 12	41.6 ± 27	-----	50.7 ± 28	10.1 ± 3	5.3 ± 3	14.9 ± 1	16.8 ± 2

1) Albite from Rantzauer Töpferbedarf (Barmstedt, Germany)
2) Albite natural rock, from Navarro River, Mendocino Co, California
3) Orthoclase natural rock, from Breckenridge, Colorado, USA
4) Microcline natural rock (amazonite), from Brazil
5) Amorphous silica (100-250 µm)
6) Amorphous silica (100-360 µm)
7) Quartz (100-250 µm)
8) Quartz (100-360 µm)
9) The specific S.A. was measured on powder samples with size fraction < 100 µm for Alb-2 and Microc, used for dissolution experiments.

The specific surface area was determined using 2-dimentional (2D) cross-section SEM images (as detailed in supplementary Information, Figure 3-16 and Figure 3-17) and presented in Table 3-1.

3.2.2 Exposure solutions

Table 3-2 summarises the solutions and storage temperatures used for the dissolution experiments. Sodium chloride (99.99%, Merck), caesium chloride (ultrapure 99.9%, Company abcr), lithium chloride (99.9%, APOLLO SCIENTIFIC), lithium hydroxide (98%, ACROS), iron (III) chloride hexahydrate (98%, Merck), magnesium chloride (99.9%, ACROS), calcium chloride (≥98%, RDTH), aluminum chloride anhydrous powder (99%, Aesar), aluminium nitrate nonahydrate (≥ 98.5, Merck), potassium hydroxide (≥85%, Fisher Chemical) and sodium hydroxide (≥98%, RDTH) were used to prepare the solutions together with ultra-pure water.

Table 3-2 Summary of solutions and storage temperatures for dissolution experiments

	Solution			Storage temperature (°C)
Alkaline solution	Element	Concentration (mM)	Salt	
100 or 400mM KOH		-----		20, 40, 60
400mM NaOH				40
100mM KOH	Al	1, 3 0.1, 0.3, 0.5, 1, 3	$AlCl_3$ or $Al(NO_3)_3.9H_2O$	20, 40
	Ca	3	$CaCl_2$	40, 60
	Li	10, 40, 100, 400	LiCl or LiOH	
	Sulfate	200	K_2SO_4	40
400mM KOH	Sulfate + Al	50 + 3	K_2SO_4 and $AlCl_3$	
	Fe	3	$FeCl_3$	
	Mg	3	$MgCl_2$	40, 60
	Na	400	NaCl	
	K	400	KCl	40
	Cs	400	CsCl	40, 60

3.2.3 Dissolution measurements

The dissolution of a solid can be followed by measuring the evolution of the surface, by the amount of ions released to the surrounding solutions or by following its weight change.

3.2.3.1

3.2.3.2 Dissolution by scratch tracking

The increase in width of scratches at the surface during dissolution was determined using a "scratch-tracking" method based on changes observed in SEM images over time as described in detail in (Chapter 2). The impregnated samples (Q-1, MicrocR, OrthoR, AlbR) were polished down to ¼ µm (by polishing machine, hard disc and diamond sprays), carbon coated and analysed by SEM and SEM/EDX in at least four different areas to assess the chemical composition and the amount of scratches. SEM images were collected before and after dissolution in different solutions at 40 °C for 21 days; the carbon coating was removed before dissolution as detailed in Chapter 2. After dissolution, the samples were washed gently with ultra-pure water and isopropanol to remove any precipitate and dried at 40 °C for 1 day before reanalysis of the sample by SEM.

In order to quantify the effect of dissolution on widening of the polishing-scratches, SEM images taken after dissolution (21 days), were spatially aligned with their corresponding SEM images before dissolution, using a "rigid body registration" algorithm, implemented at SimpleElastix image registration library (provided by Insight Segmentation and Registration Toolkit (ITK), using Python interface (Chapter 2)). The scratches at both SEM images (before and after dissolution) were segmented by applying a threshold using Avizo software (by Thermo Fisher Scientific). The scratch surface area fraction ($SSAF_i(\%)$) for each segmented binary scratch image was computed by the same software (Avizo) based on the following equation:

$$SSAF_i(\%)) = \frac{surface\ area\ of\ the\ segmented\ binary\ scratches}{surface\ area\ of\ the\ SEM\ image}$$

Equation 3-1 The scratch surface area fraction

Where i indicates the time at which the SEM image was acquired. Finally, the absolute change of scratch surface area fraction ($\Delta SSAF(\%)$) due to the dissolution was calculated by:

$$\Delta SSAF(\%) = SSAF_a(\%) - SSAF_b(\%)$$

Equation 3-2 The absolute change of scratch surface area fraction

where $SSAF_b(\%)$ is the scratch surface area before exposure and $SSAF_a(\%)$ is the scratch surface area after exposure in alkaline solution.

For each dissolution condition, the $\Delta SSAF(\%)$ was computed at least on three SEM-image-sets and the average of all values along with corresponding standard deviations was reported.

3.2.3.3 Dissolution in diluted solutions

To follow the dissolution, the increase of Si concentration in solution over time was followed in solutions for the solids (AmS-1/2, Q-1/2, Alb-1/2, Microc). For each experiment, 500 ml of solution were placed in a polypropylene container (at 20 or 40 °C) or a teflon container (at 60 °C) with 0.5 g of powder, resulting in solution to solid ratio of 1000 ml/g. Potassium or sodium hydroxide solutions were used with additions of different chloride salts to bring other ions, as summarised in Table 3-2. At each sampling time, 3ml of the solution was collected and filtered (0.2 µm nylon filter). The concentration of Si released as a function of time was measured on subsamples diluted by factor 10 using Inductively Coupled Plasma Optical Emission Spectrometry (ICP-OES; Shimadzu ICPE-9000) or ion chromatography (IC; Dionex DP ICS-3000). The pH was measured on another aliquot of the solution with a BlueLine 14 pH electrode (SI Analytics) and a Lab 850 pH meter considering calibration curve of KOH solutions (0.1, 0.2, 0.5 and 1 M KOH) as detailed in [63] and Chapter 2, and were corrected to be at the experiment temperatures. All pH values in the present paper were measured at lab temperature (23-24°C) and corrected back to the original temperature of the experiments, i.e. by deducing 0.47 pH units at 40°C and 0.99 at 60 °C.

The geochemical software GEMS [64] together with the PSI-nagra thermodynamic database [65], a cement specific database, Cemdata18 [66], and the thermodynamic data from Helgeson et al. [67] for albite and K-feldspar was used to calculate undersaturation with respect to amorphous silica, quartz, albite and K-feldspar in the solutions and potential oversaturation

with respect to C-S-H. The saturation index (SI) of the different solids corresponds to : SI = log IAP/K_{so} , where K_{so} represents the theoretical solubility product of the respective solid and IAP the ion activity product calculated based on the measured pH values and concentrations of Al, Ca, Si, K, and Na in solution. A positive saturation index (> 0) indicates that the solution is oversaturated with respect to this solid phase and this phase could possibly precipitate, while a negative value indicates under saturation.

The Si release rate from silica or feldspars, r $_{Si}$, was obtained from the slope of the curve of the normalized concentration (taking into account solution volume, mass of solid and specific surface area) of measured Si versus time, as summarised in Equation 3-3 for steady-state dissolution regime and linear trend:

$$\text{r}_{Si} = \frac{d(X)}{\Delta t} \frac{1}{m \times S \times V_{sol}}$$

Equation 3-3 The Si release rate from silica or feldspars

where m is the mass of solid, V_{sol} is solution volume, and S corresponds the initial specific surface area of the powder. All error bars were calculated with respect to 95% confidence interval. The solid was collected at the end of dissolution experiments using filter paper 2μm, washed with isopropanol and deionized water and dried at 40 °C and analysed using XRD.

3.2.3.4 Dissolution based on weight loss

In a further series of experiments, the weight changes of an amorphous silica plate (AmS-Pl) were studied after immersion in 50 ml of 400 mM KOH solution without and with 3 mM $CaCl_2$ or 400 mM LiCl at 60 °C. The plates were cleaned ultrasonically using isopropanol for few minutes and dried at 40 °C before exposure. The mass of each plate was recorded before exposure (*mb*). After 7 months of reaction, the plates were cleaned with water and isopropanol to remove the precipitates and dried at 40 °C for few hours; the plates were

weighted again after exposure (*ma*). Remaining mass (%) for each plate was calculated using the following equation:

$$\text{Remaining mass (\%)} = \frac{ma}{mb} \times 100$$

Equation 3-4 The remaining mass (%)

The mean of measurement for at least two different plates is reported. Newly formed solid in the presence of 3mM $CaCl_2$ or 400mM LiCl was collected using filter paper 2µm, washed with isopropanol and ultra-pure water and dried at 40 °C, before their characterisation by XRD.

3.3   Results

3.3.1 The effect of pH and temperature on SiO_2 dissolution

Figure 3-1 shows the increase of Si concentration, released from 0.5 g of amorphous silica with a size fraction of 100 to 250 µm (filled circles) and 100 to 360 µm (circles with cross) in 400 mM KOH as a function of time. The higher Si concentration observed for the finer amorphous silica underlines the need to normalise the measured Si concentration to the specific surface area of the solid, based on Equation 3-3. Based on the slope of the curves and the surface area as detailed in Table 3-1, the calculated dissolution rates of AmS-1 (261 ± 26)$\times 10^{-9}$and AmS-2 (242 ± 29)$\times 10^{-9}$ mol/m^2/s are comparable with a difference of < 8%. A second experiment on AmS-1 resulted in the similar dissolution rate 250 ± 47$\times 10^{-9}$ mol/m^2/s, indicating a good repeatability of the measurements and a total (experimental and systematic) error of < 5%.
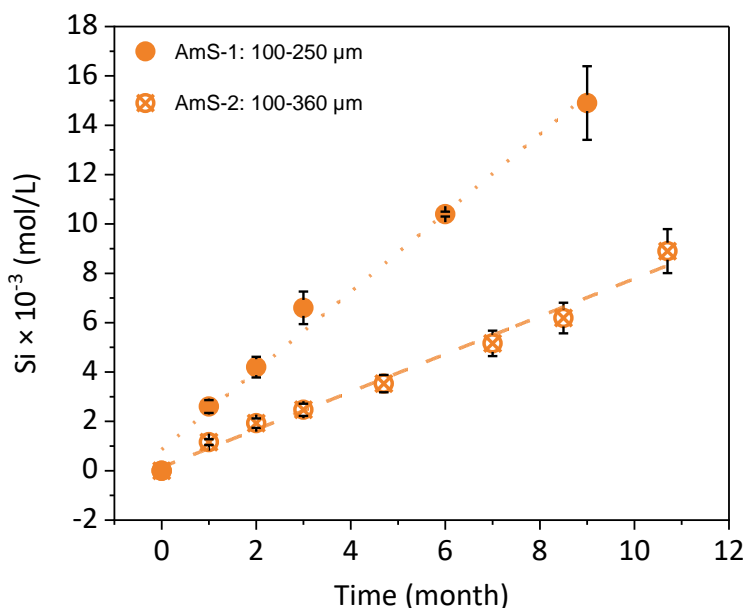
Figure 3-1 The amount of released Si (mol/L) from 0.5 g of amorphous silica with two different size fractions (AmS-1: 100 to 250 μm and AmS-2: 100 to 360 μm) in 0.5 L of 400mM KOH as a function of time at 40 °C.

The dissolution of amorphous silica in 400mM of NaOH at 40 °C (circles with cross) is $167 \pm 10 \times 10^{-9}$ mol/m^2/s, slightly slower than in 400mM KOH (half-filled circle) as shown in Figure 3-2, in agreement with the observations on quartz and silica [40,58]. The effect of pH on silica dissolution is relatively small between pH 12.4 (filled circle) and 13.0 (half-filled circle); the difference is within in the error range. Although quartz and amorphous silica have the same chemical composition, the results at 40 °C indicated amorphous silica dissolves almost 10 times faster than quartz at high pH due to the effect of crystallinity on dissolution rate.

Albite dissolves at a similar rate in 400mM of KOH (filled triangle, $0.7 \pm 0.4 \times 10^{-9}$ mol/m^2/s) as in NaOH (triangle with cross sign symbol, $1 \pm 0.4 \times 10^{-9}$ mol/m^2/s), indicating the effect of the alkali ion is negligible.
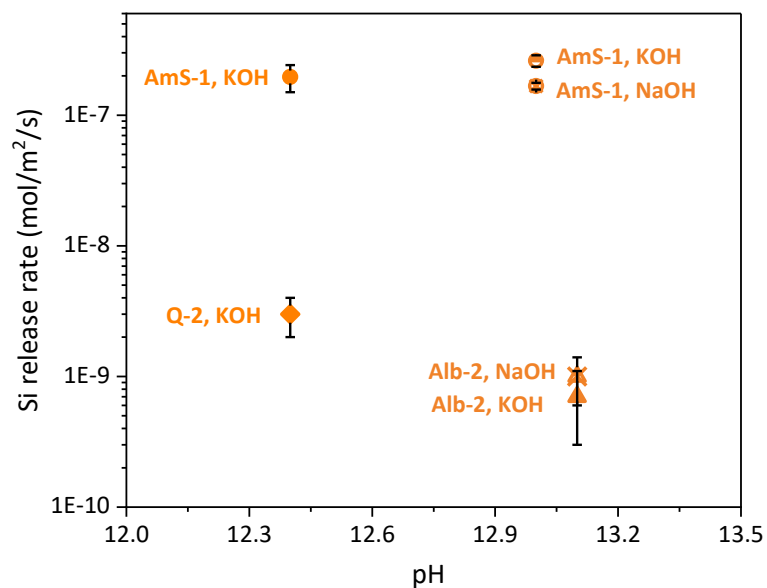
Figure 3-2 The Si release rate (mol/m^2/s) from amorphous silica (AmS-1), quartz (Q-2) and albite (Alb-2) in different solutions at 40 °C (pH values were measured at 40 °C)

Temperature as well as high pH values accelerate the dissolution rate of quartz as illustrated in Figure 3-3. Both literature data as well as our measurements show a strong increase of dissolution rate with temperature.
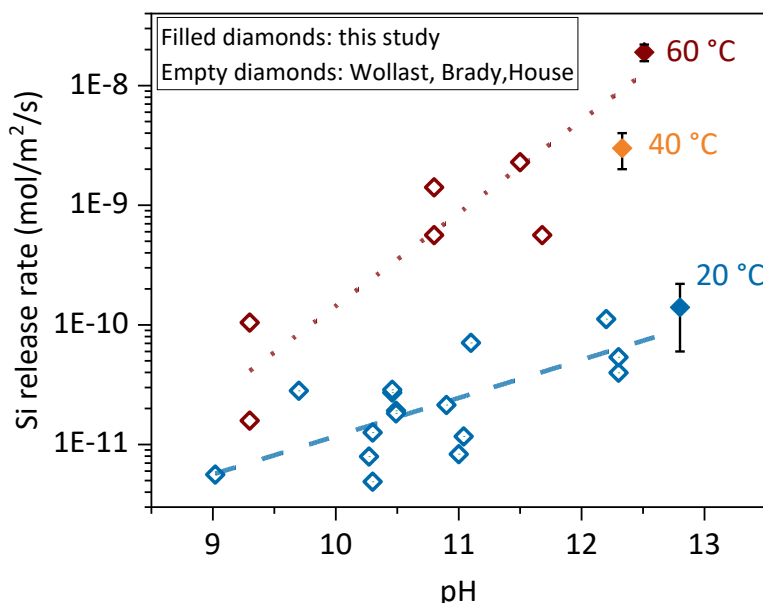
Figure 3-3 The Si release rate (mol/m^2/s) of quartz (Q) from literature: Wollast and Chou [25]; Brady and Walther [26] and House and Orr [27] (empty diamonds) and the results of this study for quartz (Q-1/2) (filled diamonds) at different temperatures (20, 40 and 60 °C) as a function of pH (pH values were reported at the experimental temperatures). Blue colour indicate experiments at 20°C, orange at 40 °C and dark red at 60°C.

Literature data [9] show a comparable increased dissolution rate at higher pH values also for albite (Na-feldspar) and K-feldspar as illustrated in Figure 3-4. At 20°C, the reported dissolution rate of albite is similar to the dissolution rate of quartz, while K-feldspar has a lower dissolution rate. In contrast, our results at 40°C indicate a very similar dissolution rate for Na-feldspar (albite; alb-1/2) and K-feldspar (microcline), while quartz has slightly a higher dissolution rate. Note, however, that we observe for the sample alb-1, which contains in addition to albite also 8% of quartz, a dissolution rate similar to quartz, underlining that all minerals present contribute to the observed Si-release rate. Thermodynamic calculations confirmed that all the solutions studied were strongly under saturated (saturation indices < 4) with respect to amorphous silica, quartz or feldspar until the end of the experiments (See Supplementary Information, Figure 3-19).

The measured dissolution rates of feldspar and quartz are almost similar and a factor of 10 to 100 higher than the dissolution rates reported for muscovite, kaolinite, biotite, … [9]: This

difference in measured dissolution rates of different minerals is in agreement with our previous work which showed higher dissolution rates of quartz and feldspars in comparison with muscovite (Chapter 2).
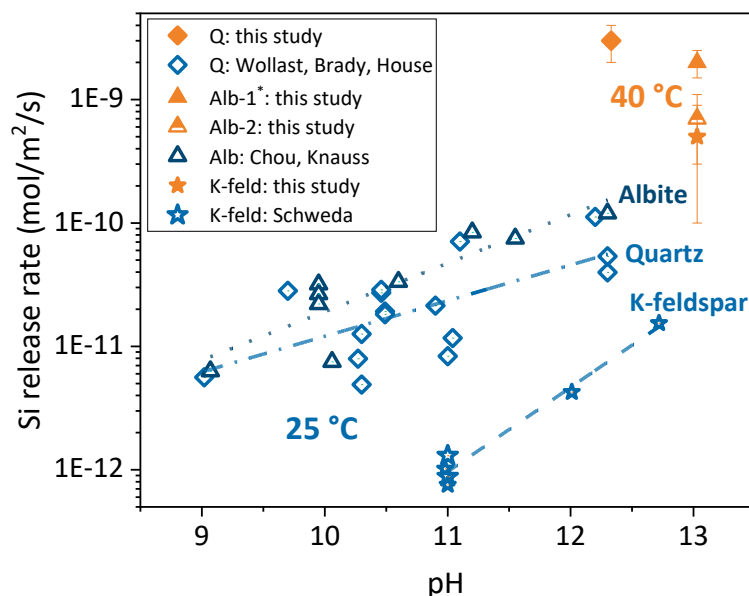
Figure 3-4 The Si release rate (mol/m^2/s) of quartz (Q), albite (Alb-1/Alb-2) and K-feldspar (K-feld) from literatures (empty dots) at 25 °C [9,24–29] and the results of this study (filled dots) at 40 °C as a function of pH. * Higher dissolution rate, as Alb-1 contains in addition 8% of quartz.

3.3.2 The effect of aluminium on the dissolution rate of silica and feldspars

3.3.2.1 Dissolution in diluted solution

Figure 3-5 shows the Si release rate (mol/m^2/s) from amorphous silica (AmS-1) as a function of Al concentration in KOH solution at pH 12.4 and 13.0. In solutions without Al, the release rates are very similar at both pH values, but are considerably slower in the presence of dissolved Al. At pH 13.0, the presence of 1 mM of Al in solution decreased amorphous silica dissolution rate 2 times; the lowest dissolution rate (4 times lower) was observed in the presence of 3 mM Al. At pH 12.4, the effect was even more clear; silica dissolution was slowed down by a factor of 9 in the presence of 1 mM Al and by a factor of 18 in the presence of 3mM

Al. The presence of different counter anions (chloride or nitrate) did not affect the dissolution rates (see Table 3-4; AmS-1 and AmS-2 in 400mM KOH with 3mM $AlCl_3$ or $Al(NO_3)_3$). This stronger inhibition of silica dissolution at lower pH values is consistent with the observations and calculations of Chappex and Scrivener [2,44]. Lower pH values increase the tendency of Al to sorb on silica and decreases its tendency to remain in solution (See Supplementary Information, Figure 3-20).

The dissolution of quartz and albite shown in Figure 3-5 is also lowered in the presence of Al. The effect of Al was stronger at 40°C than 60°C; the addition of 3mM of Al decreased the dissolution rate of quartz by a factor of 200 times at 40 °C while at 60 °C a 5 times lower dissolution rate was observed. The effect of aluminium was weaker in the case of albite.
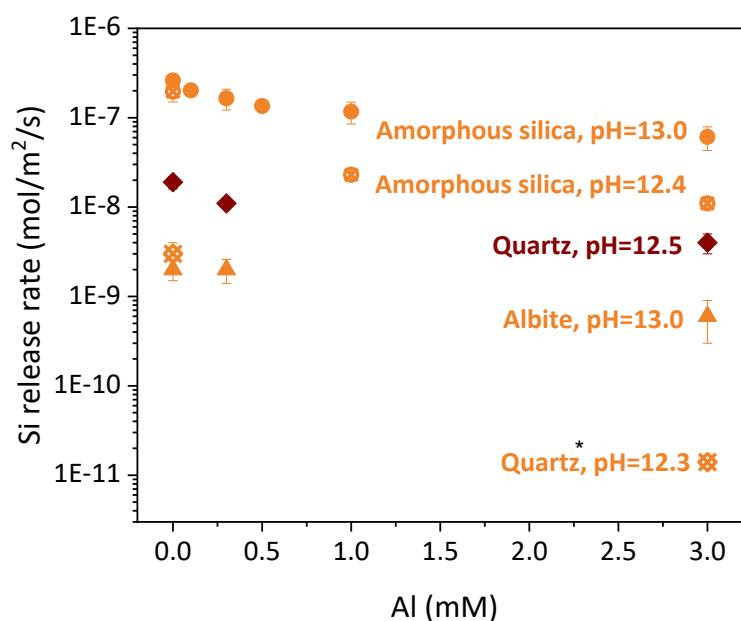
Figure 3-5 Si release rate ($mol/m^2/s$) from amorphous silica (AmS-1 at 40 °C), quartz (Q-1 at 60 °C (dark red filled diamonds), Q-2 at 40 °C (orange diamonds with cross sign symbols)) and albite (Alb-1 at 40 °C (orange filled triangles) as a function of Al concentration in pH 12.3 to 13 (pH values were measured at the experiment temperatures). * The dissolution rate is less than this number.

3.3.2.2 Surface changes during dissolution

The effect of Al on the dissolution was also followed by SEM and the progress of dissolution was quantified based on the changes in width of existing scratches as illustrated in Figure 3-6 for albite. The extent of pre-scratching was comparable for all the sample of albite as summarised in Supplementary Information, Figure 3-21. A distinct growth of pre-existing scratches is observed in the presence of KOH only, while much less change is observed in samples where in addition 3 mM of $AlCl_3$ was present, confirming the observations discussed above.
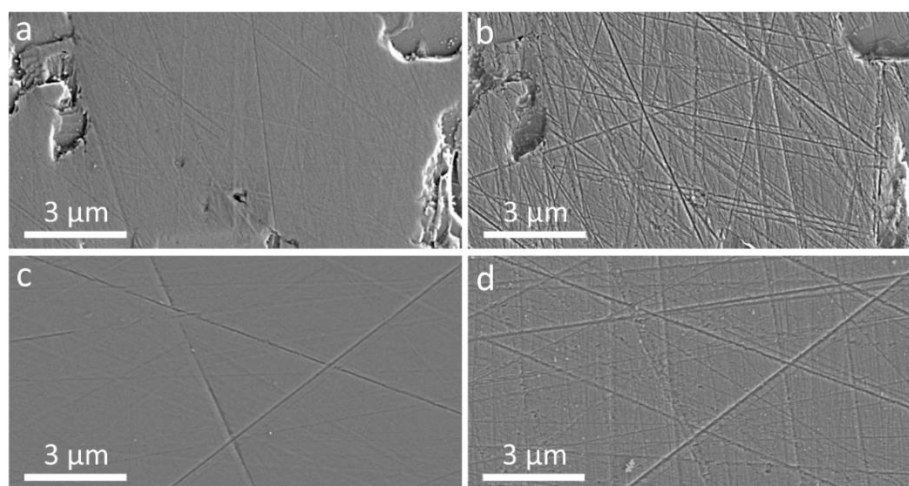
Figure 3-6 Aligned SEM secondary electron images of albite (AlbR) to quantify the width changes of scratches over time; (a and c) before dissolution, and after 21 days of dissolution in (b) 400 mM KOH and (d) 400 mM KOH + 3mM $AlCl_3$ at 40 °C

The quantification (Figure 3-7) showed a lower increase and thus less dissolution in the presence of KOH + 3 mM $AlCl_3$ than in the presence of KOH only. For all four samples, 3 mM Al decreased the dissolution rate, which is in good agreement with the results from the dissolution experiments discussed above as well as with literature data which indicated that Al in mmolar concentrations slows down the dissolution of silica [2,44], and silica rich glasses [68].

In 400mM KOH, both microcline and orthoclase (two different crystalline structures of K-feldspar) show a comparable surface reaction rate to quartz, while Na-feldspar (albite) showed slightly slower dissolution, and in the presence of Al, the differences were small.
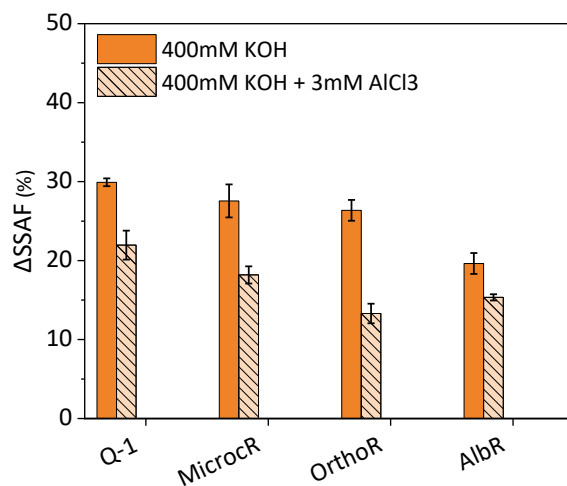
Figure 3-7 The change of scratch surface area (ΔSSAF, %) of Q-1, MicrocR, OrthoR and AlbR after 21 days of dissolution in 400mM KOH and 400mM KOH + 3mM AlCl$_3$ at 40 °C.

The results of the dissolution experiments and the increase of surface scratches underline both that Al slows down the dissolution rate of silica, quartz and feldspars, and that the effect is more distinct at lower pH values. This slower dissolution can be expected to inhibit ASR in cements with aluminium-rich SCMs such as fly ash or metakaolin [4,42,43] as well as the formation of Al-rich NASH or KASH gels instead of ASR products in the presence of Al [69].

3.3.3 The effect of calcium on dissolution rate of silica and feldspars

3.3.3.1 Dissolution by scratch tracking

Scratch tracking in the presence of 3mM CaCl$_2$ showed a clear increase of dissolution of quartz, microcline, orthoclase and albite as summarised in Figure 3-8. This increased dissolution is in agreement with observations of Dove [39,40], who observed a clear increase of

quartz dissolution in the presence of up to 10 mM calcium. This has been related to the tendency of Ca^{2+} to form monodentate surface complexes [39,40] on silica, which can accelerate dissolution kinetics [12].
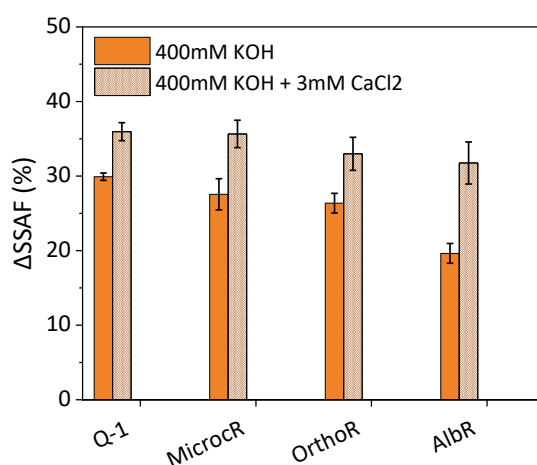
Figure 3-8 The change of scratch surface area (ΔSSAF, %) of quartz (Q-1), microcline (MicrocR), orthoclase (OrthoR) and albite (AlbR) after 21 days of dissolution in 400mM KOH and in 400mM KOH + 3mM $CaCl_2$ at 40 °C.

3.3.3.2 Dissolution in diluted solution

In contrast to the increase of scratched surface observed in the presence of Ca, the dissolution study in diluted solutions indicated an apparent decrease in dissolution rates for amorphous silica and for quartz (Table 3-3). However, SEM and XRD clearly show the formation of C-S-H (Figure 3-9) during the experiment. Thus, the slower increase of the measured Si concentrations does not mirror the dissolution rate of the amorphous silica and quartz, but rather the equilibrium between SiO_2 dissolution and C-S-H precipitation, making the calculated dissolution rates meaningless.

Table 3-3 Dissolution rates of quartz (Q), amorphous silica (AmS), albite (Alb) and microcline (Microc) in different solutions

Solid	Alkaline solution	Solution Concentration (mM)	Salt	pH [1] Initial	pH [1] Final	Storage temperature (°C)	Experiment duration (month)	$r_{Si} \times 10^{-9}$ (mol/m²/s) [2]
Q-1				12.5	12.5	60	19.7	19 ± 3
AmS-1				13.0	13.0		8.8	261 ± 26
					13.0		8.5	250 ± 47
AmS-2	400 mM KOH	--------		12.9	12.9	40	14.2	242 ± 29
Alb-1				13.0	12.9		14.2	2 ± 0.5 [3]
Alb-2				13.0	13.1		12	0.7 ± 0.4
Microc				13.0	13.1		12	0.5 ± 0.4
Calcium								
Q-1	400 mM KOH	3	CaCl₂	12.5	12.5	60	19.7	< 2 [4]
AmS-1				12.9	13.0	40	8.8	151 ± 58 [5]
Lithium								
Q-1		40	LiCl	12.4	12.4	60	19.7	30 ± 3 [6]
		400		12.5		60	19.7	26 ± 2 [6]
AmS-2		10	LiOH	12.9	12.8		14.2	261 ± 28 [6]
AmS-1		40	LiCl	13.0	13.0		8.8	255 ± 28 [6]
AmS-2		100	LiOH	12.9	12.8		14.2	191 ± 22 [6]
AmS-1	400mm KOH			13.0	13.0	40	8.8	145 ± 26 [6]
Alb-2		400	LiCl	13.0	13.2		12	0.9 ± 0.6 [6]
Microc				13.0	13.2		12	0.6 ± 0.4 [6]
Alb-1		10	LiOH	12.9	12.8		14.2	2. ± 0.5 [6]
		100					14.2	3 ± 0.6 [6]
Sulfate								
AmS-1	400mm KOH	200	K₂SO₄	13.0	13.0	40	10	197 ± 24
		3 + 50	AlCl₃ + K₂SO₄				12.4	65 ± 5

1) The pH values were measured at the experiment temperatures.
2) Si concentrations were measured using ICP-OES
3) Higher dissolution rate, as Alb-1 contains in addition 8% of quartz
4) Precipitation of C-S-H is strongly probable
5) Precipitation of C-S-H observed
6) Precipitation of Li₂SiO₃ is strongly probable, observed after 5 months of amorphous silica plate dissolution in 400mM KOH + 400mM LiCl at 60 °C
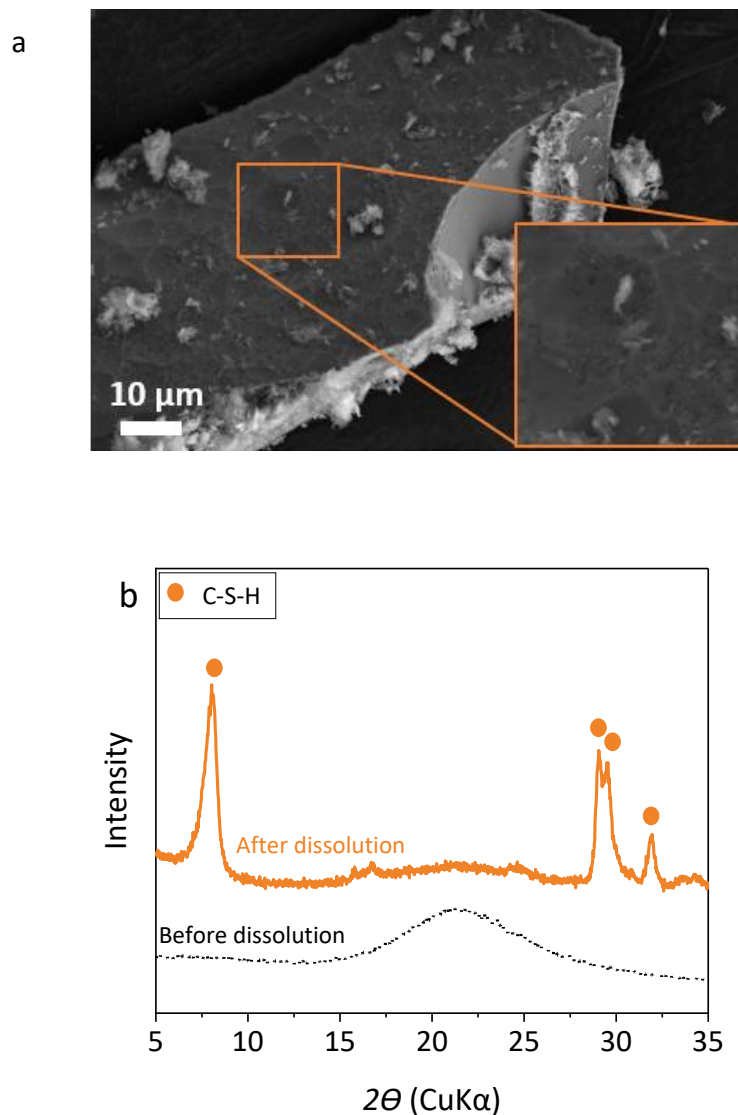
Figure 3-9 a) SEM secondary electron images and b) XRD of amorphous silica before and after 12 months of dissolution in 400mM KOH + 3mM CaCl₂ (AmS-1: amorphous SiO₂ plus C-S-H) at 40 °C.

3.3.3.3 Dissolution based on weight loss

The dissolution of amorphous silica was also followed by the decrease of the weight of plates immersed in 400mM KOH without and with 3mM CaCl₂, see Figure 3-10. The remaining mass of the samples with Ca were slightly lower than those samples exposed to KOH only, confirming the observation of the surface changes. Note that as the samples were washed with isopropanol and de-ionized water, so some C-S-H can be removed from the sample surface. Also under these conditions, the formation of C-S-H was still observed by XRD (in Supplementary Information, Figure 3-22), indicating a possibly even larger weight loss of SiO₂ in

the presence of C-S-H. The results indicate also that the presence of C-S-H did not prevent the dissolution of amorphous silica, in contrast to previous reports [49,50].
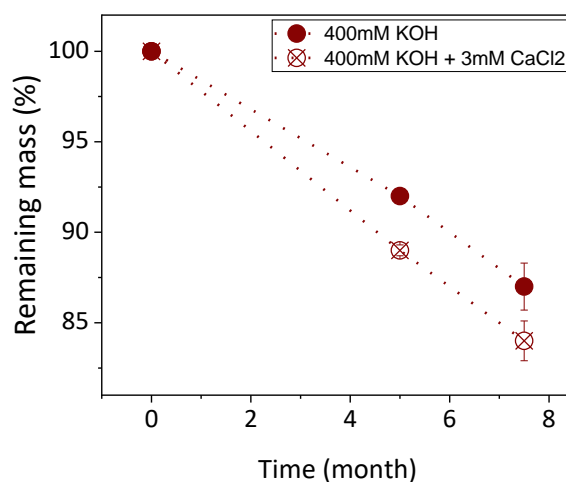
Figure 3-10 Decrease of mass (%) of AmS-PI in 400mM KOH without and with 3mM CaCl$_2$ at 60 °C as a function of time.

Some studies have suggested, based on measurements of mass loss [49,50] or silicon concentrations [51], that Ca decreases the dissolution of silica due to formation of a protective C-S-H layer on its surface. However, the study of weight losses and silicon concentrations in the presence of precipitating C-S-H contradict this hypothesis. The formation of C-S-H did not create a protective layer as the silica surface keeps reacting, as visible in the SEM image (Figure 3-9 a), and the continuing weight loss (Figure 3-10). The formation of new solids during dissolution experiments means that dissolution rates cannot be measured from the development of silicon concentrations or weighing results, as both dissolution and precipitation are occurring at the same time.

In agreement to the observations reported here, an acceleration of quartz dissolution has been reported in the presence of Ca^{2+} at near neutral pH conditions, although the effect was more moderate than observed here [39,40]. Dove has related the accelerating effect of different bivalent cations, M^{2+}, with their ability to form surface complexes $\equiv$Si–O-M$^+$ which lower the strength of the $\equiv$Si–O–Si$\equiv$ bonds and follow the size of the ion radius: Ba^{2+} > Sr^{2+} > Ca^{2+} > Mg^{2+}. Based on their sequence (which also agrees with the sequences of earth alkali

ions for sorption on C-S-H [70]), an even stronger accelerating effect of Sr^{2+}, Ba^{2+} or Ca^{2+} on SiO_2 dissolution at high pH values can be expected.

3.3.4 The effect of Fe and Mg

The presence of 3 mM Mg or Fe(III) in the starting solution did not significantly affect the dissolution rate of quartz or amorphous silica in 400mM KOH as shown in Figure 3-11. This could rather be related to the very low solubility of brucite, $Mg(OH)_2$, and hematite (or other iron hydroxides) at high pH resulting in expected Mg and Fe(III) concentrations of below 0.001 mM at pH 13 (see supplementary Information, Figure 3-20). The very low concentrations of Mg and Fe could thus explain why no effect on the dissolution rate was observed in the high pH conditions studied here.

In contrast, Dove [39,40] reported at near neutral pH conditions and at higher Mg concentrations, a slower dissolution of quartz in the presence of Mg^{2+} than in the presence of Ca^{2+} or of alkali ions, which was assigned to a lower tendency of Mg^{2+} to form surface complexes as discussed above. For iron an inhibiting effect could be expected [9,39], indicating that both Mg and Fe could potentially slow down dissolution.
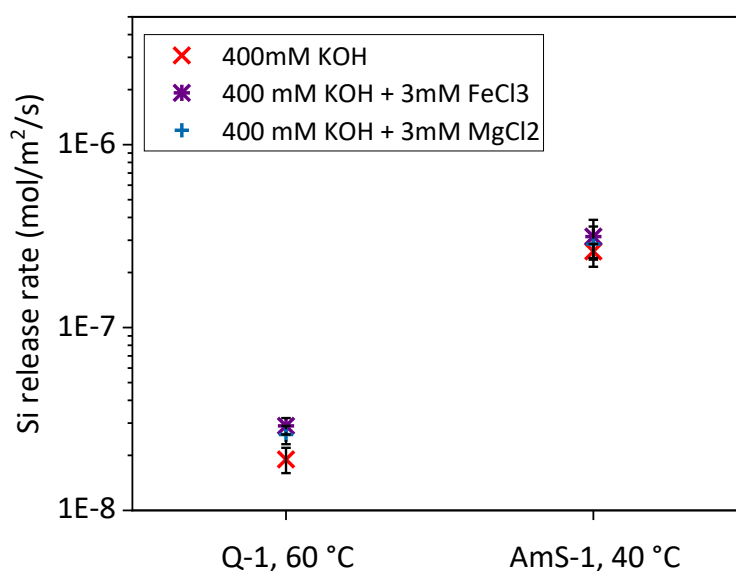
Figure 3-11 The Si release rate (mol/m^2/s) from a) Q-1 at 60 °C and b) AmS-1 at 40 °C in 400mM KOH, 400mM KOH + 3mM FeCl$_3$ and 400mM KOH + 3mM MgCl$_2$.

3.3.5 The effect of Li on dissolution rate of silica and feldspars

3.3.5.1 Dissolution by scratch tracking

The scratch-tracking technique clearly indicated that the presence of 400mM LiCl increased the dissolution rate of quartz, microcline, orthoclase and albite, as shown in Figure 3-12.
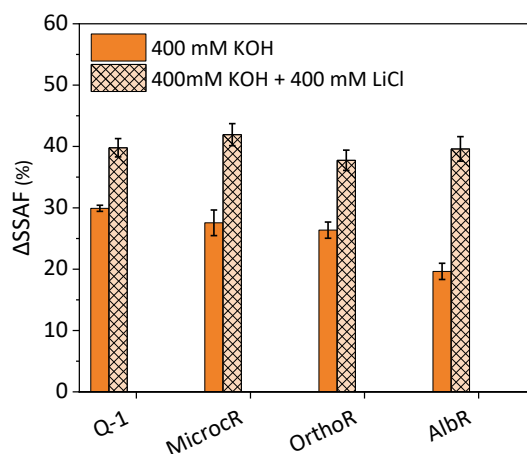

Figure 3-12 The change of scratch surface area of quartz (ΔSSAF, %) (Q-1), microcline (MicrocR), orthoclase (OrthoR) and albite (AlbR) after 21 days of dissolution in 400mM KOH and in 400mM KOH + 400mM LiCl at 40 °C.

3.3.5.2 Dissolution in diluted solution and based on weight loss

Li increased the release rate of Si from albite and microcline, while for amorphous silica and quartz slower Si release rates were measured (Table 3-3). The lower silicon concentrations observed in the presence of Li for amorphous silica and quartz could be due to formation of Li_2SiO_3 (as discussed below and as reported by [50]), which limits the Si concentrations in solution.

Figure 3-13 shows the decrease of mass (%) of a silica plate in 400mM KOH without and with 400mM LiCl. The remaining mass (%) of AmS-Pl was higher in the presence of Li, in agreement with the dissolution results but in contrast with SEM observations. The formation of Li_2SiO_3 was detected by XRD after 5 months of reaction in 400mM + 400mM LiCl (Supplementary

Information, Figure 3-22), which would explain the apparently increased mass of these samples, in agreement with the previous results of SiO_2 dissolution in the presence of lithium [50].
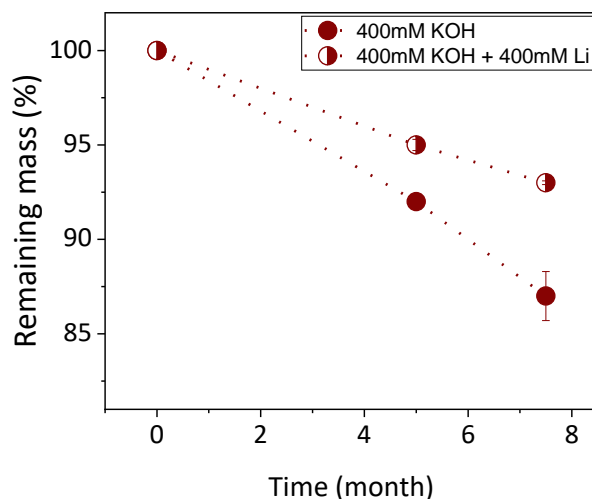
Figure 3-13 Decrease of mass of AmS-Pl in 400mM KOH without and with 400mM LiCl at 60 °C as a function of time

By scratch-tracking method, an increased dissolution of silica and feldspars was observed in the presence of Li; while the dissolution as well as the mass loss experiments showed for apparent differences in the case of SiO_2, which seems to be related to the precipitation of Li_2SiO_3 or similar Li-Si-oxides, which decreased the aqueous Si concentrations and increased the weight of the solid. Scratch-tracking method and observation of the solid surfaces showed directly that lithium can accelerate the dissolution of Si-containing solids at high pH values. It should be noted that at near neutral pH, a small reduction of silica dissolution [58] or no significant effect was observed [39,40], indicating that the pH could play an important role on the effect of Li on dissolution. Based on the observations of Dove [40], the ability of Li^+ to form surface complexes on silica could be responsible for its accelerating effect on SiO_2 dissolution.

Based on the findings discussed above, lithium rather accelerates the dissolution of silica and feldspars, and thus, it is expected to increase dissolution rate of silica-rich aggregates. The role of lithium to prevent ASR expansion is not because of any slow down of the dissolution

rate, but rather due to the formation of a different ASR product. The presence of lithium leads to an ASR product containing Li but with lower CaO/SiO_2 and $(Na+K)/Si$ [54,55].

3.3.6 The effect of Na, K and Cs

Figure 3-14 shows that the presence of additional 400mM of NaCl or KCl or CsCl had no significant effect on the dissolution rates of quartz, amorphous silica or albite, although the values measured in the presence of Cs tended to be slightly lower. This is an agreement with the observation of Dove [39,40] at near neutral pH conditions, where only a small difference between the different alkali ions on dissolution kinetics of SiO_2 was observed. Interestingly at near neutral pH values also Li shows no or only a very moderate accelerating effect [39,40], in contrast to the high pH conditions studied here, where Li shows a clearly accelerating effect resulting in the following sequence: $Li^+ >> Na^+ \approx K^+ \approx (>) Cs^+$, which follow their tendency to form surface complexes with SiO_2 as detailed in [39,40].
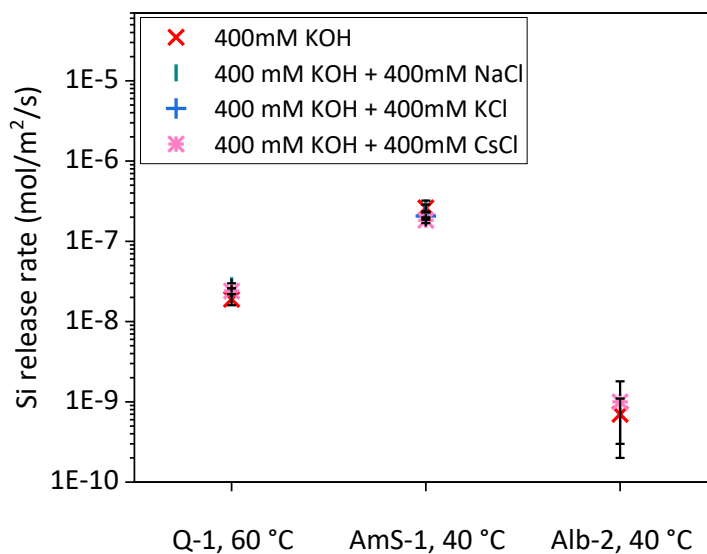
Figure 3-14 The Si release rate (mol/m^2/s) from Q-1 (at 60 °C) and AmS-1 and Alb-2 (at 40 °C) in 400mM KOH, 400mM KOH and 400mM of NaCl or KCl or CsCl.

3.3.7 Effect of sulfate

The scratch-tracking method showed that addition of 200mM of K_2SO_4 to 400mM KOH moderately increased quartz dissolution (Figure 3-15). In contrast, the dissolution studies showed no significat effect of K_2SO_4 on the dissolution rate of amorphous silica (Table 3-3). While, the presence of 50mM K_2SO_4 did not change the dissolution rate of amorphous silica (AmS-1) samples exposed to 400mM KOH + 3mM $AlCl_3$ (Table 3-3). The increased dissolution by the scratch tracking method agrees with observations at neutral pH, where an increase of silica dissolution was observed in the presence of sodium sulfate [71]. The acceleration of the dissolution rate was related to the specific adsorption of SO_4^{2-} ions on the surface of amorphous silica, resulting in a decrease in the strength of the $\equiv$Si–O–Si$\equiv$ bonds [71]. Whether specific adsorption of sulfate on SiO_2 also occurs at high pH values, where SiO_2 has a negative charge, or whether other effects are responsible for the observed increase of dissolution remains presently unclear as well as why different results were observed by the two different methods.
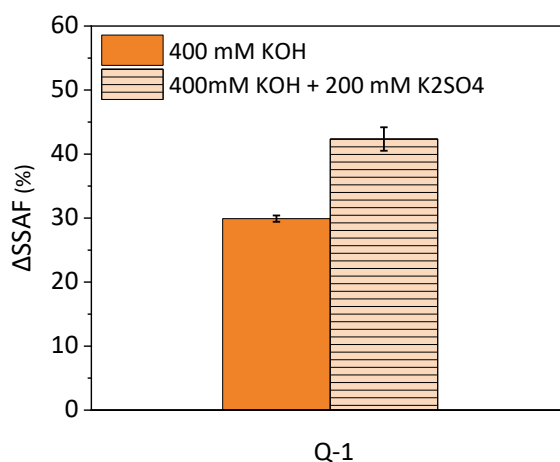
Figure 3-15 The change of scratch surface area of quartz (ΔSSAF, %) (Q-1) after 21 days of dissolution in 400mM KOH and 400mM KOH + 200mM K_2SO_4 at 40 °C.

3.4   Conclusions

The dissolution rate of silica, quartz and feldspar increased as expected with the surface area, pH values and temperature.

The comparison of different methods (increase of scratch width, measurement of the increase of Si concentrations, and measurement of weight changes) indicated that, in particular, the measurement of Si concentrations as well as the weight changes were strongly affected by the formation of secondary phases such as C-S-H and lithium silicates, which led to apparently wrong results. The direct observation of the increase of the scratched area was shown to be the most reliable method in the presence of Ca and Li where secondary solids formed, while consistent trends were observed in the absence of secondary phases.

The results showed that:

- Among all studied ions, only Al could effectively slow down the dissolution of quartz, amorphous silica, Na-feldspar and K-feldspar. The slowdown was more distinct at pH 12.5 than at pH 13, which could be associated to a higher tendency of Al to sorb on the surface at lower pH values.

- The presence of Ca accelerates dissolution of SiO_2 and feldspars, indicating that Ca is not only used to form ASR products [72] but that its presence further accelerates the dissolution.

- The presence of Fe and Mg had no significant effect on the dissolution rate, which was assigned to the very low solubility of iron hydroxide and brucite at pH 12.5 to 13.

- The presence of additional Na, K salts to KOH solutions did not affect the dissolution rate, while Cs showed a very weak suppression and Li showed a clear acceleration of SiO_2 dissolution rate. This might be related with the higher tendency of Li to form surface complexes [39,40] resulting in the following sequence of dissolution rates: $Li^+ \gg Na^+ \approx K^+ \approx (>) Cs$.

- The presence of sulfate seems also to slightly increase the dissolution of SiO_2, although the results are not that clear. Both the effect of sulfate as well as the possible

interplay between sulfate and calcium on the dissolution of SiO_2 could be further investigated.

The dissolution experiments conducted here, allowed the study of the effect of different parameters separately. In the pore solution of cements, however, many different elements are present simultaneously and their concentrations depend on pH values. The present studies underlines the importance of alkali hydroxide concentrations and thus pH values, not only for the formation of ASR products but also for the dissolution kinetics of silica-containing minerals present within the aggregates [9]. This is in good agreement with the faster expansion observed at high pH values [4,43,73,74].

The kind of alkali ions present had little influence with the exception of Li, which accelerates dissolution. Thus, the suppression or slow down of ASR in the presence of Li is not related to its effect on silica dissolution kinetics but rather to the formation of a different ASR product [54,55].

Any effect of Mg and Fe on silica dissolution kinetics is unlikely to be relevant in a cement pore solution due to extremely low Mg and Fe concentrations at high pH values. Calcium was observed to accelerate silica and feldspar dissolution. As the calcium concentrations are strongly influenced by pH value, higher calcium concentrations are present at lower pH values in PC, while the presence of Si-rich SCMs [75] has relatively little influence on the measured calcium concentrations as at the same time pH decreases. Therefore, it is rather the decrease of pH values in the pore solution of blended cements with Si-rich SCMs than lower Ca concentrations that is expected to be the reason for the slower ASR-expansion in the presence of SCMS [74,75].

Aluminium can slow down the dissolution rate of SiO_2 by 1 to 2 log units, although the effect gets weaker at high pH values. The most efficient way to increase Al concentrations in the pore solutions of cements (without increasing the pH value) is the use of Al-rich SCMs such as fly ash or metakaolin, which increases the Al-concentration in the pore solution [61,76,77], and which have been observed to contribute significantly to reduce ASR expansion.

Table 3-4 Dissolution rates of quartz, amorphous silica and albite in different solutions

Solid	Alkaline solution	Solution Concentration (mM)	Salt	pH [1] Initial	Final	Storage temperature (°C)	Technique	Experiment duration (month)	$r_{Si} \times 10^{-9}$ (mol/m²/s)
Q-2	100mM KOH			12.9	12.8	20	IC	40	0.1 ± 0.08
				12.3	12.4	40		15	3 ± 1
AmS-1				12.4			ICP-OES	8.5	196 ± 46
AmS-1	400mM NaOH	--------		13.0	13.0	40	ICP-OES	12.4	167 ± 10
Alb-2				13.0	13.1			12	1 ± 0.4
Aluminium									
Q-2	100mM KOH	3	Al(NO₃)₃.9H2O	12.8	12.8	20	IC	40	< 0.006
				12.3	12.3			15	< 0.01
AmS-1		1		12.4	12.3	40		8.5	23 ± 2
		3						8.5	11 ± 1
Q-1		0.3		12.4	12.5	60		19.7	11 ± 1
		3			12.4			19.7	4 ± 1
		0.1	AlCl₃	13.0	13.0			8.8	202 ± 20
		0.3			12.9		ICP-OES	8.8	165 ± 43
AmS-1	400mM KOH	0.5						8.8	135 ± 17
		1		12.9	13.0	40		8.8	117 ± 32
		3						12	61 ± 18
AmS-2					12.9			14.2	55 ± 8
Alb-1		0.3	Al(NO₃)₃.9H2O	12.9	12.9			14.2	2 ± 0.6
		3						14.2	0.6 ± 0.3
Iron, magnesium									
Q-1	400mM KOH	3	FeCl₃	12.4	12.5	60	ICP-OES	19.7	29 ± 3
AmS-1				12.9	12.9	40		8.8	314 ± 74
Q-1	400mM KOH	3	MgCl₂	12.4	12.5	60	ICP-OES	19.7	26 ± 3
AmS-1				12.9	12.9	40		8.8	286 ± 71
Extra alkalis; sodium, potassium, caesium									
Q-1	400mM KOH	400	NaCl	12.5	12.4	60	ICP-OES	19.7	28 ± 2
AmS-1				13.0	13.0	40		8.8	260 ± 62

AmS-1	400mM KOH	400	KCl	13.0	13.0	40	ICP-OES	10	207 ± 21
Q-1				12.5	12.4	60		19.7	24 ± 2
AmS-1	400mM KOH	400	CsCl	13.0	12.9	40	ICP-OES	8.8	183 ± 14
Alb-2				13.0	13.1			12	1 ± 0.8

The pH values were measured at the experiment temperatures.

Acknowledgements:

Supplementary information

Specific surface area

The powder (randomly sampled from a larger well-mixed batch) was impregnated in epoxy resin and was polished to 1 µm using hard disc and diamond spray. The specific surface areas of each powder was measured using 2-dimentional (2D) cross-section SEM images (Figure 3-16) after deposition of a thin carbon layer on the sample surface. Then, a shape tensor analysis (using the Avizo software (Thermo Fisher Scientific, Zuse Institute, Berlin, Germany)) was implemented to determine the bonding box extents ("a" and "b" values shown in Figure 3-17 (a)) of each individual object (powder particle) in the binary image based on their Eigenvectors/values. In order to approximate a 3-dimentional (3D) powder particle based on its 2D binary mask, the extent for the third dimension ("c" or Extent 3 = 2 $\varepsilon_3\lambda_3$) was computed as the average of its "a" and "b" values (Figure 3-17 (b)). The 3D surface area of an ellipsoid with the dimensions of a > c > b for each particle was computed (Figure 3-17 (c)). The volume of each ellipsoid was also calculated to compute the approximate mass of each particle using density of material. Finally, the specific surface area was obtained by dividing the surface area of equivalent ellipsoid to the approximate mass of each particle (with a unit of m^2/kg). A grey-level threshold was applied to the SEM image in order to produce a new binary image, differentiating the powder particles as foreground (with a constant assigned value of one to their pixels) and the one of epoxy resin as background (with a constant assigned value of zero to their pixels).
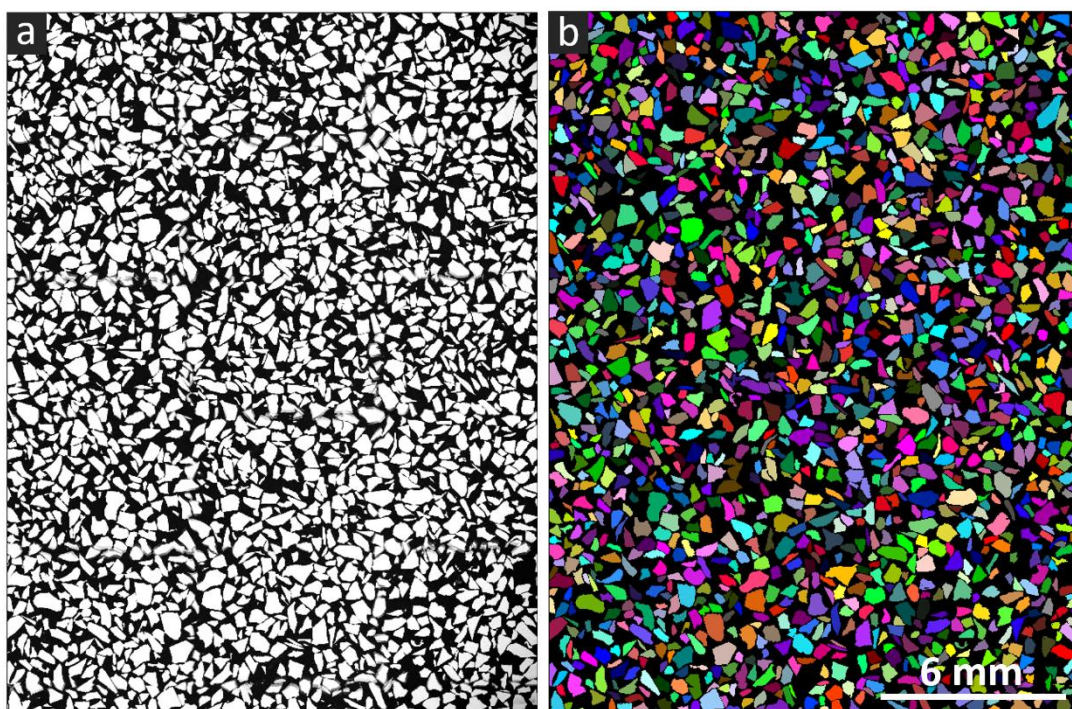
Figure 3-16 (a) An example SEM image for amorphous silica illustrating the 2D cross-section of powder particles (the micrograph was obtained by stitching several SEM images) and (b) the labeled binary particles after shape tensor analysis, each associated with a random color to demonstrate the independence of each particle.
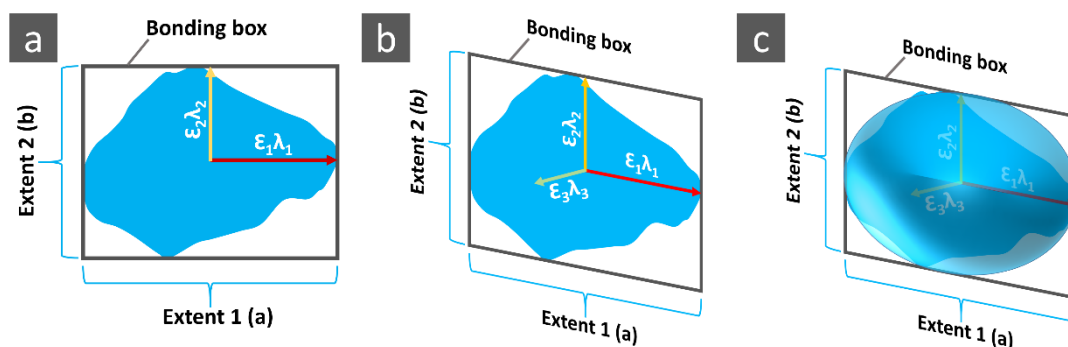
Figure 3-17 Schematic illustration of the results of shape tensor analysis on a binary mask of an individual particle: (a) 2D cross-section of a particle with shape tensor components, (b) approximated third dimension extent and (c) equivalent ellipsoid (with smooth surface) passing with dimensions of three extent values computed for the particle.

Sample characterization
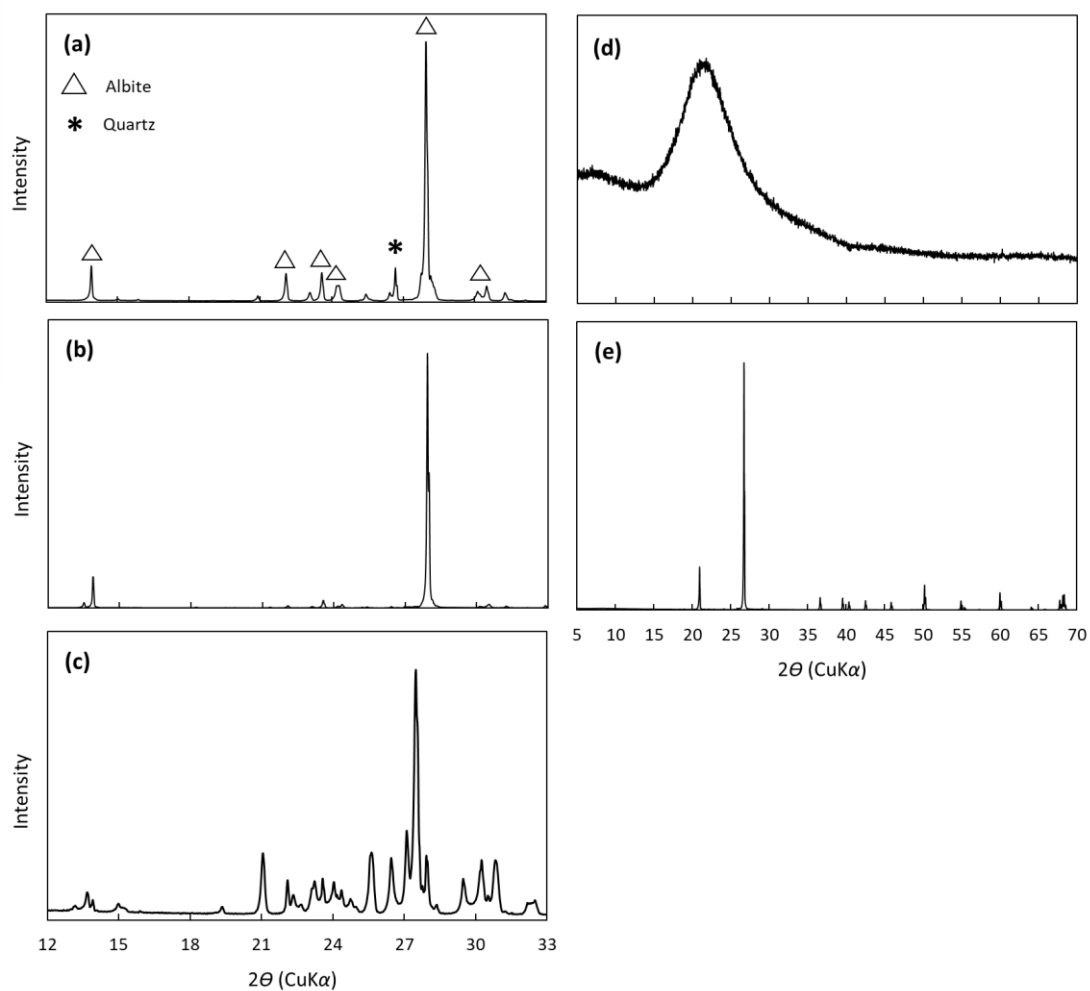
Figure 3-18 XRD patterns of a) albite (Alb-1), b) albite (AlbS/Alb-2), c) microcline (MicrocR/Microc), d) amorphous silica (AmS-1/2) and e) quartz (Q-1/2) powder before the dissolution experiments.

Saturation indices
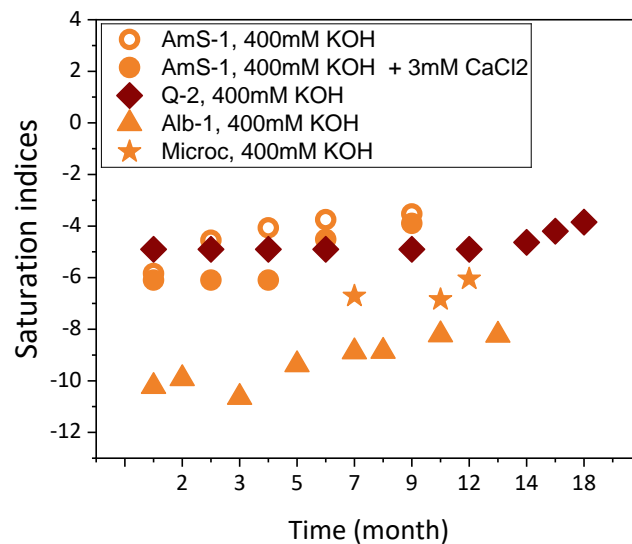
Figure 3-19 Saturation indices in solution calculated using GEMS, for dissolution of amorphous silica (AmS-1) with respect to amorphous silica, quartz (Q-1) with respect to quartz, albite (Alb-1) with respect to albite and microcline (Microc) with respect to microcline in 400mM KOH, and dissolution of amorphous silica (AmS-1) with respect to amorphous silica in 400mM KOH + 3mM $CaCl_2$ as a function of time. The storing temperatures: orange at 40 °C and dark red at 60°C.

Solubility and Al speciation
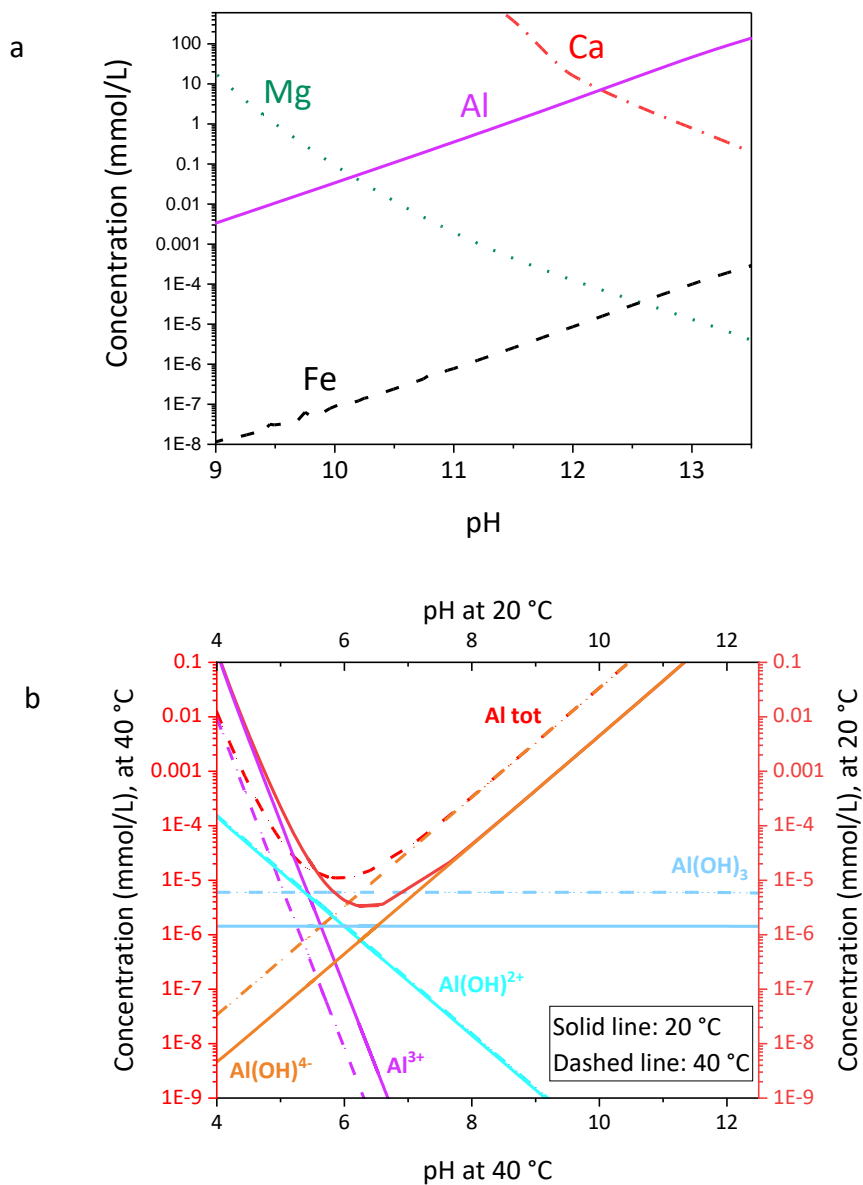
Figure 3-20 The solubility of a) gibbsite, portlandite, brucite and hematite in (mmol/L) at 40 °C and b) microcrystalline Al(OH)$_3$ and its specimens (mmol/L) as a function of pH at 20 and 40 °C, calculated by GEMS.

Scratch tracking
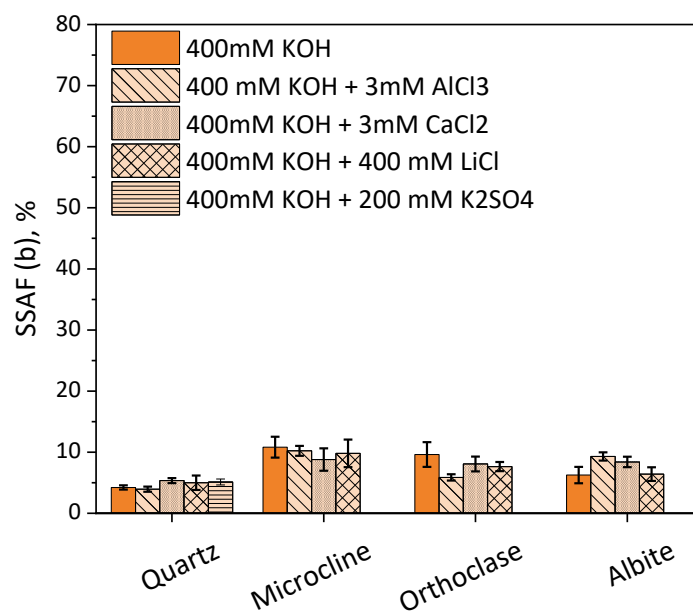
Figure 3-21 Scratched surface area fraction (SSAF, %) of quartz (Q-1), microcline (MicrocR), orthoclase (OrthoR) and albite (AlbR) before exposure to different solutions (400mM KOH, 400mM KOH + 3mM AlCl$_3$, 400mM KOH + 3mM CaCl$_2$, 400mM KOH + 400mM LiCl and 400mM KOH + 200mM K$_2$SO$_4$)

Characterization of formed solids during dissolution
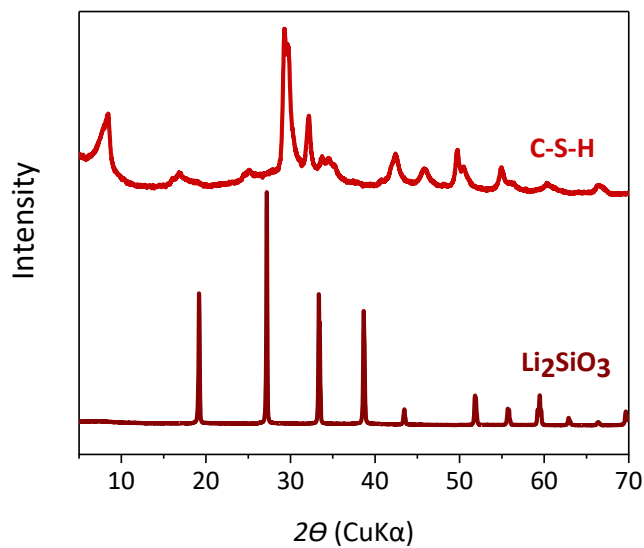
Figure 3-22 XRD patterns of C-S-H and Li_2SiO_3 which formed due to dissolution of amorphous silica plates (AmS-Pl) in 400mM KOH + 3mM $CaCl_2$ and 400mM KOH + 400mM LiCl respectively at 60 °C after 5 months.

Chapter 4 The effect of paste composition on the pore solution composition and the extent of ASR expansion

Note: This chapter is in preparation for publication in a journal. The results presented are a combination of literature review (indicated) and original work.

Contribution of the doctoral candidate: Writing of the first manuscript draft, experimental design, conduction of the original experiments shown in the manuscript.

Abstract

The alkali silica reaction can cause long-term degradation to concrete. The rate of reaction is very dependent on the composition of the pore solution. In the present study, the evolution of the pore solution composition in different cement pastes and concretes was studied at different temperatures and up to 17 months. It was found that pastes containing metakaolin had the highest amount of aluminium and the lowest amount of alkalis in the pore solution. The effect of different aggregates on the pore solution composition of concrete samples was studied. Bend aggregate, rich in feldspars, up took a noticeable amount of alkalis from the pore solution, highlighting the influence of aggregate on the pore solution composition of concrete. Measurements of expansion, revealed the noticeable effect of temperature, alkali and pH of pore solution on the extent of ASR expansion. The lowest values of ASR expansion were measured for the concretes made of blended cement pastes with low alkali and hydroxide content in their pore solution.

Keywords: Alkali silica reaction, pore solution composition, aggregate effect, paste effect, temperature effect, ASR expansion.

4.1   Introduction

Alkali Silica Reaction (ASR) [78] is a major durability issue affecting concrete. The alkaline pore solution dissolves silica-containing minerals within ASR-reactive aggregates [6]. The reaction of dissolved silica from aggregates with alkali hydroxides and calcium in the pore solution produces ASR products, which causes cracking in concrete. The pore solutions of blended cements contain various elements including alkalis (sodium and potassium), hydroxide, calcium, sulfate, silicon and aluminium. The type of cement and supplementary cementitious material (SCM) and its amount [75] affect the composition of the pore solution. In the pore solution of concrete, mainly sodium and potassium control the OH^- concentration [79]. Blended cements have been widely shown to reduce ASR expansion [4,43,73,74]. However, the aggregate type has an important influence on the amount of SCM needed to control ASR expansion [34]. Addition of extra silica from most SCMs decreases the alkalinity of the pore solution, although some SCMs (especially alkali rich fly ashes) can increase the alkali content of the pore solution [80–84]. Several researchers reported that dissolution of aggregates releases alkali into the pre solution [34,85–90]. Al-rich SCMs, for instance fly ash or metakaolin, have been reported to be more effective in preventing of ASR [4,42–44].

Lithium was reported to have the potential of controlling ASR by McCoy and Caldwell in 1951 [52]. Lithium was found to change the composition of ASR products as lower CaO/SiO_2 and $(Na+K)/Si$ were measured in the presence of lithium [54,55]. The smaller ionic radius of Li^+ and its higher charge density were proposed as the main reason for the preferential incorporation in ASR products in comparison with K^+ and Na^+, which produces non-expansive ASR products [54,55]. The amount of lithium needed to control ASR depends on different factors such as the amount and availability of alkalis (Na+K) and the aggregate type [8,52–54]. Some studies proposed that lithium decreases silica dissolution [6,57], however our recent results show that lithium increases dissolution of silica and feldspars at high pH (3.3.5), and the formation of Li_2SiO_3 interferes with measurements of silica dissolution [50] and (3.3.5).

Calcium is another element of interest. In particular, it can lead to alkali recycling by exchange with alkalis of the ASR products and forming calcium silicate hydrate (C-S-H) [6,7], which can increase alkali concentration in the solution. It was shown in our previous study using the

scratch-tracking approach that calcium increases dissolution of silica-containing minerals including quartz and feldspars at high pH values (3.3.3).

Sulfate is also present in the pore solution of paste and concrete samples. The dissolution of amorphous silica can be accelerated at high pH when sulfate is present possibly due to a specific adsorption of sulfate on its surface [91]. An increase in the dissolution rate of silica and feldspars was observed in the presence of sulfate using the scratch-tracking method in our previous study (3.3.7).

In the present study, the compositions of pore solution from different pastes and their evolution over time were measured at different temperatures up to around 17 months. The effect of different aggregates on the composition of pore solution from concrete samples was also studied. The LMC method [43,92] was used to measure ASR expansion of concrete samples made of different cement pastes and ASR-reactive Swiss aggregate. The correlation between pore solution composition and the extent of ASR expansion was investigated.

4.2   Materials and methods

4.2.1 Materials

Paste and concrete samples were made of CEM I/42.5 (Na_2O-equivalent of 0.79%) cement (PC) from Holcim. Blended cement pastes (Figure 4-1) were prepared using supplementary cementitious materials, limestone (LS) (Omya, ducral 5), coarse fly ash Maastricht (FA-c, 3080 cm^2/g) and fine fly ash Maastricht-5000 (FA-f, 5070 cm^2/g) (HeidelbergCement), metakaolin (MK) (Burgess), micro silica (SF) (Grade 983-U, Elkem Materials) (Table 4-1). Gypsum (Merck) was added to correct the sulfate balance using isothermal calorimetry experiments for the mixtures containing metakaolin (0.5% of gypsum, Figure 4-11). 400mM of LiCl (99.9%, Apollo Scientific) was added to the mixtures containing lithium. A small amount (0.9-2 l/m^3) of acrylic superplasticizer (Dynamon SR 914 – CH) was added to the mixtures containing more than 10 percent of metakaolin. De-ionized water was used to cast paste samples and tap water was used to cast concrete samples.
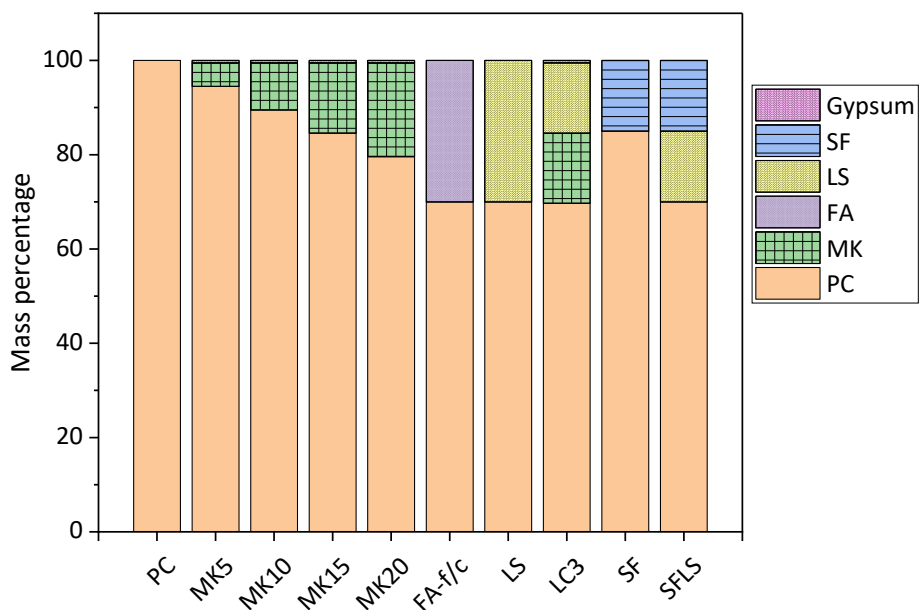
Figure 4-1 Mix design of the blended cement pastes.

Table 4-1 XRF oxide composition of the materials

Oxide wt. %	PC	FA-c	LS	MK	SF
SiO_2	20.1	59.7	0.1	52.0	99
Al_2O_3	4.6	23.3	0.001	43.8	
TiO_2	0.4	1.1	0.01	1.5	
MnO	0.05	0.03	0.003	0.01	
Fe_2O_3	3.3	6.5	0.04	0.3	
CaO	63.0	1.6	55.0	0.03	
MgO	1.8	1.0	0.1	0.01	
K_2O	1.0	2.0	0.01	0.1	-------
Na_2O	0.2	0.5	0.1	0.3	
SO_3	3.3	0.2	0.03	0.1	
P_2O_5	0.2	0.2	0.004	0.2	
Cr_2O_3	0.01	----	0.001	0.02	
L.O.I	2.1	2.3	42.5	1.5	
Total	99.9	98.4	97.9	100	

Concrete samples were made with ASR-reactive aggregates including U, B, P aggregates from Switzerland (Chapter 2) and Bend (Ben) aggregate from the US and a limestone non-ASR re-active aggregate (Cal). The chemical and mineralogical composition of the aggregates are shown in Table 4-2.

Table 4-2 Chemical and mineralogical composition of the ASR-reactive aggregates (U, B, P and Bend (Ben) aggregates) and the calcite-based non-ASR reactive (Cal) aggregates using XRF and XRD (wt.%)

Technique	Component	U	B	P	Ben	Cal
XRF (wt. %)	SiO_2	64.3	69.1	68.0		
	Al_2O_3	8.8	14.3	7.2		
	CaO	8.7	2.9	8.9		
	K_2O	2.1	3.4	2.2	------	
	MgO	2.1	1	1.9		
	Fe_2O_3	2.0	2.3	1.4		
	Na_2O	1.7	3.7	1.4		
	SO_3	0.4	0.1	0.1		
XRD (wt. %)	**Quartz**: SiO_2 [ICSD 174]	49.7	24.9	55.5	8.6	0.8
	Cristobalite: SiO_2 [ICSD 75300]		—		1.9	
	Feldspar: Albite: $NaAlSi_3O_8$ [ICSD 87657]	17.7	33.3	8.2		
	Feldspar: Albite: $NaAlSi_3O_8$ [ICSD 37653]		—		3.7	
	Feldspar: Microcline: $KAlSi_3O_8$ [ICSD 83531]	7	11.7	7.9		
	Feldspar: Orthoclase: $KAlSi_3O_8$ [ICSD 9543]	—	5.9	—		—
	Feldspar: Anorthoclase $(Na,K)AlSi_3O_8$ [ICSD 9000857]		—		41.7	
	Mica: Muscovite $KAl_2(AlSi_3O_{10})(OH)_2$ [ICSD 75952]	8.5	10.7	7.4		
	Smectite: Vermiculite $(Mg,Fe,Al)_3((Al,Si)_4O_{10})(OH)_2.4H_2O$		—		5.8	
	Calcite: $CaCO_3$ [ICSD 73446]	6.8	10.4	15.2	—	91.2
	Dolomite: $CaMg(CO_3)_2$ [ICSD 66333]	6.5	0.3	4.5	—	
	Chlorite: Clinochlore $Mg_5Al(AlSi_3O_{10})(OH)_8$ [ICSD 66258]	0.8	2.4		—	
	Amorphous/non-crystalline	3	0.4	1.3	38.3	8

Simplified pore solutions for expansion experiments were made of de-ionized water and alu-minum chloride anhydrous powder (99%, Aesar), calcium sulfate dehydrate (Roth /Merck),

sodium sulfate (99%, ACROS), calcium chloride (≥ 98%, RDTH), potassium hydroxide (Sigma Aldrich, 90%) and sodium hydroxide (ACS and ≥ 98%, RDTH).

4.2.2 Methods

4.2.2.1 Paste preparation

Paste samples were cast with a water to binder ratio of 0.6 and 0.46. The pastes were cast in polypropylene containers (250ml) after mixing at 900 rpm/min for 3-4 min. The sealed containers were stored at 20 and 40 °C.

4.2.2.2 Concrete preparation

Eight size fractions of aggregates (except Ben aggregate) were sieved (Table 4-3) and were washed with tap water and dried at 80 °C for 2 days. The size fraction of concrete samples made of Ben aggregate was 0-4 mm, similar to mortar. 1770 kg/m^3 of aggregate was used to cast the concrete and mortar samples with the cement content of 410 kg/m^3. Aggregates and cement were mixed for 2 minutes, tap water was added during half minute of mixing, and the procedure was followed by 3 minutes of mixing. Concrete samples were cast with a water to binder ratio of 0.46.

Table 4-3 Size fraction of aggregate

Size fraction (mm)	Wt. %
0.16 - 0.32	5
0.32 - 0.63	5
0.63 - 1.25	5
1.25 - 2.50	10
2.50 - 5.00	15
5.00 - 8.00	15
8.00 - 12.50	20
12.50 - 22.40	25

The samples for pore solution extraction were cast in a sealed polypropylene plastic bottles (250ml) and stored at 40 °C. The samples for the expansion study with dimension of 7×7×28 cm (three prisms for each mix) were cast in metal moulds (lubricated with oil) while at both ends of each mould, stainless pins were inserted for measuring the length of the prisms. The moulds were covered with plastic sheet to avoid evaporation, and were demoulded after 24 hours of casting. For the samples with Li, the required amount of LiCl was dissolved in the mix water to obtain 400 mmol/L of Li before mixing, and also to the simulated pore solution. The same procedure was done for the samples booseted with 1.09% of alkali, extra alkali was provided by adding NaOH and considering Na_2O eq. for the target mixes.

4.2.2.3 Pore solution measurements

Pore solution of the concrete and paste samples was extracted using a compression-testing machine. The force was variable for different paste samples from 300 to 900 kN, and from 1400 to 2200 kN for concrete samples (all samples had the same diameter). The extracted pore solution was immediately filtered after extraction using 0.2 μm nylon micro filter. In order to measure pH, 2 ml of the solution was put in a small plastic container and voltage and temperature were measured after 2 minutes of equilibration time with a pH electrode (BlueLine 14 pH, SI Analytics)) and a Lab 850pH meter. The pH readings were calibrated against potassium hydroxide solutions as detailed in [63] and Chapter 2. The remaining solution was immediately diluted 3 or 10 times using ultra-pure water, and stored in the fridge until measuring using Inductively Coupled Plasma Optical Emission Spectrometry (ICP–OES (Shimadzu ICPE–9000)), Ion Chromatography (IC (Thermo Scientific Intergrion HPIC)) or IC (Dionex DP ICS-3000 ion chromatograph).

4.2.2.4 Expansion measurements

The LMC method [43,92] was used to measure ASR expansion. A simplified pore solution for each mix was prepared based on the measured pore solution of the related concrete samples. The following main elements were added to the simplified pore solution: K, Na, Ca and sulfate (from the salts detailed in 4.2.1). Some pore solution data was not available at the

required time and the following assumption was considered to prepare simplified pore solutions. For concrete with MK5 paste and U aggregate, the simplified pore solution was made based on the data of concrete made of PC and U aggregate. For concrete with MK 10 and MK 20 and U aggregate, the simplified pore solutions were prepared based on the data of concrete made of MK 15 paste and U aggregate. After 24 hours of casting, three concrete prisms for each mix were immersed in a box containing 5 L of simplified pore solution and were stored at different temperatures 40 and 60 °C. Each box was sealed (using plastic sheet on top of the box before closing its lid) to avoid solution evaporation. The solution level was kept constant by adding extra water after monthly measurement. The length and the weight of each prism was recorded (after drying with a piece of tissue paper) as a function of time. The percentage of length change was calculated based on the following equation:

$$\frac{\Delta L}{L}(\%) = \frac{Lt - L0}{L0} \times 100$$

Equation 4-1 The percentage of length change

Where Lt is the measured length at desired time and $L0$ is the initial length before expansion (after 3 hours of immersion in the simulated solution). For each mix, the mean value was calculated considering the percentage length change of all 3 specimens.

4.3   Results

4.3.1 Expansion of concrete samples

4.3.1.1 Effect of cementitious materials (W/B=0.46)

Figure 4-2 shows the extent of ASR-expansion of concrete prisms made of different pastes and U aggregate (W/B=0.46) as a function of time a) at 40 °C and b) at 60 °C.
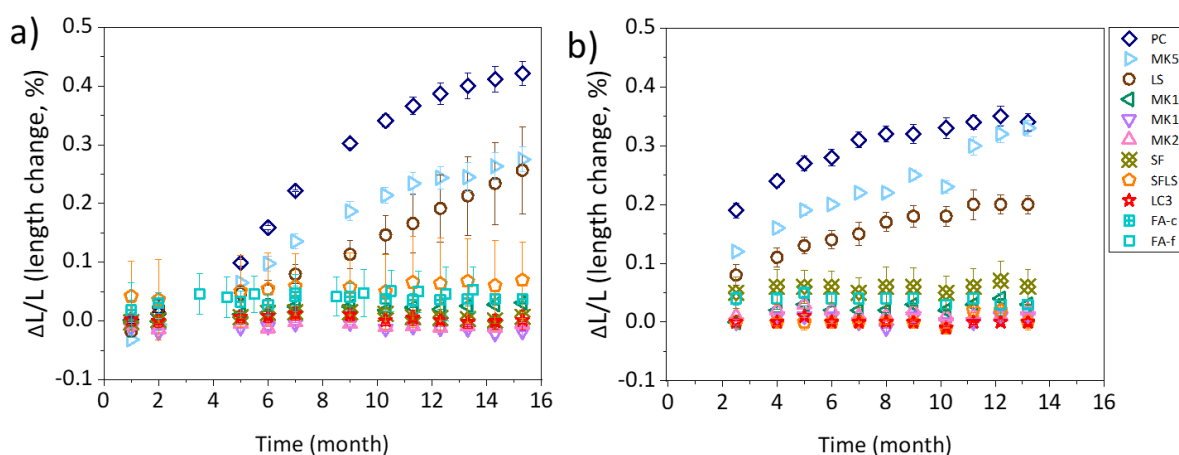
Figure 4-2 The extent of ASR-expansion of concrete prisms made of different pastes and U aggregate (W/B=0.46) as a function of time a) at 40 °C and b) at 60 °C.

Concrete prisms made of PC showed the highest expansion at both temperatures. Increasing the temperature causes a faster rate of expansion [93], while in some expansion test, alkali leaching caused lower expansion rate at higher temperature [94]. For the concrete sample made of PC 70% LS 30% and PC 95% MK 5%, the slightly lower expansion is due to dilution effect. None of the samples containing FA, MK≥10% and SF showed any expansion up to 15 months at both temperatures.

4.3.1.2 Effect of extra alkali

Figure 4-3 shows the effect of extra alkali (1.09%, addition of NaOH) on the extent of ASR-expansion for concrete prisms made of different paste and U aggregate (W/B=0.46) as a function of time a) at 40 °C and b) at 60 °C.
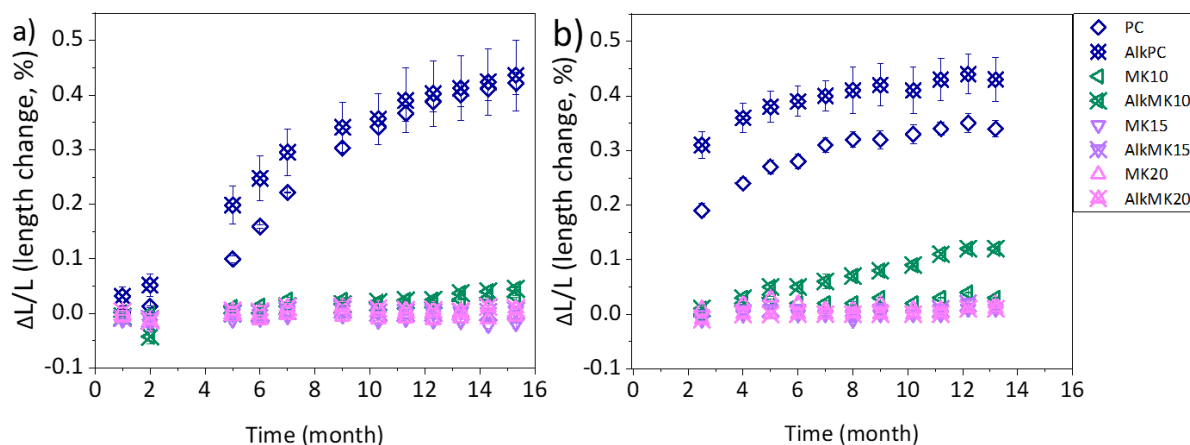
Figure 4-3 The effect of extra alkali (1.09%) on the extent of ASR-expansion for concrete prisms made of different paste and U aggregate (W/B=0.46) as a function of time a) at 40 °C and b) at 60 °C.

Addition of extra alkali causes higher dissolution rate of reactive aggregates due to higher pH of the pore solution and also more alkali to form ASR products. The addition of alkali (1.09%) to PC slightly increased the extent of expansion at 60 °C, while there was a slightly accelerating effect at 40°C. Addition of alkali (1.09%) to the pastes with high metakaolin content (MK 15 and 20% of replacement) did not affect the extent of expansion at both temperatures. Although the boosted sample with alkali 1.09% and MK10 did not expand at 40 °C, the same sample at 60 °C showed some expansion, which is very low in comparison to Alkali 1.09% +PC.

4.3.1.3 Lithium effect

Figure 4-4 demonstrates the effect of Li addition on the extent of ASR-expansion for concrete prisms made of different paste and U aggregate (W/B=0.46) as a function of time a) at 40 °C and b) at 60 °C.
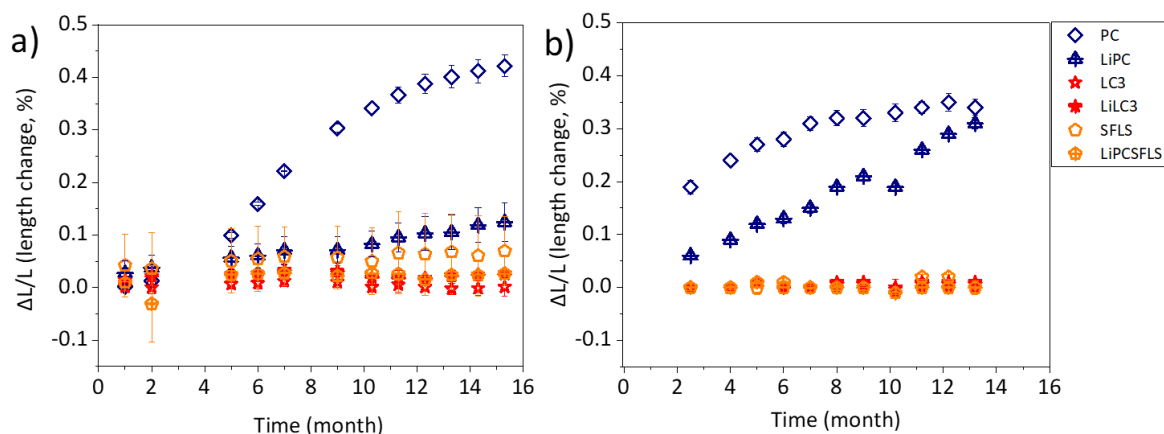
Figure 4-4 The effect of Li addition on the extent of ASR-expansion for concrete prisms made of different pastes and U aggregate (W/B=0.46) as a function of time a) at 40 °C and b) at 60 °C.

Addition of 400mM LiCl to PC decreased the extent of expansion at 40 °C, however at 60 °C, 400mM LiCl + PC 100% concrete prisms expanded significantly more than samples stored at 40 °C.

Although modification of ASR products were reported in the presence of lithium, Higher expansion was measured by adding small amounts of LiOH and Li_2CO_3 [55]. The lower expansion rate in the presence of Li also was reported in shorter period of time [8]. Therefore, as lithium is supposed to modify ASR products, its efficiency to control ASR expansion seems to depend on different factors such as temperature, the composition of aggregate and the reaction period.

4.3.2 The effect of paste composition on the pore solution composition from paste samples (W/B=0.6)

The study of pore solution compositions was done at two temperatures, 20 and 40 °C. Figure 4-5 shows a) the amount of alkalis (mmol/L) in the pore solution expressed from different pastes (W/B=0.6) and b) measured pH values as a function of time at 40 °C.
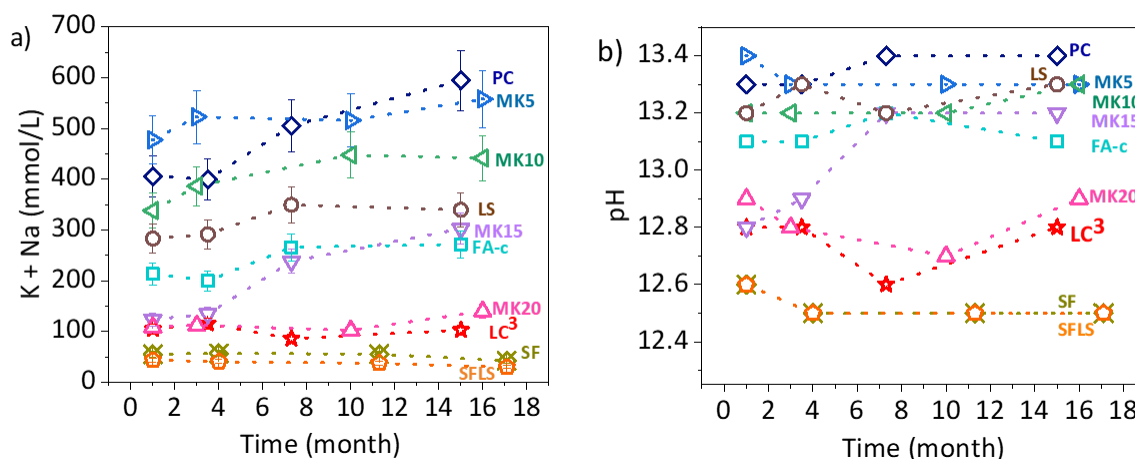
Figure 4-5 a) The amount of released alkalis (mmol/L) from different pastes (W/B=0.6) and b) pH values as a function of time at 40 °C.

At 40 and 20°C (see Table 4-4 for results at 20 °C), SF, SFLS and LC^3 released the lowest amount of alkalis in pore solution up to 17 months. The alkali content in the pore solution was almost constant for all samples; however, for PC and MK 15, the increasing trend is clear.

Figure 4-6 shows the amount of released alkalis (mmol/L) from PC and LC^3 with different water to binder ratio (W/B=0.46 and 0.6) after 28 days and at 40 °C.
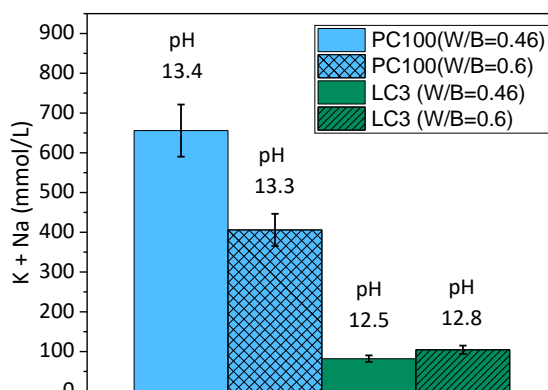
Figure 4-6 The amount of released alkalis (mmol/L) from PC and LC^3, with W/B=0.46 and 0.6 after 28 days and at 40 °C.

PC with lower W/B value released higher alkali in the pore solution in comparison with the PC sample with higher W/B; however for LC³ the changes of alkali content in pore solution with W/B is negligible. The pH values in the case of PC are almost the same for the samples with different water to binder ratios while for LC³ slightly lower pH was measured for the sample with lower water to binder ratio. The same trends of alkali and pH of pore solution were observed after 3.5 months for PC and 3 months for LC³ (Table 4-4).

Figure 4-7 shows the amount of released Al (mmol/L) from different pastes (W/B=0.6) at 40 °C as a function of time.
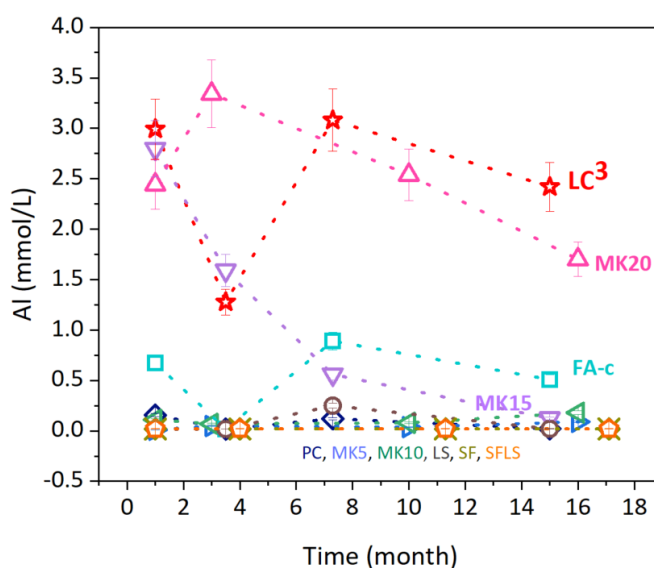
Figure 4-7 The concentration of Al (mmol/L) in the pore solution of different pastes (W/B=0.6) as a function of time at 40 °C.

Comparison of the measured Al concentrations at 20 and 40 °C (see Table 4-4 for results at 20 °C) confirms that increase of temperature increases the amount of Al in the pore solution. Moreover, the more metakaolin was present, the higher the Al concentration were measured. The LC³ blend with 15% MK has the highest concentration of Al in pore solution at both temperatures (20 and 40°C).

The measured results are in agreement with the previous reports, where an increase in Al concentration in the pore solution was measured for Al-rich SCMs replacement in blended cement pastes [42,43]. For blended cement, the amount of alkali depends also on the amount of alkali in SCMs [82–84]. Pore solution of PC contains the highest amount of alkali and thus pH values (Figure 4-5). In this case, high Ca/Si C-S-H forms, which binds less alkali, and therefore, more alkali remains in the pore solution [4]. For those samples wih Si-rich SCMs such as FA, MK and SF, the alakli content is not only lowered by teh dissolution of the PC, but also by the lowering of Ca/Si in C-S-H, which increases the alkali uptake by C-S-H (cit), and thus lowers the alklai concentration in the solution.

4.3.3 The effect of aggregate mineralogy on solution composition of a) PC on b) blended cements

Figure 4-8 shows the amount of alkalis (mmol/L) in the pore solution of PC or LC[3] pastes (No agg.) and different concretes made of PC or LC[3] and different aggregates (W/B=0.46); and pH values after 28 days at 40 °C. Pore solutions of concretes made of PC with Cal, U and B had slightly lower alkali concentrations in comparison with the PC paste and concrete made with P aggregate. Surprisingly, the pore solution of concrete made of PC with Ben aggregate showed the lowest alkali concentrations. For LC[3], pore solutions of concrete samples made of P, Cal and U aggregates had slightly higher alkali concentrations compared to the paste (no. agg.), and again very low alkali concentrations were measured for the concrete made of Ben aggregate.
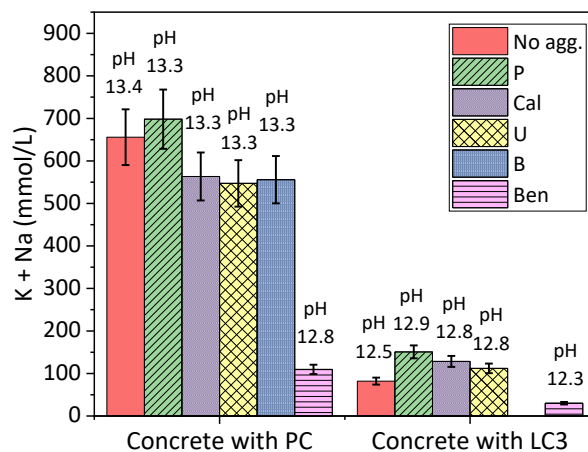
Figure 4-8 The amount of released alkalis (mmol/L) from PC or LC³ pastes (No agg.) and different concretes made of PC or LC³ and different aggregates (W/B=0.46); and pH values after 28 days at 40 °C.

Various reactions may affect alkali concentration; release of alkali due to feldspar dissolution within aggregate; uptake of alkali by C-S-H; uptake of alkali by silica from aggregate or by ASR products. Compared to the same samples made with PC, the total amount of alkalis for the samples made by LC³ are dramatically lower.

Figure 4-9 shows the Al concentration (mmol/L) of the extracted pore solution from PC or LC³ pastes (No agg.) and different concrete samples made of PC or LC³ and different aggregates (W/B=0.46) after 28 days at 40 °C.
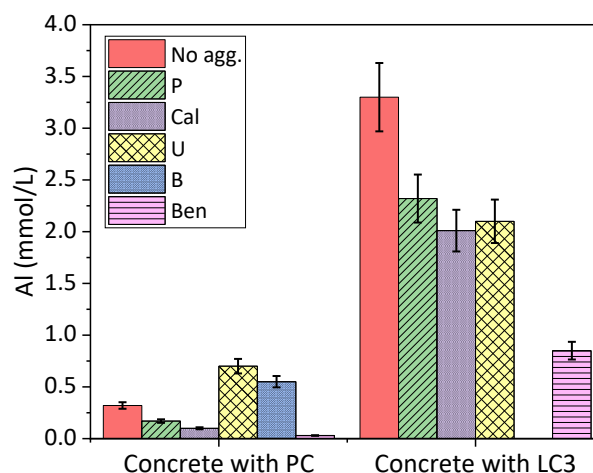
Figure 4-9 The Al concentration (mmol/L) of the extracted pore solution from PC or LC^3 pastes (No agg.) and different concrete samples made of PC or LC^3 and different aggregates (W/B=0.46) after 28 days at 40 °C.

The amount of Al in the pore solution is very low for PC and all concrete samples made of PC, and the maximum amount of Al in pore solution belongs to concrete samples made of U and B aggregates (probably due to feldspar dissolution, as U and B samples contain 24 and 50 wt.% of feldspars). For concrete samples made of LC^3 and P, Cal and U aggregates, the amount of Al is lower. For concretes made of Ben aggregate this drop in Al concentration is higher. In our previous work, it was shown that 1mM of Al decreased dissolution rate of silica (quartz & amorphous silica) noticeably at 40 °C (note that the pH values in this paper are reported at 25 °C, and in our previous work at 40°C) (3.3.2). Therefore, for concrete samples made with LC^3, there is still an effective amount of Al in the pore solution to suppress ASR. For older samples (after 3-4 months of casting), the same trends of alkali and Al concentrations were measured for all samples made of PC or LC^3 pastes and the mentioned concretes (Table 4-5).

4.3.4 Effect of alkali and pH in the pore solution on expansion

The rates of expansion for concrete samples (%/month) were calculated from the slope of the expansion curves as a function of time at 40 °C up to 15 months (shown in Figure

4-2). By assuming that the pore solution composition does not change noticeably after 1 month, the alkali content of the pore solution was taken after 1 month (For MK5, 10 and 20 after 1.7 months) and at 40 °C (Table 4-6).

Figure 4-10 shows the rate of expansion (%/month) as a function of K + Na (mmol/L) in the extracted pore solution from different concretes made of U aggregate (W/B=0.46) after 1/1.7 months and at 40 °C. The higher pH values and alkali concentrations in the pore solution accelerated ASR expansion. The apparent threshold is below 300 mmol/L of total amount of alkalis (K + Na) in the pore solution.
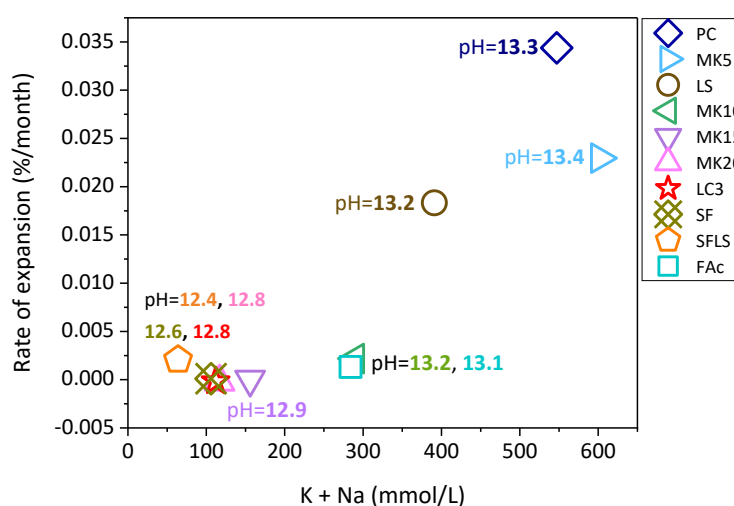
Figure 4-10 The rate of expansion (%/month) as a function of K + Na (mmol/L) in the extracted pore solution from different concretes made of U aggregate (W/B=0.46) after 1/1.7 months and at 40 °C.

For this length of exposure, the expansion results show no difference between SF and MK samples. While we expect the MK samples to be more efficient to supress ASR in the long term, as the blended cement pastes with metakaolin > 10%, in addition to having low alkali content in the pore solution, release higher Al concentration. For the more expanded samples, PC, MK 5 and LS, the Ca and sulfate concentrations were higher than the other samples (except samples containing SF) (Table 4-6).

In our previous study (Chapter 3), dissolution experiments revealed that Ca and sulfate in-crease silica and feldspar dissolution at high pH, which both minerals are present in U aggre-gate. However, the amount of alkali and pH values showed a clearer trend for the ASR expan-sion for all concrete samples. Thus, the present results can be explained purely on the basis of pH.

4.4　Conclusions

Measuring of ASR expansion for concrete samples, made of ASR-reactive Swiss ag-gregate (U aggregate) and different cement pastes, revealed the highest expansion rate for the paste having 100% of Portland cement at 40 and 60 °C. However, all concrete samples containing fly ash, metakaolin (≥10%) and micro silica showed no expansion at either temper-ature over the experiment duration (14/15 Months). The higher expansion rates were meas-ured at higher temperature. Addition of extra alkali (1.09%) accelerated expansion rate at higher temperature (60 °C), but no effect was observed at 40 °C. Addition of 400mM LiCl slowed down the expansion rate at 40 °C, however at 60 °C, higher expansion rate was meas-ured. The effect of paste composition on the pore solution composition in long term showed that LC^3 and blended pastes having SF provided the lowest alkali and hydroxide contents in the pore solution up to 17 months. The noticeable effect of aggregate mineralogy was meas-ured on the alkali content of pore solution. The Bend aggregate, which contains mainly feld-spar, up took up a huge amount of alkali from the pore solution of concrete made of Portland cement paste. Therefore, up taking alkali by silica from aggregate is another reaction to affect alkali content of the pore solution. A clear trend of alkali content in the pore solution was observed on the extent of ASR expansion. The highest extent of expansion was measured for the concrete samples with high alkali and hydroxide contents within their pore solutions at 40 °C.

Table 4-4 Elemental concentrations (mmol/L) and pH values in the pore solution from different paste samples at different temperatures (°C)

Paste (wt.%)	W/B	Storage temperature (°C)	Time (month)	K (mmol/L)	Na (mmol/L)	Al (mmol/L)	Ca (mmol/L)	Sulfate [1] (mmol/L)	Si (mmol/L)	pH [2]	Pressure (KN)	Technique
PC 100	0.6	20	1	316	89	0.68	1.37	2.46	0.35	13.3	300	ICP-OES
			3.5	302	86	0.02	1.83	2.92	0.02	13.4	400	
			7.3	408	114	0.17	1.70	8.43	0.15	13.4	800	IC
			15	405	124	0.07	1.73	8.79	< LOQ [3]	13.4	900	
		40	1	315	91	0.16	1.90	14.90	0.14	13.3	400	ICP-OES
			3.5	305	95	0.02	1.74	17.85	0.02	13.3	400	
			7.3	394	111	0.12	1.74	27.04	0.10	13.4	800	IC
			15	457	137	0.02	3.29	28.68	< LOQ	13.4	900	
	0.46		1	527	129	0.32	1.58	35.63	0.27	13.4	400	IC
			3	528	134	0.10	1.55	39.70	0.13	13.4	450	
PC 95 + MK 5	0.6	20	1	261	136	0.04	2.28	0.97	< LOQ	13.3	800	IC
			3	310	182	0.06	2.50	2.56	< LOQ	13.3		
			10	343	199	0.07	1.92	7.06	0.15	13.3		
			16	345	196	0.08	1.86	7.99	< LOQ	13.3		
		40	1	310	167	0.01	3.96	13.36	< LOQ	13.4	800	IC
			3	328	195	0.05	2.58	19.64	< LOQ	13.3		
			10	325	191	0.04	2.03	20.08	0.04	13.3		
			16	352	206	0.09	2.12	35.94	< LOQ	13.3		
PC 90 + MK 10	0.6	20	1	177	100	0.77	1.12	0.47	< LOQ	13.2	800	IC
			3	191	121	0.76	1.41	0.76	< LOQ	13.2		
			10	211	133	0.40	2.00	1.34	0.20	13.2		
			16	208	140	0.25	1.45	1.87	< LOQ	13.2		
		40	1	210	128	0.11	1.63	3.45	< LOQ	13.2	800	IC
			3	235	152	0.07	4.64	8.96	< LOQ	13.2		
			10	275	172	0.08	3.14	16.66	0.06	13.2		
			16	267	174	0.18	2.63	19.92	< LOQ	13.3		

Paste (wt.%)	W/B	Storage temperature (°C)	Time (month)	K (mmol/L)	Na (mmol/L)	Al (mmol/L)	Ca (mmol/L)	Sulfate [1] (mmol/L)	Si (mmol/L)	pH [2]	Pressure (KN)	Technique
PC 85 + MK 15	0.6	20	1	128	45	1.72	0.73	0.52	0.35	13.0	700	ICP-OES
			3.5	135	55	0.68	0.70	0.45	0.02	13.1		
			7.3	166	66	1.50	0.90	0.87	0.25	13.1	800	IC
			15	177	75	0.46	1.00	0.72	< LOQ[3]	13.3	900	
		40	1	92	32	2.80	0.59	9.00	0.58	12.8	700	ICP-OES
			3.5	97	38	1.59	0.71	9.99	0.54	12.9	700	
			7.3	170	67	0.56	0.95	4.37	0.22	13.2	400	IC
			15	214	89	0.12	2.41	5.80	< LOQ	13.2	400	
PC 80 + MK 20	0.6	20	1	90	62	1.90	1.15	0.35	0.08	13.0	800	IC
			3	86	63	2.45	1.27	0.36	0.08	12.9		
			10	90	68	1.51	0.92	0.58	0.22	13.0		
			16	93	79	1.42	1.05	0.78	0.17	13.0		
		40	1	62	46	2.44	0.99	1.46	0.18	12.9	800	IC
			3	64	48	3.34	0.89	7.92	0.29	12.8		
			10	55	47	2.54	0.60	6.60	0.38	12.7		
			16	77	63	1.70	1.17	3.65	0.24	12.9		
PC 70 + FA 30	0.6	20	1	234	72	0.16	2.99	0.97	0.07	13.2	400	ICP-OES
			3.5	172	62	0.62	0.97	0.95	0.02	13.2	400	
			7.3	213	73	0.48	1.31	2.08	0.25	13.2	800	IC
			15	219	78	0.83	1.68	1.38	< LOQ	13.2	900	
		40	1	161	52	0.67	1.07	2.46	0.29	13.1	400	ICP-OES
			3.5	144	55	0.02	0.97	13.52	0.02	13.1	400	
			7.3	196	70	0.89	0.80	6.04	0.30	13.2	800	IC
			15	196	75	0.51	1.11	3.72	< LOQ	13.1	900	

Paste (wt.%)	W/B	Storage temperature (°C)	Time (month)	K (mmol/L)	Na (mmol/L)	Al (mmol/L)	Ca (mmol/L)	Sulfate [1] (mmol/L)	Si (mmol/L)	pH [2]	Pressure (KN)	Technique
LC³ PC70MK15LS15	0.6	20	1	77	34	1.82	0.76	0.37	0.25	12.9	500	ICP-OES
			3.5	81	35	0.90	0.89	0.29	0.02	12.9	600	
			7.3	106	45	1.95	0.91	0.76	0.27	12.9	800	IC
			15	108	47	1.98	0.98	0.57	0.04	13	900	
		40	1	72	33	2.99	0.59	4.81	0.37	12.8	500	ICP-OES
			3.5	80	36	1.28	0.66	3.81	0.02	12.8	600	
			7.3	58	27	3.08	0.40	12.41	0.49	12.6	400	IC
			15	70	33	2.42	0.54	5.98	0.21	12.8		
	0.46		1	59	23	3.3	0.44	12.12	0.44	12.5	400	IC
			3	59	24	2.6	0.66	13.37	0.51	12.5	450	
PC 70 + LS 30	0.6	20	1	215	65	0.02	1.51	1.03	0.02	13.3	300	ICP-OES
			3.5	208	66	0.02	2.94	1.55	0.02	13.3	400	
			7.3	286	84	0.08	2.53	3.90	0.09	13.3	800	IC
			15	287	92	0.03	4.16	2.85	< LOQ[3]	13.3		
		40	1	218	65	0.02	2.32	5.40	0.02	13.2	300	ICP-OES
			3.5	220	71		3.13	7.55	0.02	13.3		
			7.3	267	82	0.25	1.89	7.60	0.14	13.2	400	IC
			15	257	82	< LOQ	3.39	5.62	< LOQ	13.3		
PC70LS15SF15	0.6	20	1	27	25		14.83	0.24	0.04	12.7	500	IC
			4	16	18	< LOQ	5.92	0.10	0.06	12.5		
			11.3	11	14		8.27	0.13	0.08	12.4		
			17.1	9	12		9.61	0.21	< LOQ	12.5		
		40	1	20	23		7.26	0.34	0.12	12.6	500	IC
			4	17	24	< LOQ	3.46	0.39	0.21	12.5		
			11.3	14	23		7.23	0.42	0.10	12.5		
			17.1	11	19		8.21	0.36	< LOQ	12.5		

Paste (wt.%)	W/B	Storage temperature (°C)	Time (month)	K (mmol/L)	Na (mmol/L)	Al (mmol/L)	Ca (mmol/L)	Sulfate [1] (mmol/L)	Si (mmol/L)	pH [2]	Pressure (KN)	Technique
PC 85 + SF 15	0.6	20	1	40	34		7.76	0.24	0.09	12.7	500	IC
			4	26		< LOQ[3]	0.18	0.26	8.64	12.5		
			11.3	23	27		0.20	0.22	7.46	12.4		
			17.1					0.30	13.21	12.4		
		40	1	26	29		6.37	0.36	0.11	12.6	500	IC
			4	25	32	< LOQ	0.24	0.63	4.64	12.5		
			11.3	23			0.41	0.65	3.95	12.5		
			17.1	18	25		2.43	0.48	0.33	12.5		

1) Sulfate concentrations were measured using IC for all samples
2) The pH values were measured at 25 °C.
3) LOQ = Limit of Quantification

Table 4-5 The ion concentrations (mmol/L) in the pore solution from different concretes (W/B=0.46) at 40 °C, measured using IC and the pH values

Paste (wt.%)	Aggregate	Time (month)	K (mmol/L)	Na (mmol/L)	Al (mmol/L)	Ca (mmol/L)	Sulfate (mmol/L)	Si (mmol/L)	pH [1]	Pressure (KN)
PC 100	U	1	421	126	0.70	0.86	27.76	0.78	13.3	1800
		3	378	124	0.14	0.55	30.83	3.00	13.2	
	P	1	496	202	0.17	0.93	51.83	1.36	13.3	2000
		3	474	206	0.36	0.17	53.80	12.46	13.3	
	B	1	346	210	0.55	0.87	22.71	1.10	13.3	
		4	375	241	0.25	0.75	38.03	0.96	13.3	
	Ben	1	17	93	0.03	3.82	0.53	0.03	12.8	
		4	22	108	0.08	1.93	1.31	0.10	12.8	2200
	Cal	1	347	217	0.10	1.21	21.80	0.04	13.3	2000
		4	379	246	0.19	1.15	34.77	< LOQ[2]	13.3	
LC³ PC70MK15LS15	U	1	76	36	2.10	0.58	3.10	0.40	12.8	1400
		3	70	37	1.22	0.63	5.30	0.49	12.7	
	P	1	109	42	2.32	0.32	4.99	1.09	12.9	2000
		3	114	43	1.99	0.56	5.96	0.74	12.9	
	Ben	1	8	22	0.85	4.12	0.66	0.24	12.3	
		3	7	20	0.75	2.40	0.63	0.20	12.2	2200
	Cal	1	87	42	2.01	0.29	2.98	0.64	12.8	1800
		3	93	46	1.85	0.49	3.44	0.41	12.9	2000

1) The pH values were measured at 25 °C.
2) LOQ = Limit of Quantification

Table 4-6 The ion concentrations (mmol/L) in the pore solution from different concretes (W/B=0.46) with U aggregate at 40 °C, measured using IC and the pH values

Paste (wt.%)	Time (month)	K (mmol/L)	Na (mmol/L)	Al (mmol/L)	Ca (mmol/L)	Sulfate (mmol/L)	Si (mmol/L)	pH [1]	Pressure (KN)
PC 100	1	421	126	0.70	0.86	27.76	0.78	13.3	1800
	3	378	124	0.14	0.55	30.83	3.00	13.2	
PC95+MK5	1.7	443	159	0.07	2.51	2.00	< LOQ[2]	13.4	
PC90MK10	1.7	204	86	0.45	0.86	3.57	0.18	13.2	
PC85MK15	1	86	70	1.83	0.44	2.37	0.52	12.9	
	4	84	71	1.58	0.60	3.28	0.42	12.9	
PC80MK20	1.7	75	42	2.29	0.58	2.50	0.40	12.8	
LC³ (PC70MK15LS15)	1	76	36	2.1	0.58	3.10	0.40	12.8	
	3	70	37	1.2	0.63	5.30	0.49	12.7	2000
PC70FA30	1	172	112	0.50	0.70	6.17	0.69	13.1	
	4	144	103	0.43	0.79	7.63	0.83	13.0	
PC70LS30	1	230	161	0.05	1.63	9.46	0.13	13.2	
	4	187	155	0.09	0.98	12.29	0.97	13.1	
PC70SF15LS15	1	32	32	0.04	4.46	11.71	0.08	12.4	
	4	40	38	0.07	2.33	15.72	0.11	12.5	
PC85SF15	1	57	49	0.05	2.18	13.37	0.19	12.6	
	4	66	59	0.1	2.08	15.69	0.13	12.7	

1) The pH values were measured at 25 °C.
2) LOQ = Limit of Quantification

Acknowledgements:

Supplementary information

Calorimetry

a)

b)
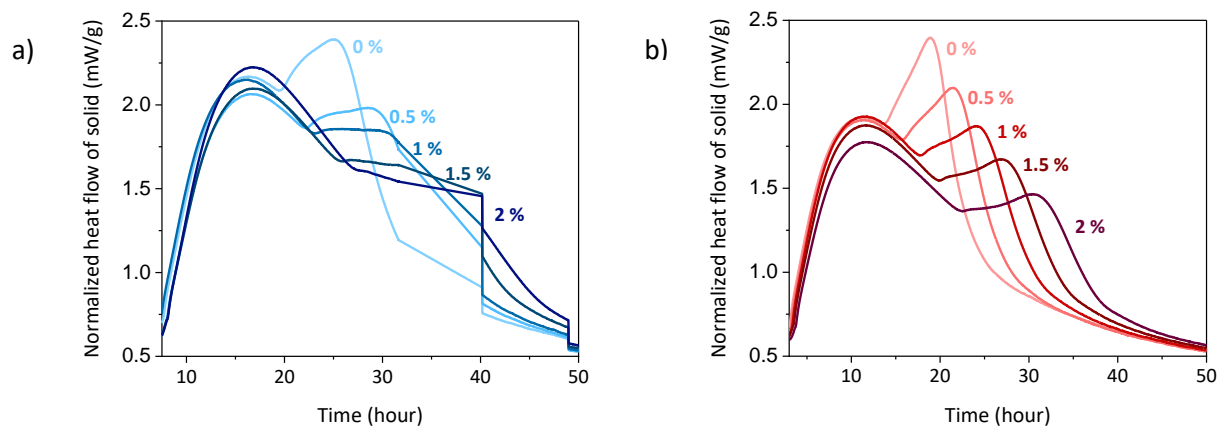
Figure 4-11 Normalized heat flow of a) PC85MK15 and b) LC^3 (mW/g) with different gypsum content.

Chapter 5   Conclusions and perspectives

5.1   Conclusions

The main goal of the present project was to identify the main factors affecting the dissolution kinetics of reactive minerals within natural aggregates. Since natural aggregates can have very complicated mineralogy, the dissolution kinetics of model solids was studied with different approaches; solution analysis and the scratch-tracking method. The scratch-tracking method was introduced as a new image-based method. This method helps to have a closer look at the dissolution kinetics of the solid surfaces; where formation of new precipitates causes uncertainties and misunderstanding in the interpretation of measurements from the solution study.

In parallel, the evolution of the pore-solution composition was tracked for different pastes in long term experiments. As ASR is a long-term reaction, this analysis provides useful knowledge of pore solution composition in long term. Adding aggregates to cement paste provides new surfaces for further reactions in a concrete sample. Therefore, the effect of aggregate mineralogy was investigated on pore solution composition. Finally, the expansion tests (based on LMC method) were done at different temperatures to determine which concrete samples were resistant to ASR. The expansion results gave an insight into the link between the results of the dissolution experiments and the pore solution analysis.

The ASR reactivity of three aggregates from different locations in Switzerland was investigated using conventional expansion and dissolution tests. The scratch-tracking method revealed the faster dissolutions of feldspar and quartz, while mica reacted negligibly. These observations were confirmed by solution analysis, which showed a clear increase of dissolved Si for all aggregates and of K and Al for the aggregates rich in feldspar. Similar trends were measured in expansion and aggregate dissolution experiment. However, dissolution experiments and expansion tests are different and both tests have complex interactions. Therefore, the extent of ASR expansion cannot be simply correlated to the dissolution results.

The dissolution rates of the amorphous and crystalline model solids were studied at different temperatures and at high pH. The solution analysis was done to calculate the dissolution rates based on the amount of released Si from each solid. For example, Figure 5-1 shows the summary of dissolution rates of amorphous silica in different solutions at 40 °C. In comparison with silica dissolution rate in reference solution (400mM of KOH), among all elements, the only efficient element to slow down silica dissolution is aluminum. The higher concentration of aluminum was added to the solution, the lower dissolution rate was measured. Even though a high water to solid ratio was used in the experiments to try and avoid precipitation, the formation of C-S-H and lithium silicates were observed, which interfered with the interpretation of the dissolution rates. However, the dissolution could be quantified directly using the scratch-tracking method. In the case of Cs and sulfate, further investigation is needed to clarify the real effect of these elements as scratch-tracking method indicated increase in dissolution rate of quartz in the presence of sulfate.
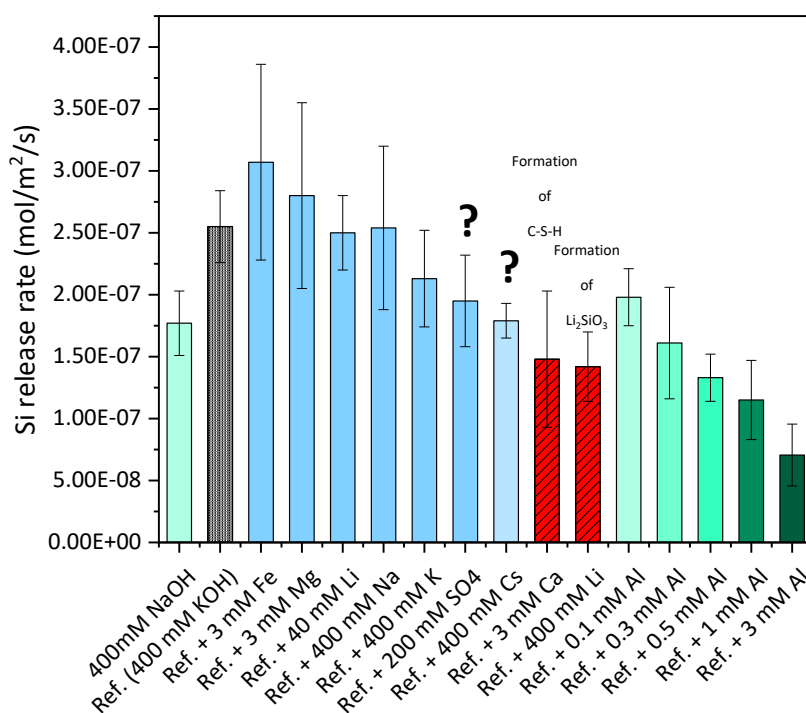
Figure 5-1 The summary of dissolution rates of amorphous silica in different solutions at 40 °C

Figure 5-2 shows an overview of dissolution results based on both solution study and scratch-tracking method for quartz, feldspars and amorphous silica. The dissolution results at high pH showed an

increase in dissolution rates of quartz and feldspars in the presence of lithium, calcium and sulfate, while, no significant effect was measured in the presence of iron, magnesium and additional NaCl, KCl or CsCl. However, slower dissolution rates of quartz, amorphous silica and Na and K-feldspar at 20, 40 and 60 °C were measured in the presence of aluminium.
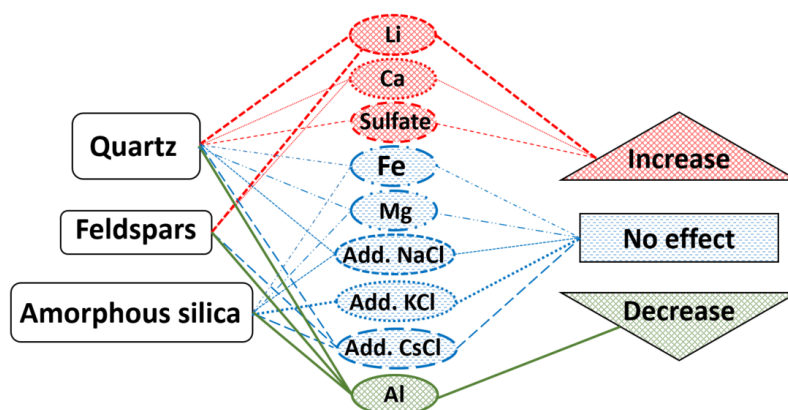
Figure 5-2 The summary of dissolution results

The pore solution analysis indicated that the pastes containing metakaolin provide the highest amount of Al and the lowest amount of alkalis up to 15-17 months. The pore solution results of mortar samples made of the Bend aggregate, rich in feldspars, showed this aggregate up took a significant amount of alkalis from the pore solution. This highlights the effect of aggregate mineral-ogy on the composition of the pore solution for mortars and concretes.

The noticeable effects of temperature, alkali and pH of pore solution were observed on the extent of ASR expansion for concretes, made of Swiss ASR-reactive aggregate and different cement pastes. The lowest ASR expansion values were measured for the concretes made of blended cement pastes with low alkali and hydroxide content in their pore solutions. The addition of 1.09% of extra alkali had no effect on the expansion trends for samples made of PC and blended cement pastes with different relatively high substitutions of metakaolin (10, 15 and 20% of metakaolin in the cement paste) at 40 °C. While at 60 °C, higher expansion was observed for the samples made of PC and blended cement paste with 10% substitution of metakaolin, in contrast to the samples made of

blended cement pastes with 15 and 20% substitutions of metakaolin. The presence of 400mN of Li slowed down expansion at 40 °C, while, noticeably higher expansion was measured at 60 °C.

5.2 Perspectives

Figure 5-3 shows schematically the different steps of ASR. ASR initiates due to the dissolution of silica-containing minerals within reactive aggregate, resulting in formation of ASR products in the presence of calcium and alkalis from the pore solution. The filling of macroscopic cracks with ASR products creates additional cracks, and this process continues to create a network of ASR cracking in concrete.

Different factors affect the dissolution of silica-containing minerals within aggregates, and consequently the extent of ASR expansion such as moisture, temperature and composition of pore solution within concrete. In addition, if aggregates may react with the pore solution and they release or take up alkalis (as it was shown in the present study for the Bend aggregate), and so in turn influence the reaction. Therefore, the type of the aggregates used and the paste composition affect the composition of pore solution, and then the composition of pore solution changes the dissolution kinetics of silica-containing minerals within aggregates. The use of local aggregate is desirable economically and the environmental factors cannot be controlled. Indeed, the adjustable aspect is the change of pore solution composition to slow down aggregate dissolution, formation of ASR products and suppress ASR. This goal is achievable by the use of appropriate blended cement pastes with Supplementary Cementitious Materials (SCMs).
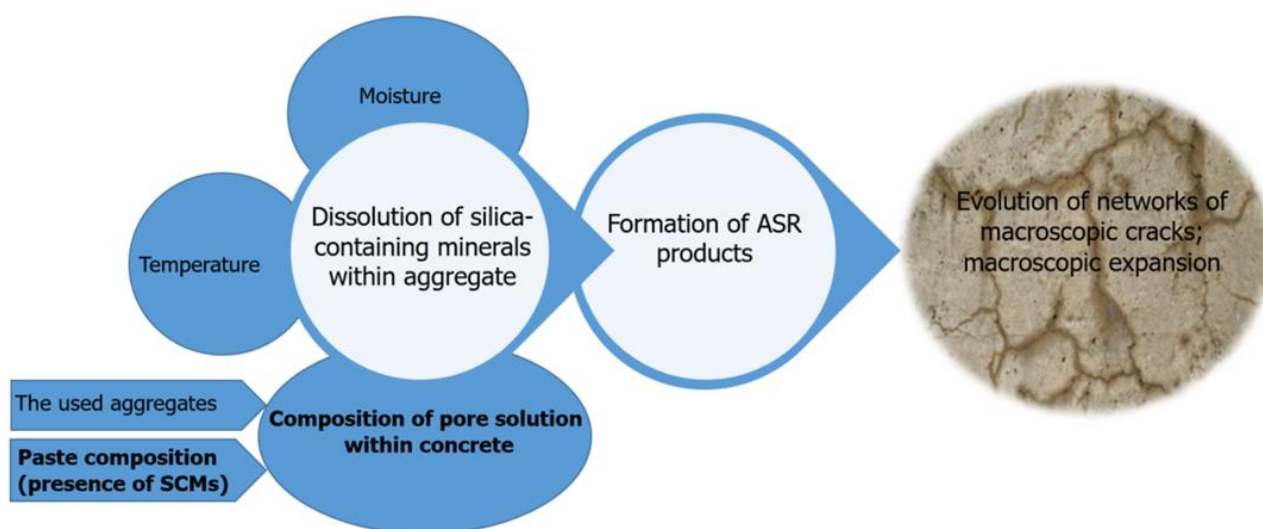
Figure 5-3 Overview of the steps of ASR, and the factors affecting the extent of expansion.

In order to introduce the best paste composition to lower damage risk, ASR-reactivity of aggregate should be assessed, as the first step. It is essential to identify the type and the amount of reactive minerals in the target aggregate. After that, it would be possible to find the appropriate substitution of SCMs in the cement paste to control the dissolution kinetics of these reactive minerals within the target aggregate. However, the results of this project indicated how the formation of new solids during dissolution experiments gives misleading results if the ASR-reactivity of aggregate is assessed directly in the solution. Moreover, it is impossible to indicate the type of reactive minerals using solution analysis. For example, if both quartz and feldspars are present in an aggregate, by measuring solution composition, the source of measured Si due to dissolution in unclear. Also, new protocols to assess ASR-reactivity of aggregate are needed to be introduced after analysing the majority of natural aggregates.

A new image-based method was introduced in the present project to find which minerals within an aggregate are reactive. The effect of solution composition on the extent of dissolution was assessed in the presence of the same amount of hydroxide and pH values. The sensitivity of the scratch-tracking method to different pH values can be tested. After that, this method can help to study the dissolution of minerals in different pH values.

The results showed the Bend aggregate has a noticeable tendency to up take alkalis from the pore solution. However, it is not clear how this phenomenon affects the dissolution rate and ASR reactivity. This is important as ASR in concrete occurs where a small volume of pore solution is present. Further investigations should be done to answer these questions.

The pore solution composition and ASR-expansion were investigated for concrete samples in this project; however, analysing the composition and structures of ASR products provide more information about the mechanisms, which the use of blended cement paste slows down ASR.

The results of the pore solution study and the extent of ASR expansions revealed the dominant effect of alkalis on the ASR expansion where the samples made of blended cement pastes, low in both alkali and aluminium in the pore solution, showed no expansion at both 40 and 60 °C. Also, longer term investigations should be done to clarify the real effect of aluminium on slowing down ASR for the blended cement pastes with Al-rich SCMs such as metakaolin.

The effect of lithium on ASR is still unclear. The scratch-tracking method revealed a higher dissolution rate in the presence of lithium. More studies should be done to clarify the real lithium effect on ASR expanding in concretes.

References

[1]   L. Valentini, M. Favero, M.C. Dalconi, V. Russo, G. Ferrari, G. Artioli, Kinetic model of calcium-silicate hydrate nucleation and growth in the presence of PCE superplasticizers, Cryst. Growth Des. 16 (2016) 646–654. doi:10.1021/acs.cgd.5b01127.

[2]   T. Chappex, K.L. Scrivener, The effect of aluminum in solution on the dissolution of amorphous silica and its relation to cementitious systems, J. Am. Ceram. Soc. 96 (2013) 592–597. doi:10.1111/jace.12098.

[3]   A. Merz, C., Leemann, Validierung der AAR-Prüfungen für Neubau und Instandsetzung, 2012.

[4]   T. Chappex, K. Scrivener, Alkali fixation of C-S-H in blended cement pastes and its relation to alkali silica reaction, Cem. Concr. Res. 42 (2012) 1049–1054. doi:10.1016/j.cemconres.2012.03.010.

[5]   L.S. Dent Glasser, N. Kataoka, The chemistry of "alkali-aggregate" reaction, Cem. Concr. Res. 11 (1981) 1–9. doi:10.1016/0008-8846(81)90003-X.

[6]   F. Rajabipour, E. Giannini, C. Dunant, J.H. Ideker, M.D.A. Thomas, Alkali-silica reaction: current understanding of the reaction mechanisms and the knowledge gaps, Cem. Concr. Res. 76 (2015) 130–146. doi:10.1016/j.cemconres.2015.05.024.

[7]   L.S. Dent Glasser, N. Kataoka, The chemistry of "alkali-aggregate" reaction, Cem. Concr. Res. 11 (1981) 1–9.

[8]   A. Leemann, L. Lörtscher, L. Bernard, G. Le Saout, B. Lothenbach, R.M. Espinosa-Marzal, Mitigation of ASR by the use of $LiNO_3$ - characterization of the reaction products, Cem. Concr. Res. 59 (2014) 73–86. doi:10.1016/j.cemconres.2014.02.003.

[9]   S.L. Brantley, A.F. White, J.D. Kubicki, Kinetics of Water-Rock Interaction, 2008. doi:10.1007/978-0-387-73563-4.

[10]   A. Leemann, L. Holzer, Alkali-aggregate reaction-identifying reactive silicates in complex aggregates by ESEM observation of dissolution features, Cem. Concr. Compos. 27 (2005) 796–801. doi:10.1016/j.cemconcomp.2005.03.007.

[11]   G. Yuan, Y. Cao, H. Schulz, F. Hao, J. Gluyas, K. Liu, A review of feldspar alteration and its geological significance in sedimentary basins: from shallow aquifers to deep hydrocarbon

reservoirs, Eartf-Sci. Rev. (2019). doi:10.1016/j.earscirev.2019.02.004.

[12] W. Stumm, J.J. Morgan, Aquatic Chemistry: Chemical Equilibria and Rates in Natural Waters, American Library Association, 1996. doi:10.5860/choice.33-6312.

[13] S. Race, ASTM C 289. Annual book of ASTM standards. American society for testing materials., Philadelphia, 1916.

[14] H. Menendez, E., Fournier, B., Santos, A., Justnes, RILEM TC 219-ACS, AAR-8: Determination of alkalis releasable by aggregates in concrete, RILEM/TC-ACS. (2014) 1–12. rilem/tc-acs/aar-8/draft February 14.

[15] S. Chatterji, Chemistry of alkali-silica reaction and testing of aggregates, Cem. Concr. Compos. 27 (2005) 788–795. doi:10.1016/j.cemconcomp.2005.03.005.

[16] SIA MB 2042, Vorbeugung von Schäden durch die Alkali-Aggregat-Reaktion (AAR) bei Betonbauten, Schweizerischer In-genieur- und Architektenverein (2012), https://www.sia.ch/de/dienstleistungen/artikelbeitraege/detail/article/neues-merkblatt-sia-2042/. [Accessed: 11-Jan-2021/ (accessed March 14, 2021).

[17] A. Leemann, C. Merz, Long-term efficiency of silica fume and fly ash to suppress ASR in field structures, Proc. 16th Int. Conf. Alkali-Aggregate React. Concr. (2021) 367–379. https://www.dora.lib4ri.ch/empa/islandora/object/empa%3A25553/ (accessed June 9, 2021).

[18] B.C. Lowekamp, D.T. Chen, L. Ibáñez, D. Blezek, The Design of SimpleITK, Front NEUROINFORM. 7 (2013) 1–14. doi:10.3389/fninf.2013.00045.

[19] C. Bärtschi, Kieselkalke der Schweiz: Charakterisierunq eines Rohstoffs aus geologischer, petroqraphischer, wirtschaftlicher und umweltrelevanter Sicht, Beitr. Geol. Schweiz. Geotechn. 97 (2012) 1–160.

[20] M. Rooms, B. Statements, Standard test method for potential alkali reactivity of aggregates (mortar-bar), Test. 04 (2010) 1–5. doi:10.1520/C1260-14.

[21] 219-ACS : Alkali aggregate reaction in concrete structures: performance testing and appraisal.

[22] A. Leemann, I. Borchers, M. Shakoorioskooie, M. Griffa, C. Müller, P. Lura, Microstructural

analysis of ASR in concrete - accelerated testing versus natural exposure, Proc. Int. Conf. Sustain. Mater. Syst. Struct. (SMSS2019). Durability, Monit. Repair Struct. (2019) 222–229. https://www.dora.lib4ri.ch/empa/islandora/object/empa%3A19231/ (accessed June 8, 2021).

[23] A. Leemann, Z. Shi, J. Lindgård, Characterization of amorphous and crystalline ASR products formed in concrete aggregates, Cem. Concr. Res. 137 (2020). doi:10.1016/j.cemconres.2020.106190.

[24] P.M. Dove, S.F. Elston, Dissolution kinetics of quartz in sodium chloride solutions: analysis of existing data and a rate model for 25°C, Geochim. Cosmochim. Acta. 56 (1992) 4147–4156. doi:10.1016/0016-7037(92)90257-J.

[25] R. Wollast, L. Chou, In Physical and Chemical Weathering in Geochemical Cycles (ed. A. Lerman and M. Maybeck), Springer Netherlands, 1988. doi:10.1007/978-94-009-3071-1.

[26] P. V. Brady, J. V. Walther, Kinetics of quartz dissolution at low temperatures, Chem. Geol. 82 (1990) 253–264. doi:10.1016/0009-2541(90)90084-K.

[27] W.A. House, D.R. Orr, Investigation of the pH dependence of the kinetics of quartz dissolution at 25°C, J. Chem. Soc. Faraday Trans. 88 (1992) 233–241. doi:10.1039/FT9928800233.

[28] L. Chou, R. Wollast, Steady-state kinetics and dissolution mechanisms of albite., Am. J. Sci. 285 (1985) 963–993. doi:10.2475/ajs.285.10.963.

[29] K.G. Knauss, T.J. Wolery, Dependence of albite dissolution kinetics on pH and time at 25°C and 70°C, Geochim. Cosmochim. Acta. 50 (1986) 2481–2497. doi:10.1016/0016-7037(86)90031-1.

[30] K. Lammers, M.M. Smith, S.A. Carroll, Muscovite dissolution kinetics as a function of pH at elevated temperature, Chem. Geol. 466 (2017) 149–158. doi:10.1016/j.chemgeo.2017.06.003.

[31] K.G. Knauss, W. Thomas J, Muscovite dissolution kinetics as a function of pH and time at 70°C, Geochim. Cosmochim. Acta. 53 (1989) 1493–1501. doi:10.1016/0016-7037(89)90232-9.

[32] E.H. Oelkers, J. Schott, J. Gauthier, T. Herrero-roncal, An experimental study of the dissolution

mechanism and rates of muscovite, 72 (2008) 4948–4961. doi:10.1016/j.gca.2008.01.040.

[33] D. De Paiva Gomes Neto, H. Conceição, V.A.C. Lisboa, R.S. De Paiva Santana, L.S. Barreto, Influence of granitic aggregates from Northeast Brazil on the alkali-aggregate reaction, Mater. Res. 17 (2014) 51–58. doi:10.1590/S1516-14392014005000045.

[34] C. Drolet, J. Duchesne, B. Fournier, Effect of alkali release by aggregates on alkali-silica reaction, Constr. Build. Mater. 157 (2017) 263–276. doi:10.1016/j.conbuildmat.2017.09.085.

[35] P.M. Dove, N. Han, A.F. Wallace, J.J. De Yoreo, Kinetics of amorphous silica dissolution and the paradox of the silica polymorphs, Proc. Natl. Acad. Sci. 105 (2008) 9903–9908. doi:10.1073/pnas.0803798105.

[36] P.M. Dove, The dissolution kinetics of quartz in sodium chloride solutions at 25° to 300°C, Am. J. Sci. 294 (1994) 665–712. doi:10.2475/ajs.294.6.665.

[37] J.P. Icenhower, P.M. Dove, The dissolution kinetics of amorphous silica into sodium chloride solutions: effects of temperature and ionic strength, Geochim. Cosmochim. Acta. 64 (2000) 4193–4203. doi:10.1016/S0016-7037(00)00487-7.

[38] A. Vollpracht, B. Lothenbach, R. Snellings, J. Haufe, The pore solution of blended cements: a review, Mater. Struct. Constr. 49 (2016) 3341–3367. doi:10.1617/s11527-015-0724-1.

[39] P.M. Dove, The dissolution kinetics of quartz in aqueous mixed cation solutions, Geochim. Cosmochim. Acta. 63 (1999) 3715–3727. doi:10.1016/S0016-7037(99)00218-5.

[40] P.M. Dove, C.J. Nix, The influence of the alkaline earth cations, magnesium, calcium, and barium on the dissolution kinetics of quartz, Geochim. Cosmochim. Acta. 61 (1997) 3329–3340. doi:10.1016/S0016-7037(97)00217-2.

[41] W.L. Marshall, J.M. Warakomski, Amorphous silica solubilities-II. Effect of aqueous salt solutions at 25°C, Geochim. Cosmochim. Acta. 44 (1980). doi:10.1016/0016-7037(80)90281-1.

[42] J. Zhou, K. Zheng, Z. Liu, L. Chen, N. Lippiatt, Use of γ-Al$_2$O$_3$ to prevent alkali-silica reaction by altering solid and aqueous compositions of hydrated cement paste, Cem. Concr. Res. 124 (2019). doi:10.1016/j.cemconres.2019.105817.

[43] M.J. Tapas, L. Sofia, K. Vessalas, P. Thomas, V. Sirivivatnanon, K. Scrivener, Efficacy of SCMs to mitigate ASR in systems with higher alkali contents assessed by pore solution method, Cem. Concr. Res. 142 (2021) 106353. doi:10.1016/j.cemconres.2021.106353.

[44] T. Chappex, K.L. Scrivener, The influence of aluminium on the dissolution of amorphous silica and its relation to alkali silica reaction, Cem. Concr. Res. 42 (2012) 1645–1649. doi:10.1016/j.cemconres.2012.09.009.

[45] K.J. Hünger, The contribution of quartz and the role of aluminum for understanding the AAR with greywacke, Cem. Concr. Res. 37 (2007) 1193–1205. doi:10.1016/j.cemconres.2007.05.009.

[46] R.K. Iler, Effect of adsorbed alumina on the solubility of amorphous silica in water, J. Colloid Interface Sci. 43 (1973) 399–408. doi:10.1016/0021-9797(73)90386-X.

[47] L. Nicoleau, E. Schreiner, A. Nonat, Ion-specific effects influencing the dissolution of tricalcium silicate, Cem. Concr. Res. 59 (2014) 118–138. doi:10.1016/j.cemconres.2014.02.006.

[48] B.R. Bickmore, K.L. Nagy, A.K. Gray, A.R. Brinkerhoff, The effect of $Al(OH)_4^-$ on the dissolution rate of quartz, Geochim. Cosmochim. Acta. 70 (2006) 290–305. doi:10.1016/j.gca.2005.09.017.

[49] H. Maraghechi, F. Rajabipour, C.G. Pantano, W.D. Burgos, Effect of calcium on dissolution and precipitation reactions of amorphous silica at high alkalinity, Cem. Concr. Res. 87 (2016) 1–13. doi:10.1016/j.cemconres.2016.05.004.

[50] B. Zhou, Z. Mao, M. Deng, Reaction of quartz glass in lithium-containing alkaline solutions with or without Ca, R. Soc. Open Sci. 5 (2018). doi:10.1098/rsos.180797.

[51] T. Oey, E.C. La Plante, G. Falzone, Y.H. Hsiao, A. Wada, L. Monfardini, M. Bauchy, J.W. Bullard, G. Sant, Calcium nitrate: a chemical admixture to inhibit aggregate dissolution and mitigate expansion caused by alkali-silica reaction, Cem. Concr. Compos. 110 (2020). doi:10.1016/j.cemconcomp.2020.103592.

[52] W.J. McCOY, A.G. Caldwell, New approach to inhibiting alkali-aggregate expansion, ACI J. Proc. 47 (1951) 693–706. doi:10.14359/12030.

[53]   X. Feng, M.D.A. Thomas, T.W. Bremner, B.J. Balcom, K.J. Folliard, Studies on lithium salts to mitigate ASR-induced expansion in new concrete: a critical review, Cem. Concr. Res. 35 (2005) 1789–1796. doi:10.1016/j.cemconres.2004.10.013.

[54]   X. Mo, Laboratory study of LiOH in inhibiting alkali-silica reaction at 20 °C: A contribution, Cem. Concr. Res. 35 (2005) 499–504. doi:10.1016/j.cemconres.2004.06.003.

[55]   M. Kawamura, H. Fuwa, Effects of lithium salts on ASR gel composition and expansion of mortars, Cem. Concr. Res. 33 (2003) 913–919. doi:10.1016/S0008-8846(02)01092-X.

[56]   C. Tremblay, M.A. Bérubé, B. Fournier, M.D.A. Thomas, K.J. Folliard, Effectiveness of lithium-based products in concrete made with Canadian natural aggregates susceptible to alkali-silica reactivity, ACI Mater. J. 104 (2007) 195–205. doi:10.14359/18583.

[57]   C. Tremblay, M.A. Bérubé, B. Fournier, M.D. Thomas, K.J. Folliard, Experimental investigation of the mechanisms by which $LiNO_3$ is effective against ASR, Cem. Concr. Res. 40 (2010) 583–597. doi:10.1016/j.cemconres.2009.09.022.

[58]   S. Plettinck, L. Chou, R. Wollast, Kinetics and mechanisms of dissolution of silica at room temperature   and   pressure,   Mineral.   Mag.   58A   (1994)   728–729. doi:10.1180/minmag.1994.58a.2.116.

[59]   T. Oey, E.C. La Plante, G. Falzone, K. Yang, A. Wada, M. Bauchy, J.W. Bullard, G. Sant, Topological controls on aluminosilicate glass dissolution: complexities induced in hyperalkaline aqueous environments, J. Am. Ceram. Soc. 103 (2020) 6198–6207. doi:10.1111/jace.17357.

[60]   T. Oey, E. La Plante, Y.-H. Hsiao, G. Falzone, G. Sant, The role of barrier layers and reactive site deactivation on dissolution suppression: implications on mitigating alkali-silica reaction, in: 15th Int. Congr. Chem. Cem., Prague, Czech Republic, 2019.

[61]   F. Deschner, B. Lothenbach, F. Winnefeld, J. Neubauer, Effect of temperature on the hydration of Portland cement blended with siliceous fl y ash, Cem. Concr. Res. 52 (2013) 169–181. doi:10.1016/j.cemconres.2013.07.006.

[62]   B. Lothenbach, F. Winnefeld, C. Alder, E. Wieland, P. Lunk, Effect of temperature on the pore

solution, microstructure and hydration products of Portland cement pastes, Cem. Concr. Res. 37 (2007) 483–491. doi:10.1016/j.cemconres.2006.11.016.

[63]   B. Traynor, H. Uvegi, E. Olivetti, B. Lothenbach, R.J. Myers, Methodology for pH measurement in high alkali cementitious systems, Cem. Concr. Res. 135 (2020) 106122. doi:10.1016/j.cemconres.2020.106122.

[64]   D.A. Kulik, T. Wagner, · Svitlana, V. Dmytrieva, G. Kosakowski, F.F. Hingerl, K. V Chudnenko, · Urs, R. Berner, D.A. Kulik, · G Kosakowski, F.F. Hingerl, T. Wagner, S. V Dmytrieva, K. V Chudnenko, GEM-Selektor geochemical modeling package: revised algorithm and GEMS3K numerical kernel for coupled simulation codes, Comput Geosci. 17 (2013) 1–24. doi:10.1007/s10596-012-9310-6.

[65]   T. Thoenen, W. Hummel, U. Berner, E. Curti, The PSI/Nagra Chemical Thermodynamic Database 12/07 Nuclear Energy and Safety Research Department Laboratory for Waste Management (LES), (2014).

[66]   B. Lothenbach, D.A. Kulik, T. Matschei, M. Balonis, L. Baquerizo, B. Dilnesa, G.D. Miron, R.J. Myers, Cemdata18: A chemical thermodynamic database for hydrated Portland cements and alkali-activated materials, Cem. Concr. Res. 115 (2019) 472–506. doi:10.1016/j.cemconres.2018.04.018.

[67]   H.C. Helgeson, J.M. Delany, H.W. Nesbitt, D.K. Bird, Summary and Critique of the Thermodynamic Properties of Rock-Forming Minerals., 1978.

[68]   R. Snellings, Solution-controlled dissolution of supplementary cementitious material glasses at pH 13: the effect of solution composition on glass dissolution rates, J. Am. Ceram. Soc. 96 (2013) 2467–2475. doi:10.1111/jace.12480.

[69]   Z. Shi, B. Ma, B. Lothenbach, Effect of Al on the formation and structure of alkali-silica reaction products, Cem. Concr. Res. 140 (2021) 106311. doi:10.1016/j.cemconres.2020.106311.

[70]   G.D. Miron, D.A. Kulik, Y. Yan, J. Tits, B. Lothenbach, Parameterization of C-S-H-(N)-(K) sublattice solid solution model for alkali uptake, Cem. Concr. Res. Submitted (2021).

[71]   S. Bai, S. Urabe, Y. Okaue, T. Yokoyama, Acceleration effect of sulfate ion on the dissolution

of amorphous silica, J. Colloid Interface Sci. 331 (2009) 551–554. doi:10.1016/j.jcis.2008.11.076.

[72] Z. Shi, B. Lothenbach, The role of calcium on the formation of alkali-silica reaction products, Cem. Concr. Res. 126 (2019) 105898. doi:10.1016/j.cemconres.2019.105898.

[73] T. Ramlochan, M. Thomas, K.A. Gruber, Effect of metakaolin on alkali-silica reaction in concrete, Cem. Concr. Res. 30 (2000) 339–344. doi:10.1016/S0008-8846(99)00261-6.

[74] M. Thomas, The effect of supplementary cementing materials on alkali-silica reaction: a review, Cem. Concr. Res. 41 (2011) 1224–1231. doi:10.1016/j.cemconres.2010.11.003.

[75] A. Vollpracht, B. Lothenbach, R. Snellings, J. Haufe, The pore solution of blended cements: a review, Mater. Struct. Constr. 49 (2016) 3341–3367. doi:10.1617/s11527-015-0724-1.

[76] F. Deschner, F. Winnefeld, B. Lothenbach, S. Seufert, P. Schwesig, S. Dittrich, F. Goetz-Neunhoeffer, J. Neubauer, Hydration of Portland cement with high replacement by siliceous fly ash, Cem. Concr. Res. 42 (2012) 1389–1400. doi:10.1016/j.cemconres.2012.06.009.

[77] F. Avet, K. Scrivener, Investigation of the calcined kaolinite content on the hydration of Limestone Calcined Clay Cement (LC^3), Cem. Concr. Res. 107 (2018) 124–135. doi:10.1016/j.cemconres.2018.02.016.

[78] D.E. Stanton, The expansion of concrete through reaction between cement and aggregate, Am. Soc. Civ. Eng. 66 (1940) 1781–1811.

[79] S. Diamond, A review of alkali-silica reaction and expansion mechanisms 1. Alkalies in cements and in concrete pore solutions, Cem. Concr. Res. 5 (1975) 329–345. doi:10.1016/0008-8846(75)90089-7.

[80] A.M. Boddy, R.D. Hooton, M.D.A. Thomas, Effect of product form of silica fume on its ability to control alkali-silica reaction, Cem. Concr. Res. 30 (2000) 1139–1150. doi:10.1016/S0008-8846(00)00297-0.

[81] A.M. Boddy, R.D. Hooton, M.D.A. Thomas, The effect of the silica content of silica fume on its ability to control alkali-silica reaction, Cem. Concr. Res. 33 (2003) 1263–1268. doi:10.1016/S0008-8846(03)00058-9.

[82]   M.H. Shehata, M.D.A. Thomas, Use of ternary blends containing silica fume and fly ash to suppress expansion due to alkali-silica reaction in concrete, Cem. Concr. Res. 32 (2002) 341–349. doi:10.1016/S0008-8846(01)00680-9.

[83]   J.A. Larbi, A.L.A. Fraay, J.M.J.M. Bijen, The chemistry of the pore fluid of silica fume-blended cement systems, Cem. Concr. Res. 20 (1990) 506–516. doi:10.1016/0008-8846(90)90095-F.

[84]   M. Kawamura, K. Takemoto, Correlation between pore solution composition and alkali silica expansion in mortars containing various fly ashes and blastfurnace slags, Int. J. Cem. Compos. Light. Concr. 10 (1988) 215–223. doi:10.1016/0262-5075(88)90051-6.

[85]   J.H.P. van Aardt, S. Visser, Calcium hydroxide attack on feldspars and clays: Possible relevance to Cement-aggregate reactions, Cem. Concr. Res. 7 (1977) 643–648. doi:10.1016/0008-8846(77)90046-1.

[86]   D. Stark, M. Bhatty, ALKALI-SILICA REACTIVITY: EFFECT OF ALKALI IN AGGREGATE ON EXPANSION, ASTM Spec. Tech. Publ. (1986).

[87]   W. Yujiang, D. Min, T. Mingshu, Alkali release from aggregate and the effect on AAR expansion, Mater. Struct. Constr. 41 (2008) 159–171. doi:10.1617/s11527-007-9227-z.

[88]   F. Locati, S. Marfil, E. Baldo, P. Maiza, Na_2O, K_2O, SiO_2 and Al_2O_3 release from potassic and calcic-sodic feldspars into alkaline solutions, Cem. Concr. Res. 40 (2010) 1189–1196. doi:10.1016/j.cemconres.2010.04.005.

[89]   C. Drolet, J. Duchesne, B. Fournier, Validation of the alkali contribution by aggregates to the concrete pore solution, Cem. Concr. Res. 98 (2017) 10–23. doi:10.1016/j.cemconres.2017.04.001.

[90]   M. Berra, U. Costa, T. Mangialardi, A.E. Paolini, Application of an innovative methodology to assessing the alkali-silica reaction in concrete, Mater. Struct. Constr. 48 (2015) 2727–2740. doi:10.1617/s11527-014-0349-9.

[91]   S. Bai, S. Urabe, Y. Okaue, T. Yokoyama, Acceleration effect of sulfate ion on the dissolution of amorphous silica, J. Colloid Interface Sci. 331 (2009) 551–554. doi:10.1016/j.jcis.2008.11.076.

113

[92] T. Chappex, L. Sofia, K. Scrivener, A robust testing protocol for the assessment of ASR reactivity of concrete, in: 15th Int. Conf. Alkali Aggreg. React. Concr., Sao Paulo, Brazil, 2016.

[93] B.P. Gautam, D.K. Panesar, The effect of elevated conditioning temperature on the ASR expansion, cracking and properties of reactive Spratt aggregate concrete, Constr. Build. Mater. 140 (2017) 310–320. doi:10.1016/j.conbuildmat.2017.02.104.

[94] J.H. Ideker, B.L. East, K.J. Folliard, M.D.A. Thomas, B. Fournier, The current state of the accelerated concrete prism test, Cem. Concr. Res. 40 (2010) 550–555. doi:10.1016/j.cemconres.2009.08.030.

Curriculum Vitae

MAHSA BAGHERI

mahsa.bagheri@epfl.ch /mahsa.bagheri987@gmail.com

PERSONAL INFORMATION

Date of birth	31-07-1987
Natinality	Iranien
Languages	Persian (native speaker)
	English (advance user)

EDUCATION

2017-2021	Doctor of Science (Ph.D.)
	ÉCOLE POLYTECHNIQUE FÉDÉRALE DE LAUSANNE (EPFL)
	Construction Materials Laboratory (LMC)
	Thesis nominated for EPFL distinction
2010-2013	Master of Physical Chemistry
	Bu-Ali Sina University
	23 September 2013
2005-2009	Bachlor of Applied Chemistry
	Bu-Ali Sina University
2004-2005	Pre-Uni (Mathematics Sciences)
	Mahdieh pre-university school
2003-2004	Diploma (Mathematics and Physics)
	Shahid Marzieh Khonsari high school

PUBLICATIONS

o **Bagheri, M.**, Azizian, S., Jaleh, B., Chehregani, A. (2014), Adsorption of Cu (II) from aqueous solution by micro-structured ZnO thin films, Journal of Industrial and Engineering Chemistry, 20, 2439-2446.

o Azizian, S., **Bagheri, M.** (2014), Enhanced adsorption of Cu^{2+} from aqueous solution by Ag doped nano-structured ZnO, Journal of Molecular Liquids, 196, 198-203.

o Zolfigol, M. A., Khazaei, A., Safaiee, M., Mokhlesi, M., Rostamian, R., **Bagheri, M.**, Shiri, M., Kruger, H. G. (2013), Application of silica vanadic acid as a heterogeneous, selective and highly reusable catalyst for oxidation of sulfides at room temperature, Journal of Molecular Catalysis A: Chemical, 370, 80-86.